



**TECHNISCHE
UNIVERSITÄT
WIEN**

**VIENNA
UNIVERSITY OF
TECHNOLOGY**

DISSERTATION

Application of Mid-Infrared Quantum Cascade Lasers for Quantitative Analysis in Aqueous Phase

ausgeführt zum Zwecke der Erlangung des akademischen Grades eines Doktors der
technischen Wissenschaften unter der Leitung von

Ao.Univ.Prof. Dipl.-Ing. Dr.techn. Bernhard Lendl
E164-AC

Institut für Chemische Technologien und Analytik

eingereicht an der Technische Universität Wien
Fakultät für Technische Naturwissenschaften und Informatik

von

Dipl.-Ing. Stefan Schaden

Matrikelnummer: 9625044
Simmeringer Hauptstraße 192A/1/20, 1110 Wien

Wien, am 20.05.2006

Deutsche Kurzfassung

Das Ziel dieser Arbeit war es, das Potential von Quanten Kaskaden Lasern als Lichtquelle für die Infrarotspektroskopie in wässriger Phase für neue Anwendungen zu evaluieren und zu testen. Dabei wurden die Vorteile von Quanten Kaskaden Lasern (QCL) gegenüber herkömmlicher Fourier-Transformations-Infrarot (FTIR) Techniken hinsichtlich der signifikant erhöhten Strahlleistung und Einfachheit des optischen Designs ausgenutzt um möglichst kompakte und leistungsfähige Analysensysteme zu entwickeln. Es wurden verschiedene Konzepte von Fliessystemen zur Probenvorbereitung bzw. Überführung der Probe in die Messzelle angewandt. Des weiteren kamen innovative Konzepte der QCL Messtechnik für wässrige Systeme wie die simultane Messung mit zwei Lasern oder Wellenlängemodulation zum Einsatz.

Die Forschungsergebnisse dieser Dissertation liegen in Form von 5 Publikationen vor, welche in internationalen wissenschaftlichen Journalen veröffentlicht (**Publikation I** und **II**) zur Veröffentlichung angenommen (**Publikation III**) bzw. eingereicht wurden (**Publikationen IV** und **V**).

In **Publikation I** wird erstmals die Verknüpfung von Kapillarelektrophorese (CE) mit QCL basierender online Infrarotdetektion gezeigt. Dazu wurde eine speziell für die CE-IR Kopplung entwickelte Durchflusszelle eingesetzt. Die bisher veröffentlichten CE-FTIR Experimente verwendeten optischen Weglängen von 10-15 μm . Diese konnten durch den Einsatz eines QCLs auf 60 μm gesteigert werden. Mit Hilfe gruppenspezifischer Detektion (Kohlenhydrate) wurden die Analyten quantifiziert.

Publikation II beschäftigt sich mit der erstmaligen simultanen Messung mit 2 QCLs in wässriger Phase. Zur Realisierung wurde ein optischer Aufbau verwendet, welcher die Beprobung einer Messzelle mit zwei Laserstrahlen ermöglichte (Dual-QCL System). Es konnte gezeigt werden, dass durch die Absorptionsmessung an zwei verschiedenen Wellenlängen mit jeweils einem QCL trotz Überlappung der Absorptionsbanden von Glucose und Natriumacetat eine quantitative Analyse beider Substanzen möglich ist.

Die Möglichkeit mehrere Wellenlängen gleichzeitig zu messen wurde in **Publikation III** eingesetzt um eine Onlineanalyse eines Reaktionsgemisches durchzuführen. Es wurde die

Oxidation von Sulfit zu Sulfat mittels Wasserstoffperoxyd untersucht. Die hohe Zeitauflösung des Dual-QCL Systems ermöglichte eine Echtzeit Überwachung der Sulfat-Bildung und des Wasserstoffperoxyd-Abbaus.

Die Korrektur von Basislinienänderungen mittels Modulation der Laserwellenlänge wird in **Publikation IV** gezeigt. Hier wird durch periodische Änderung der Betriebsparameter eines QCLs eine Absorptionsmessung an zwei Wellenlängen ermöglicht. Die erhaltene Information wird zur Basislinienkorrektur genutzt um den Einfluss variierender Sachrosekonzentrationen auf die CO₂-Messung zu kompensieren.

Eine weitere Publikation dieser Dissertation (**Publikation V**) gibt einen Überblick über die Eigenschaften von QCLs und ihre Anwendungen in der Gas- und Flüssigphase. Dabei werden sowohl die unterschiedlichen Analysentechniken besprochen, als auch deren zahlreiche Einsatzgebiete.

Abstract

The aim of this thesis was to explore the potential of Quantum Cascade Lasers as light source for infrared spectroscopy in aqueous phase for new applications. The advantages of Quantum Cascade Lasers (QCL) compared to fourier transform infrared techniques (FTIR) concerning the significantly higher light power and the simplicity of the optical design were used to develop compact and powerful analytical methods. Different kinds of flow systems for sample preparation as well as for filling the sample cell were investigated. Additionally innovative concepts for QCL based sampling techniques for aqueous systems such as simultaneous measuring with two QCLs or wavelength modulation were performed.

The research results of this thesis are present in 5 papers, which already have been published (**paper I and II**), are accepted for publication (**paper III**) or have been submitted for publication (**paper IV and V**) in international scientific journals.

Paper I reports for the first time the on-line hyphenation of a QCL based IR detection to a capillary electrophoresis (CE) system. In order to succeed with this hyphenation a dedicated IR-transparent flow cell was constructed. The assessable optical path length could be increased, from the until now published 10-15 μm in CE-FTIR experiments to 60 μm by use of this powerful mid-infrared laser. Functional group detection i.e. carbohydrate-detection, was accomplished for quantifying the analytes.

The first simultaneous measurements of two analytes in aqueous solution employing two quantum cascade lasers is presented in **paper II**. For the realization an optical set-up was developed allowing sampling of one flow cell with two QCL beams (Dual-QCL system). The information of both wavelengths was used for quantitative analysis of glucose and sodium acetate even if they showed strong overlapping absorption bands typically found in condensed phase.

The possibility of measuring at two wavelengths simultaneously was applied in **paper III** for on-line monitoring of a chemical reaction. The Oxidation of sulphite to sulphate by hydrogen peroxide was investigated. The short time constant of the system allowed direct, real-time monitoring of sulphate formation and hydrogen peroxide depletion.

The compensation of baseline drifts via wavelength modulation is shown in **paper IV**. Periodical modulation of the QCL driving parameters allows alternating measurements on two distinct wavelengths. The gained information is used to perform a baseline correction in order to compensate for influences on the signal of the CO₂ measurement arising from changes in matrix composition.

Another paper included in this thesis (**paper V**) reviews the characteristics of QCLs and their use in gaseous and liquid phase. Different measurement techniques are as well discussed as their numerous fields of applications.

Acknowledgement

Zuerst möchte ich mich bei Bernhard Lendl für die Ermöglichung dieser Dissertation sowie das in mich gesetzte Vertrauen bedanken. Für die Zusammenarbeit und die zur Verfügung gestellten Geräte im QCL-CE Projekt bedanke ich mich bei Bo Karlberg und Malin Kölhed.

Bei Ana Dominguez-Vidal bedanke ich mich vor allem für die Hilfe bei der Fertigstellung des CO₂ Papers. Wolfgang Ritter sei für die zahlreichen teils fruchtbaren teils aber auch nur unterhaltsamen Diskussionen im Laufe der Dissertation gedankt. Bei dem Rest der Arbeitsgruppe – Johannes Frank, Markus Schaufler, Nina Kaun, Stephan Kulka, Johannes Schnöller, Mercedes López Pastor, Guillermo Quintas Soriano, sowie den „Ehemaligen“ und den zahlreichen Gästen bedanke ich mich für das freundschaftliche Arbeitsklima, und den internationalen Flair den ich in der Gruppe genießen durfte.

Alexander Smutni hat mir dankenswerter Weise geholfen, die Dissertation von Fehlern im Englischen zu befreien. Aber auch bei meinen restlichen Freunden möchte ich mich hier bedanken für die schönen Zeiten während der Dissertation und jenen die noch folgen werden.

Bei Zaneta bedanke ich mich für vieles. Insbesondere für ihre Unterstützung und das Verständnis wenn ich einmal weniger Zeit hatte.

Meiner Familie danke ich für die Unterstützung und die Zahlreichen kleinen Dienste, die mir mehr Zeit für meine Arbeit einräumten.

Dankeschön!

Table of Content

Deutsche Kurzfassung.....	II
Abstract.....	IV
Acknowledgement.....	VI
Table of Content.....	VII
List of Publications	IX
List of abbreviations.....	X

1. IR-Spectroscopy.....	1
1.1. Theory of infrared absorption.....	1
1.2. Gained information of infrared absorption spectra.....	4
1.3. Infrared spectroscopy in aqueous phase	5
1.4. Fourier transform infrared spectroscopy (FTIR)	6
2. Quantum cascade lasers	7
2.1. Theory of lasers.....	7
2.1.1. Stimulated emission.....	7
2.1.2. Population inversion.....	8
2.1.3. Resonance of a standing wave.....	8
2.2. Quantum cascade laser –principle of operation.....	9
2.2.1. Properties of quantum cascade lasers	11
2.3. Fields of application in analytical chemistry.....	13
2.4. Comparison of the light power of a QCL-System and a FTIR spectrometer	14
2.4.1. Light power of a QCL system.....	14
2.4.2. Light power of a FTIR spectrometer	15
2.4.2.1. Spectral intensity	16
2.4.2.2. Throughput of a spectrometer.....	16
2.4.2.3. Efficiency of a spectrometer.....	17
2.4.2.4. Calculation of the light power	17
3. Concepts for quantitative QCL based analysis in aqueous phase	19
3.1. Capillary electrophoresis	21
3.1.1. Theoretical background.....	21
3.1.2. Principle of capillary zone electrophoresis	22
3.1.3. Injection of the sample	24

3.1.3.1.	Hydrodynamic injection.....	25
3.1.3.2.	Electrokinetic injection.....	25
3.1.4.	Detection.....	25
3.1.4.1.	Interface for online QCL detection in capillary electrophoresis	26
3.2.	<i>Flow injection analysis</i>	27
3.3.	<i>Continuous on-line measurements</i>	29
3.4.	<i>Wavelength modulation of the QCL for background compensation</i>	29
3.4.1.	Investigation of the pH-dependent concentration of CO ₂ (aq).....	30
3.4.1.1.	Motivation.....	30
3.4.1.2.	Experimental.....	31
3.4.1.3.	Results and discussion.....	32
3.4.2.	Investigation of water baseline changes due to relevant constituents of beverages.....	33
3.4.2.1.	Motivation.....	33
3.4.2.2.	Experimental.....	34
3.4.2.3.	Results and discussion.....	35
3.4.2.4.	Conclusion	41
4.	Laser instrumentation and signal processing	43
4.1.	<i>General Devices</i>	43
4.1.1.	Function Generator	43
4.1.2.	Computer Interface	43
4.2.	<i>Laser driving units</i>	44
4.2.1.	Alpes Lasers starter kit.....	44
4.2.2.	Quanta-BP	45
4.3.	<i>Evaluation of the detector signal</i>	46
4.4.	<i>Software</i>	47
4.5.	<i>Apparatus</i>	48
4.5.1.	Paper I.....	48
4.5.2.	Paper II and III	49
4.5.3.	Paper IV.....	50
5.	References.....	53
6.	Appendix.....	56
	<i>Paper I</i>	56
	<i>Paper II</i>	63
	<i>Paper III</i>	69
	<i>Paper IV</i>	85
	<i>Paper V</i>	106
	<i>Curriculum Vitae</i>	151

List of Publications

“ On-Line hyphenation of quantum cascade laser and capillary electrophoresis”

M. Kölhed, S. Schaden, B. Karlberg, and B. Lendl, *Journal of Chromatography A* **1083**,199 (2005).

“ Simultaneous measurement of two compounds in aqueous solution with dual quantum cascade laser absorption spectroscopy” S. Schaden, A. Domínguez-Vidal, and B. Lendl, *Applied Physics B: Lasers and Optics* **83**,135 (2006).

“Online reaction monitoring in liquid phase using two mid-IR quantum cascade lasers simultaneously” S. Schaden, A. Dominguez-Vidal, and B. Lendl, *Applied Spectroscopy* **60**, (2006) in press.

“Quantum cascade laser modulation for correction of matrix induced background changes in aqueous samples” S. Schaden, A. Domínguez-Vidal, and B. Lendl, *Applied Physics B: Lasers and Optics*, submitted for publication

“Quantum cascade lasers: a promising light source for vibrational spectroscopy” S. Schaden, L. Hvozdar, A. Müller B. Lendl, *Applied Spectroscopy*, submitted for publication

List of abbreviations

ATR	Attenuated Total Reflection
BGE	Background Electrolyte
BNC	Bayonet Nut Connector
CE	Capillary Electrophoresis
CI	Computer Interface
CIEF	Capillary Isoelectric Focusing
CITP	Capillary Isotachopheresis
CW	Continues Wave
CZE	Capillary Zone Electrophoresis
DC	Direct Current
DFB	Distributed Feed Back
EOF	Electroosmotic Flow
FIA	Flow Injection Analysis
FTIR	Fourier Transform Infrared
HPLC	High Performance Liquid Chromatography
IR	Infrared
LASER	Light Amplification by Stimulated Emission of Radiation
LED	Light Emitting Diodes
MBE	Molecular Beam Epitaxy
MCT	Mercury Cadmium Telluride
MEKC	Micellar Electrokinetic Chromatography
MID-IR	Middle Infrared
MLR	Multiple Linear Regression
PC	Personal Computer
PLS	Partial Least Squares
PTFE	Polytetraflouroethane
QCL	Quantum Cascade Laser
SMB	Sub-Miniature-B
SNR	Signal to Noise Ratio
TTL	Transistor-Transistor-Logic
UV	Ultra Violet
VDC	Volt Direct Current

1. IR-Spectroscopy

1.1. Theory of infrared absorption

Every molecule has a certain number of vibrational degrees of freedom. In case of a linear molecule with n atoms this number is $3n-5$ and for a non linear molecule $3n-6$. Every vibration of the molecule is a linear combination of these vibrational degrees of freedom. The vibration of a molecule consisting of two atoms can be described using the model of the quantum harmonic and anharmonic oscillator where the quantum anharmonic oscillator takes into account the asymmetry of attraction and repulsion forces as well as the dissociation of the molecule. Therefore the quantum anharmonic oscillator is more appropriate. Both models show a quantisation of the allowed energy states. The energy diagram of the quantum anharmonic oscillator is given in Figure 1.

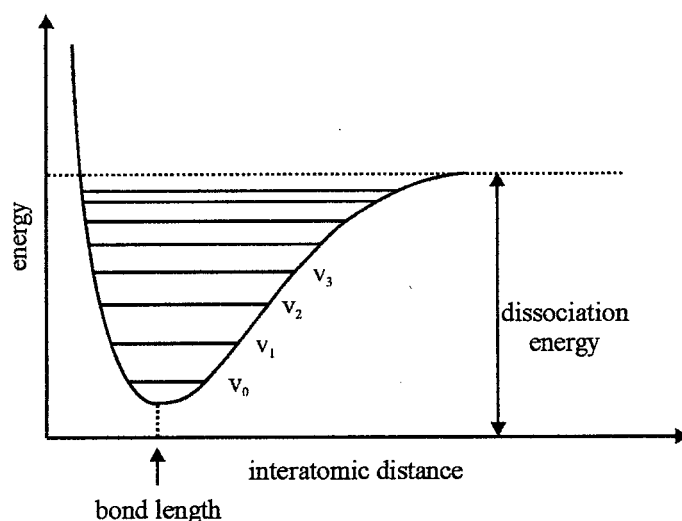


Figure 1: Energy level diagram of a quantum anharmonic oscillator.

The spacing of the energy levels is not equidistant as it is for the harmonic oscillator. It is getting smaller with rising vibrational quantum number (v) and breaks up into a continuum when the dissociation energy is reached. The quantum mechanic selection rules allow transitions between energy levels of $\Delta v = \pm 1$ as well as for higher transitions, called overtones ($\Delta v = \pm 2, \pm 3$ etc.). But the probability decays exponentially with Δv .

The population density of the different energy levels shows a Boltzmann distribution. Therefore the ground state of a vibrational system shows always the highest population density and also the highest probability that a transition caused by excitation takes place. This is also referred to as the excitation of the fundamental vibrations ($\nu_0 \rightarrow \nu_1$). Excitations of higher energy levels (e.g. $\nu_1 \rightarrow \nu_2$, or $\nu_2 \rightarrow \nu_3$) are called Hot Bands and show a decreasing probability with rising ν .

It is also possible that two vibrations of a molecule are excited by one energy quant. This phenomenon is called combination vibration. Therefore the excitation energy must be equal to the total energy difference of the ground and excited state of both vibrations. Another special case of excited vibrations is the so called differential vibration. A energy quant equal to the energy difference of the first states of two different vibrations causes the transition of the first state of vibration A to the first state of vibration B under relaxation of vibration A to the ground state. An overview of the different discussed vibrational excitations is given in Figure 2.

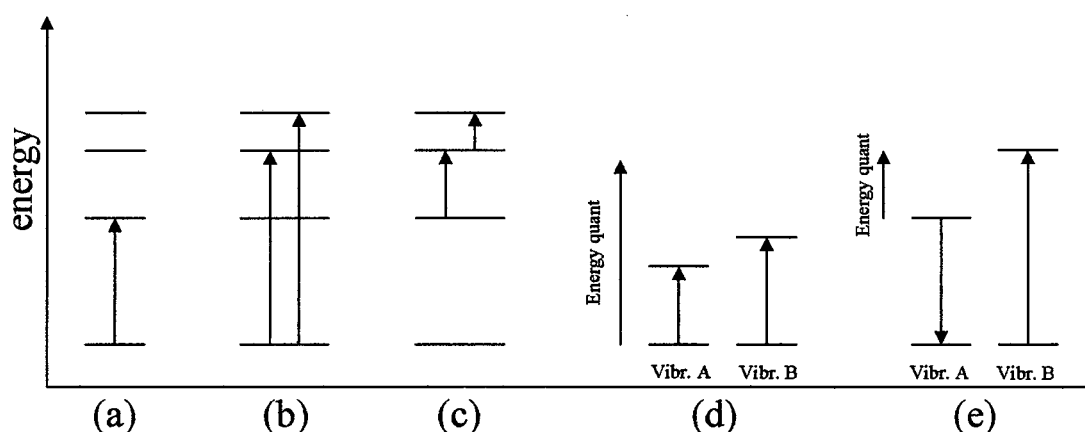


Figure 2: Different vibrational excitations: (a) transition from the ground state to the first excited state – fundamental vibration (b) transition from the ground state to higher excited states – overtones (c) transition from excited states to the next higher state – Hot Bands (d) excitation of a combination vibration (e) excitation of a differential vibration

If the excitation of vibrations is caused by the absorption of a photon, the energy of the photon has to be in resonance with the involved energy levels. The energy (E) of a photon with a given frequency (ν) can be calculated using the following equation

$$E = h\nu \quad \text{Equation 1.1}$$

in which h is Planck's constant having the value $6.6260755 \cdot 10^{-34}$ J·s.

Transitions of vibrational states show typically smaller energy differences than the transition of electron states. Hence the exciting photons show wavelength beyond the red part of the visible light, the infrared region. Beside the resonance of the absorption there exists another precondition for the excitation by absorption of infrared light. The excited vibrations within a molecule must cause a net change in the dipole moment of the molecule.

The term infrared covers the range of the electromagnetic spectrum between 0.75 and 1000 μm . In the context of infrared spectroscopy, wavelength is given in terms of wavenumbers, which have the unit cm^{-1} . Therefore the infrared region extends from 13300 to 10 cm^{-1} . This range is divided into three sections according to the vibrations that are excited. The near infrared region excites overtones and combinations of the fundamental vibrations. The photons of the middle infrared region have lower energy and cause excitation of the fundamental vibrations that show higher intensities. The third region is the far infrared. The excited vibrations are intermolecular vibrations. The borders of the three infrared ranges are not sharp as some molecules have their fundamental vibrations in an energy range where other already show some overtones. This applies also to the border of fundamental and intermolecular vibrations. However an overview of a common classification of the three infrared regions is given in Table 1.

Region	Wavenumber range (cm^{-1})
Near	13300 - 4000
Middle	4000 - 400
Far	400 - 10

Table 1: Classification of the three infrared ranges.[1]

For infrared spectroscopy different kinds of light sources are used, depending on the observed wavelength region. For near infrared spectroscopy glowing tungsten filament, halogen lamps as well as diode lasers or Light Emitting Diodes (LED) can be used. For mid infrared spectroscopy broadband emitters like globars, Nernst lamps or coils of chrome-nickel alloy are available. Mid infrared light sources for spectroscopy with minor spectral width but higher light intensities are for example semiconductor lasers. The spectral region of the far infrared can be exploited using light sources like high-pressure mercury lamps or nowadays also accessible synchrotron radiation and so called terahertz quantum cascade lasers.

1.2. Gained information of infrared absorption spectra

Comparison of many IR-spectra showed, that functional groups (e.g. C=O, =CH₂, -C=C-, C-Cl, C≡N aso.) show absorption bands at the same or nearly the same wavenumber, even if they are present in different chemical environments. For example the carbonyl group of aldehydes, ketones, esters and carboxylic acids show strong absorption at around 1710 cm⁻¹. Hence spectra of chemical pure, unknown substances showing absorption bands at 1710 cm⁻¹ indicate a carbonyl group in the structure of the investigated substance. Therefore IR-spectroscopy is an important technique for the evaluation of the structure of organic compounds and also for identification purposes and quality control. For the last two applications the comparison of the obtained IR-spectrum with a spectra library is often used. The most characteristic part of the spectrum of a certain molecule is the region from about 1500 to 500 cm⁻¹. This region usually contains vibrations including movements of many atoms. As the signature of these vibrations is highly characteristic for a certain molecule this spectral region is also called the fingerprint region [2].

IR-absorption spectroscopy is not only used in qualitative but also in quantitative analysis. The absorption obeys the law of Lambert-Beer.

$$A = \varepsilon \cdot c \cdot l = \log \frac{I_0}{I} \quad \text{Equation 1.2}$$

A is the Absorbance [AU], ε the molar absorptivity [l/(mol*cm)], c the concentration of the analyte [mol/l] and l the path length [cm]. I_0 is the light intensity before and I the light intensity after the sample cell. I_0 is normally measured as single beam background spectrum of the sample cell filled with sample matrix without the analyte. That way the absorption of the cell or the background medium can be compensated. The changes in the absorption at specific wavenumbers are used to determine the concentration of an analyte. Even when other analytes show partly overlapping absorption the evaluation of the absorption at multiple wavenumbers can be used to determine the concentration of all analytes [3]. In this case multivariate calibrations such as partial least squares (PLS) or multiple linear regression (MLR) have to be used.

Additional to information about the constitution of a molecule or the concentration of an analyte, IR-spectroscopy is also able to determine latent variables that are the result of the composition of a mixture and are influenced by many different substances. As an example the determination of the octane number of gasoline [4,5] can be mentioned.

1.3. Infrared spectroscopy in aqueous phase

Water itself is strongly absorbing infrared light. Due to interactions of the molecules in condensed phase, the absorption bands of water are broad. Water has two main regions of absorption, namely the bending vibration, which is located around 1640 cm^{-1} and the symmetric and asymmetric stretching vibration that are separated in the gas phase but are absorbing strongly in the entire region between 3600 and 3000 cm^{-1} in the condensed phase. There is a small but significant combination band of the bending and libration modes at 2150 cm^{-1} [6]. The spectra given in Figure 3 additionally shows absorption at around 1000 cm^{-1} and beyond arising from the used window material (CaF_2).

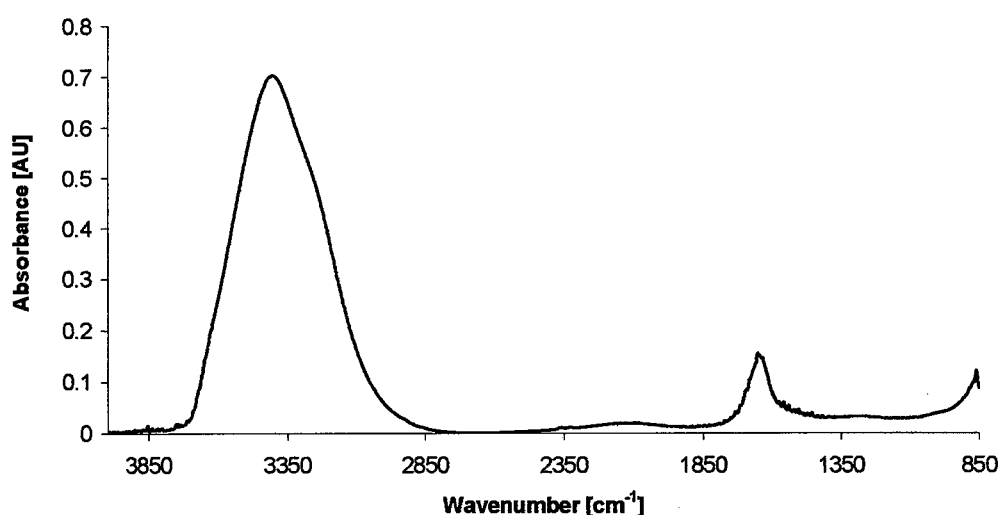


Figure 3: FTIR absorption spectrum of a water film between two CaF_2 windows.

The self-absorption of water restricts the optical path of transmission cells and also the limit of detection of the analytes.

1.4. Fourier transform infrared spectroscopy (FTIR)

The use of FTIR spectrometers has main advantages compared to spectrometers using prisms or gratings. The radiation is not separated into single wavelengths. The interferogram contains the information of all of them, in the Fourier transform, this information is extracted for all wavelengths simultaneously. This so-called multiplex advantage [7] results in an improvement of the signal to noise ratio. Another advantage, known as the Connes advantage [7], addresses the fact that a HeNe laser is used as an internal wavelength calibration standard. Hence FTIR-Spectrometers show high wavelength stability. The third advantage of FTIR-Spectrometers is the throughput of light. In a Michelson interferometer the throughput is higher in comparison to a grating or prism spectrometer. An increase of the light intensity allows higher path length and results in higher signals. Nevertheless to increase the light power significantly, IR spectroscopic principles with different light sources were developed. At this point infrared lasers are one of the most promising tools for the future. Due to the strong MID-IR absorption of water and because of the limited brightness of thermal IR-light sources (globar), which are used in state-of-the-art FTIR spectrometer, MID-IR transmission measurements in aqueous phase require a very short ($<50\text{ }\mu\text{m}$) optical path. For measurements in the biological interesting area at 1640 cm^{-1} (amide I band) even optical paths below $10\text{ }\mu\text{m}$ have to be used. The necessity of using short optical paths is also a serious problem in process analytical applications due to easy clogging of the flow-cell.

2. Quantum cascade lasers

2.1. Theory of lasers

A Laser (Light Amplification by Stimulated Emission of Radiation) is an optical source that emits photons in a beam with very special characteristics. Normally not all of these characteristics apply to a particular type of laser. The laser light shows high intensities, it is strongly parallel, monochrome, coherent and can be tuned. Lasers can operate in continuous wave (cw) mode or pulsed mode, where ultra short pulses of femto seconds are achievable. The basic principles are the stimulated emission, the occurrence of population inversion and resonance. For a better understanding a short introduction in these principles will be given in the following section.

2.1.1. Stimulated emission

Electrons in atoms, ions or molecules can be excited by absorption of light or by an energy transfer upon impacts. The excited energy level can decay directly by emission of a photon, via an intermediate state (e.g. fluorescence) or via a radiation less process. Normally the photons are isotropically radiated. Every direction is statistically equal. The number of emitted photons is proportional to the number of excited electrons. Alternatively, if a photon hits the excited particle and the energy of the photon is in resonance with the transition between excited and ground state of the particle, the emission is stimulated. In that case the emitted photon shows the same energy, orientation and phase as the stimulating one. The emitted number of photons is proportional to the number of excited electrons as well as to the number of stimulating photons.

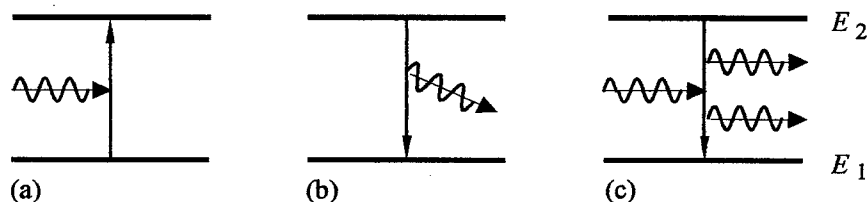


Figure 4: Absorption of a photon (a), spontaneous emission of a photon, random orientation (b) and light stimulated emission, emitted photon has the same orientation and phase than the stimulating one (c).

Photons can also be absorbed if they hit a particle in the ground state. Stimulated emission and absorption are two competing processes, where the ratio of particles in the ground state and in the excited state determines the main process. Therefore light amplification is only possible if a higher number of electrons are located in the excited state than in the ground state. This phenomenon is called population inversion.

2.1.2. Population inversion

Systems in equilibrium show a distribution of the electrons between two energy states according to the Maxwell-Boltzmann distribution:

$$\frac{N_2}{N_1} = \frac{g_2}{g_1} \cdot e^{-\left(\frac{E_2 - E_1}{kT}\right)} \quad \text{Equation 2.1}$$

Where N_x is the number of electrons in the energy state x , g_x is the statistical weight of the energy state x , k is the Boltzmann constant ($1.38 \cdot 10^{-23}$ J/K) and T the temperature of the system in K.

If the temperature is infinitely high, the maximum ratio of N_2 to N_1 is reached with 1:1. The realisation of a population inversion is only possible by an input of energy - different than heat - into the system. This procedure is called pumping. Additionally at least three energy levels are involved, where the radiant transition takes place only between two levels. The third level is used for the pumping process. An example is shown in Figure 5. To hold up the population inversion the lifetime of E_2 has to be significantly longer than the one of E_3 .

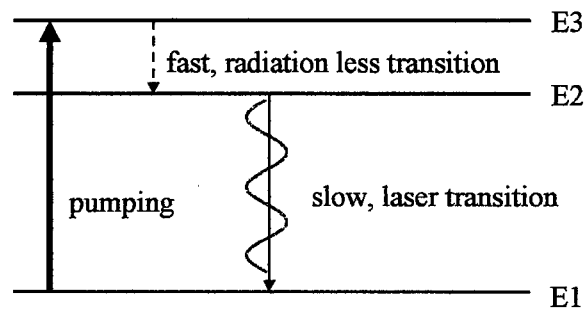


Figure 5: Energy levels of a laser system

2.1.3. Resonance of a standing wave

The emitted photons are reflected at the end of the laser medium and can induce stimulated emission of further photons. This leads to light cascades and a high degree of amplification. It is maximized if the photons can form a standing wave. Therefore the reflecting parts form a resonator. Its length (L) and the wavelength of the photons (λ) have to fulfil the following equation, wherein m is an integer.

$$L = m \frac{\lambda}{2} \quad \text{Equation 2.2}$$

2.2. Quantum cascade laser –principle of operation

Quantum cascade lasers are semiconductor lasers that differ in a fundamental way from conventional diode lasers. Diode lasers show a bipolar transition that takes place between energy bands where conduction electrons and band holes recombine across the band gap (p and n structure). The chemical system determines the band gap and therefore also the wavelength of the emitted light. In contrast QCLs are unipolar lasers where the light generation is based on intersubband transition within the conduction band [8]. The electron states arise from size quantisation in semiconductor heterostructures. A heterostructure consists of layers from at least two different materials. Layers with higher (“barrier” layer) and lower (“well” layer) band edges alternate. In such a system the conduction band edges of the two materials form a step structure, as shown in Figure 6. If the thickness of the layer is in the range of several atomic monolayers, the fact that the electron is a wave cannot be neglected. The allowed states in this structure correspond to standing waves. The former continuum of the states above the band gap breaks up into a set of discrete quantized states. The layer thickness of the well layers determines the spacing between the energetic states.

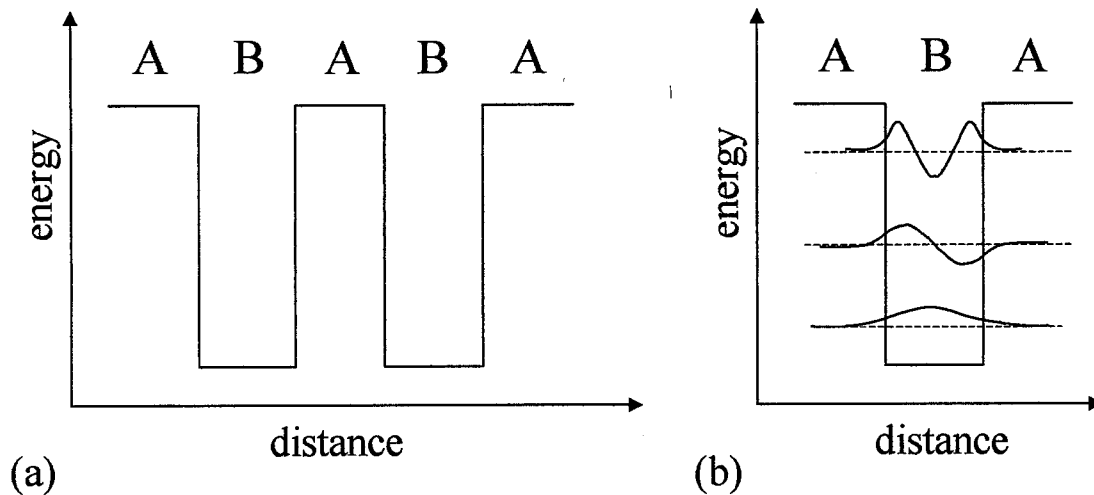


Figure 6: Energy diagram of the conduction band of a heterostructure consisting of barrier layers A and well layers B (left) and the quantisation of the energy states (right).

If a barrier layer thin enough separates the well layers, the wave functions can overlap and form a hybrid state. As a result electrons can physically move from one well layer to the other one, even if they do not have enough energy to pass over the barrier (see Figure 7). This phenomenon is called tunnelling.

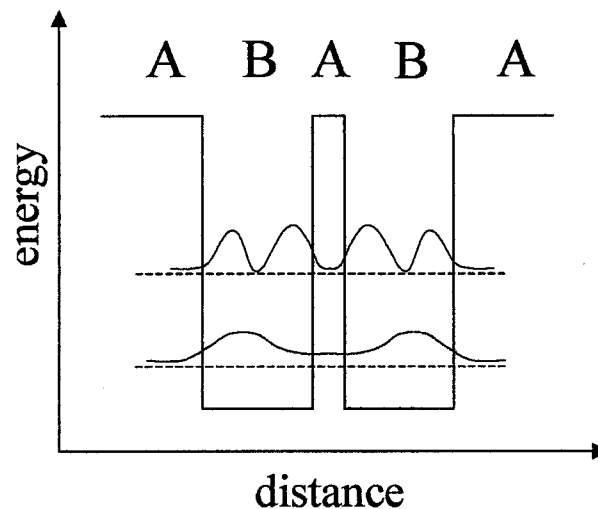


Figure 7: Hybrid state formed by overlapping wave functions of electrons in neighbouring well layers B separated by thin barrier layers A.

A quantum cascade laser is realised as a sequence of well and barrier layers. By variation of the layer thickness a pair of injection region and active region is realised. This pair is repeated n times. The heterostructure of the active region generates three coupled energetic levels. Figure 8 shows a simplified energy diagram. The electrons are injected into the third energy level by means of the electrical current. The radiant

transition takes place between the third and the second level. The subsequent transition (from level 2 to level 1) is tailored to be in resonance with the longitudinal optical phonon energy. Therefore it is several orders of magnitude faster than the transition for photon emission. As a result population inversion is assured. Additionally electrons are extracted from level 2 and 1 into the next injection region very fast. The extraction of electrons from level 3 is a forbidden transition.

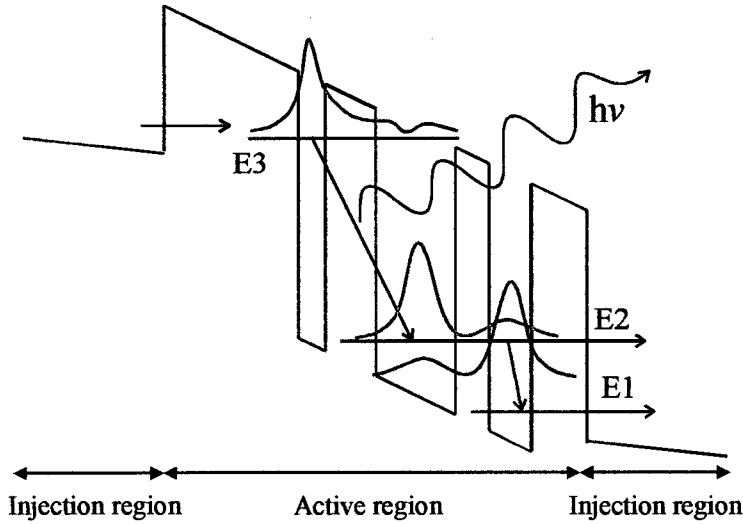


Figure 8: Energy diagram of an active region. Radiant transition $E3 \rightarrow E2$ (slow), non radiant transition $E2 \rightarrow E1$ (fast), electron extraction from E1 and E2 into the next injection region (fast).

There is a high demand on the layer resolution of such heterostructures. The edges between the well and barrier layers have to be sharp. The lack of an appropriate manufacturing technique for such hetero structures, delayed the practical realisation of QCLs. 24 years after the first theoretical proposals [9] Faist et. al. was using molecular beam epitaxy (MBE) to grow the substrate for the first working QCL.

2.2.1. Properties of quantum cascade lasers

The first QCL realised in 1994 [8] had to be operated in pulsed mode at cryogenic temperatures (max. of 88 K). Room temperature operating was not possible. Fast development in the field of heterostructure engineering lead to rapid improvements of the performance of QCLs. Nowadays room temperature operating for pulsed as well as for continuous wave (cw) mode is realised. An overview of the milestones in the history of QCL technology is given in Table 2.

Year	Milestones	Puplication	
1994	First QCL	Science 264, 533	J. Faist et al.
1995	CW operation	Appl. Phys. Lett. 68, 3057	J. Faist et al.
1996	Room temperature operation with high power	Appl. Phys. Lett. 67, 3680	J. Faist et al.
1997	Room temperature operation in single mode (DFB)	Appl. Phys. Lett. 70, 2670	J. Faist et al.
1998	New material used: GaAs/AlGaAs	Appl. Phys. Lett. 73, 3486	C. Sirtori et al.
2002	cw operation above room temperature	Science 295, 301	M. Beck et al.

Table 2: Milestones in QCL development until 2002

As discussed in the previous chapter, the spacing between the energy levels of a QCL is determined by the thickness of the well layers. Hence the wavelength can be tailored by bandstructure engineering over a wide spectral region and to the particular need of the application using the same semi-conducting material. This gives access to wavelength regions not accessible with diode lasers. The mechanism of light generation from the intersubband transition is liable to a selection rule that causes a polarisation of the generated light. The polarisation plane is linearly with the electric field and perpendicular to the layers.

It is possible to tune the emission wavelength of a QCL in the range of 0.4% around the central wavelength. This can be done either by changing the heat sink temperature or by adding a DC component to the laser driving current. In both cases a change of the resonator length is responsible for tuning according to Equation 2.2. The resonator of a QCL can be designed as a Fabry-Pérot type or a Distributed Feed Back (DFB) type. Fabry-Pérot QCLs show normally a multimode performance. The mode spacing depends on the length of the resonator. But most applications such as chemical sensing and pollution monitoring require a tunable light source with a narrow line width. With the DFB technology these demands are fulfilled. In DFB lasers a grating is etched into the active medium perpendicular to the resonator length [10]. The allowed standing waves formed inside the resonator are coupling with the grating so that only one narrow mode is amplified. The mode is determined by the grating period.

QCLs show a high beam divergence. The full divergence angle is about 60 degrees perpendicular to the layer and 20 degrees parallel to the layers. The reason can be

found in the diffraction at the output slit of the cavity, that is direct proportional to the wavelength and indirect proportional to the square of the slit diameter.

2.3. Fields of application in analytical chemistry

Infrared laser absorption spectroscopy is an extremely effective tool for the detection of molecular trace gases [11]. The usefulness of the laser spectroscopy approach is limited by the availability of convenient tunable sources in the region of fundamental vibrational absorption bands from 3 to 20 μm . Properties of QCL like tuning range over few wavenumbers or tailoring the emission frequency by band structure engineering as well as room temperature operation and a compact design make them well suitable for the demands of chemical sensing applications. Beside direct absorption based spectroscopic techniques QCLs permit the use of advanced detection techniques that significantly improve the SNR of trace gas spectra and decrease the sensor size. Sensors based on cavity ringdown spectroscopy [12,13], integrated cavity output spectroscopy [14], photo acoustic spectroscopy [15,16] as well as Faraday modulation spectroscopy [17] have been reported. The field of application ranges from atmospheric trace gas detection, pollution monitoring to spectroscopic studies and medical diagnostics.

In condensed phase absorption bands are much broader than in gas phase, furthermore spectral overlap of different analytes is frequent. At first glance this situation seems to discourage the use of QCLs for measurements of liquids. However, because of the high spectral power density compared to thermal light sources (see chapter 2.4), QCLs may bring about substantial advantages also for liquid phase measurement. Sensitivity and robustness of liquid phase measurements is hampered by strong solvent absorption that requires very short optical paths length in transmission measurement. Using QCLs allows extending the optical path for transmission measurements of aqueous samples from typically 8-30 μm for FTIR-Spectroscopy [18,19] to about 120-250 μm [20]. In case direct measurements do not offer sufficient selectivity a flow system for sample modulation may be added prior to detection. This was demonstrated for a flow injection system performing a selected chemical reaction that induces traceable changes in analyte absorption bands [21] as well as for separation techniques such as high performance liquid chromatography [22] and within this thesis for capillary electrophoresis. If separation of the analytes or

selective reactions cannot be performed other strategies to measure interfering analytes have to be developed. A possible solution is the application of more than one laser or wavelength modulation of one laser. Both possibilities have been investigated within this thesis.

2.4. Comparison of the light power of a QCL-System and a FTIR spectrometer

One of the most often highlighted advantages of QCLs for applications in condensed phase is their high light power compared to other MID-IR sources. As already discussed in chapter 1.3, IR-spectroscopy in aqueous systems suffers from strong solvent absorption. This limits the optical path and as a consequence increases the limits of detections. QCLs show a light power in the milliwatt range if operated in cw mode and even higher in pulsed mode. Conventional MID-IR sources used in FTIR spectrometers (e.g. globars) show similar light powers. But contrary to globars, QCLs focus the whole power in a small spectral region. Therefore they show much higher light power for particular wavelength compared to globars. To give an estimation of the difference, in the following section the throughput of an FTIR spectrometer is calculated and compared with the throughput of an optical set-up for absorption measurements with QCLs.

2.4.1. Light power of a QCL system

The light power received at the detector of a QCL system (P_{QCL}) depends mainly on the emission power of the QCL, and losses at the optics (efficiency of light collection and the losses due to absorption). As the optics can be built with only two mirrors (or lenses), losses due to imperfect alignment play a minor roll. For calculations of P_{QCL} , the specifications of QCLs used for this work where taken. The QCLs were operated in pulsed mode. Data sampling was only performed within the pulses. Between the pulses the detector signal was not evaluated. Theoretically variations of the duty cycle and hence variations in average power would not have affected the signal intensity. Therefore the effective used power of the QCLs was the pulse power and not the average power. The specifications of the laser power are given for pulse duration of 50 ns and a repetition period of 2.5 μs . This is equal to a duty cycle of 2%. Hence the

given values for the average power have to be multiplied by 50 to obtain the pulse power.

As QCLs show a strong beam divergence the efficiency of the collecting optic has to be calculated. The beam shows a full divergence angle of about 60 degrees perpendicular to the layer and 20 degrees parallel to the layers. The producer of the QCL specifies that $f/1$ optics - as used for this thesis - will typically collect about 70% of the emitted output power. Further the reflectivity of the used mirrors has to be considered. The manufacturer specifies the reflectivity with 95%. For calculations of the whole losses an optical set-up consisting of 4 mirrors was assumed.

Two QCLs were investigated for this calculation, one with an emission maximum at 1080 cm^{-1} (QCL1), the other one with a maximum at 1393 cm^{-1} (QCL2). Table 3 summarize the given parameters of the laser as well as the calculated P_{QCL} .

	Emission maximum [cm ⁻¹]	Spectral width [cm ⁻¹]	Average power [mW]	Pulse power [mW]	P_{QCL} [mW]
QCL1	1080	81	20	1000	570
QCL2	1393	83	8	400	228

Table 3: Parameters of the investigated QCLs including the calculated light power received at the detector P_{QCL} .

2.4.2. Light power of a FTIR spectrometer

To calculate the effective light power of a spectrometer, it has to be considered that not only the emission of the light source is crucial, but also many other parameters have an influence. The power P_{FTIR} received at the detector of a spectrometer is determined by the spectral intensity ($U_{\bar{\nu}}(T)$) of the light source (expressed as the amount of energy per unit time per unit surface area per unit solid angle per unit frequency), the throughput (Θ) and efficiency (ξ) of the spectrometer as well as by the desired spectral width ($\Delta\bar{\nu}$), as given in Equation 2.3. [7]

$$P_{\text{FTIR}} = U_{\bar{\nu}}(T) \cdot \Theta \cdot \xi \cdot \Delta\bar{\nu} \quad [\text{W}] \quad \text{Equation 2.3}$$

All these values depend on further parameters that will be explained consequently in the following section.

2.4.2.1. Spectral intensity

The spectral intensity of a blackbody source is given through the Plank's law. Higher temperatures lead to higher emission power but also to a shift of the emission maximum to shorter wavelengths.

$$U_{\bar{\nu}}(T) = \frac{C_1 \bar{\nu}^3}{e^{C_2 \bar{\nu}/T} - 1} \quad [W / (sr \cdot cm^2 \cdot cm^{-1})] \quad \text{Equation 2.4}$$

C_1 and C_2 are the first and second radiation constants, having the values

$$C_1 = 1.191 \cdot 10^{-12} [W/cm^2 sr (cm^{-1})^4]$$

and

$$C_2 = 1.439 [K cm].$$

2.4.2.2. Throughput of a spectrometer

The throughput of a spectrometer can be either limited by the maximum allowed solid angle of the beam (Ω_I) or by the physical constraints of the optics such as size of the detector. Ω_I itself is determined by the desired resolution of the spectrum ($\Delta \bar{\nu}$) and the maximum wavenumber ($\bar{\nu}_{max}$) in the spectrum according to Equation 2.5.

$$\Omega_I = \frac{2\pi \Delta \bar{\nu}}{\bar{\nu}_{max}} \quad [sr] \quad \text{Equation 2.5}$$

The throughput (Θ_I) is then determined by the product of Ω_I and the area of the mirrors in the interferometer being illuminated (A_M).

$$\Theta_I = \frac{2\pi A_M \Delta \bar{\nu}}{\bar{\nu}_{max}} \quad [cm^2 \cdot sr] \quad \text{Equation 2.6}$$

If the optic is determining the throughput of the spectrometer mostly the size of the detector is giving the limitation. The throughput (Θ_D) is then the product of the detector area (A_D) and the solid angle of the beam being focused on the detector (Ω_D).

$$\Theta_D = A_D \Omega_D \quad [cm^2 sr] \quad \text{Equation 2.7}$$

Ω_D can be calculated from the maximum half-angle of convergence achievable from the detectors foreoptics (α_M) according to Equation 2.8.

$$\Omega_D = 2\pi(1 - \cos \alpha_M) \quad [\text{sr}] \quad \text{Equation 2.8}$$

2.4.2.3. Efficiency of a spectrometer

There are several factors contributing to the efficiency of a spectrometer such as beam splitter efficiency, losses at the mirrors, radiation obscured by the mounting hardware for the reference laser, the emissivity of the global source and losses due to imperfect optical alignment. The very complex correlation between all this factors makes it hard to find a suitable mathematical expression. For this reason an experimental verified value for ξ was used as a base for further calculations. Mattson [23] found the efficiency of a Nicolet 7199 spectrometer to be 0.096. As an assumption that this value is a good approximation for other spectrometer, a value of 0.1 was used for the calculation.

2.4.2.4. Calculation of the light power

Typically globars used in FTIR spectroscopy have a working temperature of 1300° C. The spectral intensity was calculated for different wavenumbers, according to the maximum emission of the QCLs used in this thesis.

Wavenumber [cm^{-1}]	Spectral energy density [$\text{W/sr cm}^2 \text{cm}^{-1}$]
1080 (QCL1)	0.00089
1393 (QCL2)	0.00125

Table 4: Spectral energy densities of a global at different wavenumbers.

The highest possible throughput of a spectrometer is Θ_D . If using a detector with an element size of 2 mm^2 and an α_M of 45° (usual the maximum) the following values can be calculated:

$$AD = 0,04 \text{ [cm}^2\text{]}$$

$$\Omega_D = 1.84 \text{ [sr]}$$

$$\Theta_D = 0,0736 \text{ [cm}^2 \text{ sr]}$$

For the spectral width in Equation 2.3 the spectral width of the QCLs was used. The calculated P_{FTIR} for different spectral regions are given in Table 5.

Central Wavenumber [cm^{-1}]	Spectral width [cm^{-1}]	P_{FTIR} [mW]
1080 (QCL1)	81	0.505
1393 (QCL2)	83	0.726

Table 5: Results of the calculations for the power received at the detector of a FTIR spectrometer P_{FTIR} for different spectral regions.

The comparison of P_{QCL} and P_{FTIR} shows that the effective light power P_{QCL} is up to three orders of magnitude higher than P_{FTIR} for the same spectral region. This underlines clearly the advantages and the high potential of QCL based absorption spectroscopy for aqueous systems. Based on the absorption of water measured with an FTIR spectrometer and an optical path of 25 μm it can be calculated that for the QCLs under study an optical path of 154 μm (QCL1) and 124 μm (QCL2) respectively would result in the same light intensity received at the detector compared with the 25 μm used in the FTIR measurement. This means an increase of the optical path and hence also an increase of the sensitivity of around 5 to 6 times.

3. Concepts for quantitative QCL based analysis in aqueous phase

To optimize and control industrial production processes, there is an increased need for real-time and reliable information about concentration of chemical species in the process. In an ideal case continuous measurements are done in-line with sensors possessing the required selectivity and long time stability. Due to their characteristics, QCLs hold promise to be used in robust and compact sensing devices that are addressing these needs. Nevertheless depending on the sample matrix, the type of measurement as well as on the information needed different kind of process measurements may be performed [24], as displayed in Figure 9. Starting with off-line measurements where the sample is collected at the plant and analysed in a laboratory, measurements can be performed at-line with instruments located in the plant, on-line by instruments interfaced to the chemical process or in-line applying sensors directly inserted into the process stream.

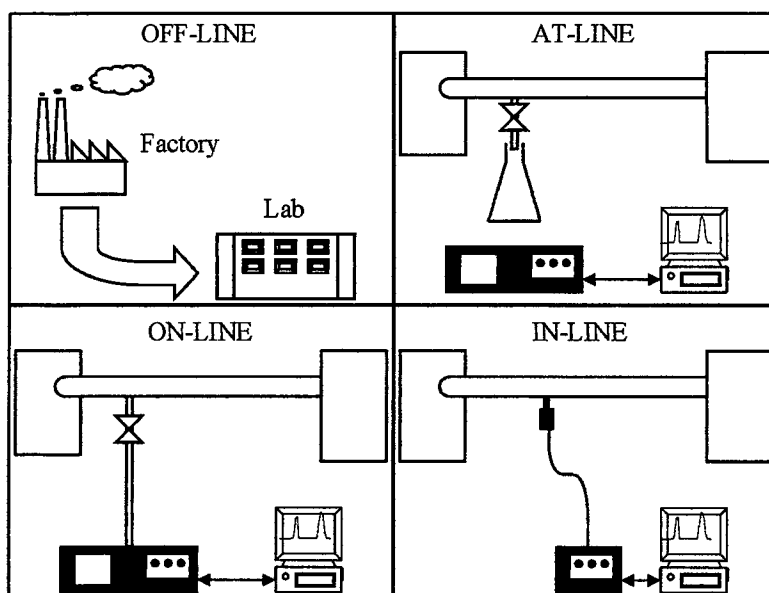


Figure 9: Types of process measurements.

If the sample matrix requires a sophisticated measurement technique with a challenging sample treatment including the modulation of the sample, measurements are performed mostly off-line or at-line. For measurements in aqueous phase there is a large family of methods based on sample injection into a flowing stream, which carries the analyte through a chemical modulator into a detector [25]. This includes

chromatography, electrophoresis, filed flow fraction as well as flow injection analysis (FIA). The basic differences between the methods can be seen in the kind of chemical modulator. The originally square wave input, provided by sample injection is modified to a chromatogram, electropherogram, fractogram or fiagram.

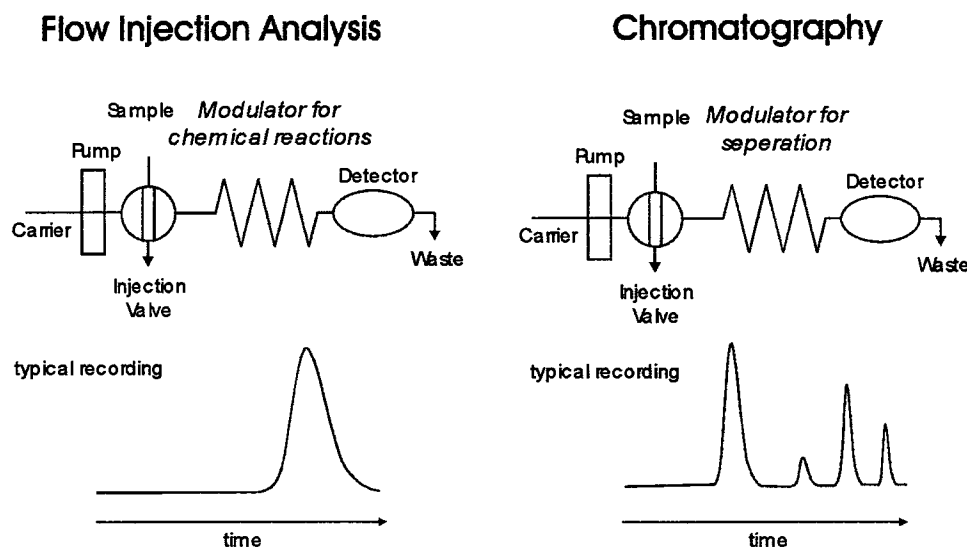


Figure 10: Comparison of flow injection analysis and chromatography.

Most modulators aim on the separation of the sample. Multiple peak recording is typical for these techniques. The realisation of a QCL based quantitative measurement in combination with a separation technique prior to detection was demonstrated within this theses for capillary electrophoresis in **paper I**.

In case of FIA the chemical modulator consists of a reaction coil where the injected analyte disperses and reacts with the components of the carrier stream. No separation is obtained and only a single peak is delivered per injection. The high grade of automation accessible with FIA systems turns them into a powerful tool for on-line measurements. Additionally FIA recordings include measurements of the baseline before and after the sample plug passes the detector. This information can be used for compensating slow baseline drifts. The application of a QCL based detection system for flow injection analysis is presented in **paper II**.

If the sample does not require a chemical modulation prior to detection the realisation of an on-line measurement is much easier. The process can be sampled automatically. Analytes are measured without any further separation or reaction performed. **Paper III** reports the application of a dual-QCL system for such an on-line measurement. The system has already the potential to perform measurements in-line. But mostly the

composition of the process matrix and its changes inhibit the application of in-line sensors due to the limited selectivity for the analyte of interest in the presence of the matrix. In-line sensor working independently from the process matrix are therefore of high interest. A possible concept for such a sensor is presented in **paper IV**, where the modulation of a QCL is used to compensate for matrix changes.

The different concepts of the flow systems used in this thesis are presented in the following chapters.

3.1. Capillary electrophoresis

3.1.1. Theoretical background

Electrophoresis means the movement of a charged species under the influence of an electric field. Electrophoresis based separation techniques rely on the different migration of analytes according to their size and charge. The limits for the separation efficiency of the method are given from thermal diffusion and convection. For this reason electrophoresis was traditionally performed in anti-convective media, such as polyacrylamide or agarose gels. Normally such systems suffer from long analysis time, low efficiency and difficulty in automation.

Capillary electrophoresis (CE) is performed in capillaries with an inner diameter of typically 25-75 μm . The high ratio of surface area to volume ensures an effective dissipation of the generated heat, even if capillaries show a high resistance and hence enable application of very high electrical fields [26]. As a consequence electrical fields of up to 500 V/cm can be applied that lead to short analysis times and high separation efficiency. Additionally CE demands small sample volumes typically in the low nL range. To show the simplicity of a CE system, a typical set-up is given in Figure 11. Two buffer reservoirs are filled with background electrolyte (BGE). A fused silica capillary containing the same BGE is connecting the two reservoirs. The high voltage system composed by a power supply and two electrodes contacting each one of the reservoirs is used to apply up to 30 kV. Within the capillary an optical detection window is integrated.

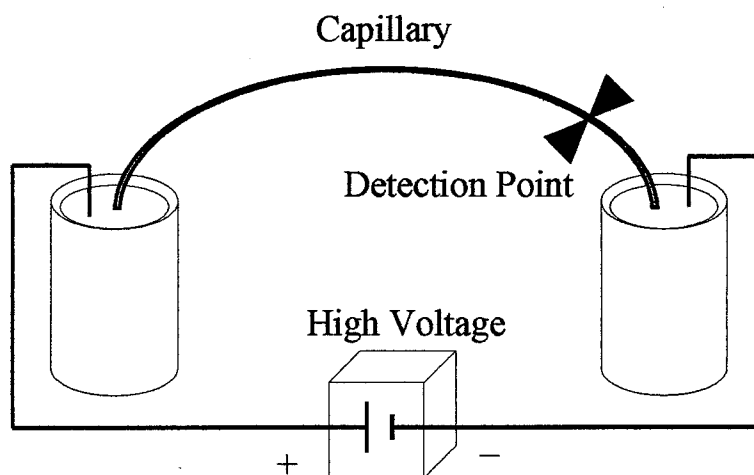


Figure 11: Schematically drawing of a CE System.

CE offers a wide spectrum of operation modes, including capillary zone electrophoresis (CZE), micellar electrokinetic chromatography (MEKC), capillary gel electrophoresis, capillary isoelectric focusing (CIEF) and capillary isotachopheresis (CITP). In the context of this work only the basic form of CE namely CZE has been used and is therefore described in this section. But it has to be mentioned that the basics presented here are valid for all CE operation modes.

3.1.2. Principle of capillary zone electrophoresis

The separation of analytes is based on the difference in their ion velocity (v_I) that is given by the electrophoretic mobility (μ_e) and the applied electric field (E) as described in Equation 3.1.

$$v_I = \mu_e E \quad \text{Equation 3.1}$$

Two forces, the electric force (F_E) and the frictional force (F_F) define the electrophoretic mobility. A charged particle in an electrical field is affected by F_E , given in Equation 3.2.

$$F_E = qE \quad \text{Equation 3.2}$$

Where q is the effective ion charge. F_E causes the ions to move to the counter electrode. Additionally moving particles in a medium are affected by F_F that shows an inverse direction. For a spherical ion F_F is defined as given in Equation 3.3.

$$F_F = -6\pi\eta r v_I \quad \text{Equation 3.3}$$

Where η is the solution viscosity and r the ion radius. In steady state condition both forces are equal but opposite.

$$qE = 6\pi\eta r v_I \quad \text{Equation 3.4}$$

Using Equation 3.1 and Equation 3.4 μ_e can be expressed as follows

$$\mu_e = \frac{q}{6\pi\eta r} \quad \text{Equation 3.5}$$

It can be clearly seen that μ_e increases for higher charged and/or smaller particles.

The silanol groups on the surface of fused silica capillaries have a pH value ranging from 2 to 5. BGEs showing a higher pH deprotonate the silanol groups. Positive counter ions form a double layer next to the capillary wall to uphold charge balance (see Figure 12), which creates a potential difference, the so-called zeta potential (ζ). If voltage is applied across the capillary counter ions are moving towards the cathode (negative). The solvated counter ions in combination with the viscosity of the BGE drags the whole bulk towards the cathode, as long as the inner diameter of the capillary does not exceed a critical value (200 to 300 μm). This phenomenon is referred to as electroosmotic flow (EOF). The total velocity (v_T) of particles in CE is composed as v_I and the velocity of the EOF (v_{EOF}) that are both proportional to the electric field.

$$v_T = v_I + v_{EOF} = (\mu_e + \mu_{EOF})E \quad \text{Equation 3.6}$$

Where μ_{EOF} is the mobility of the EOF. It is defined via the zeta potential as well as the viscosity and dielectric constant of the BGE.

$$\mu_{EOF} = \frac{\varepsilon\zeta}{\eta}$$

Equation 3.7

The configuration of the analytes according to their mobility is shown in Figure 12.

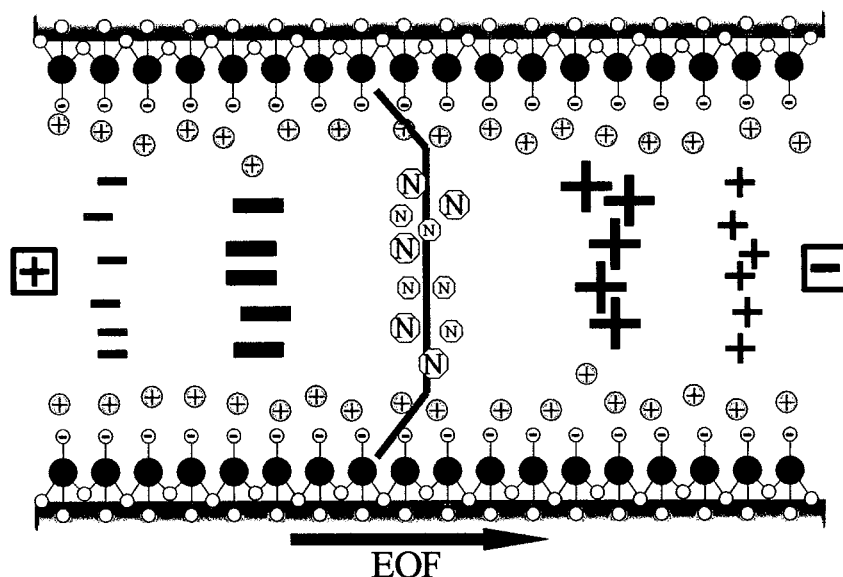


Figure 12: Differential solute migration superimposed on EOF in CE. The blue line indicates the flow profile.

The driving force of the EOF shows some advantages compared to pressure gradients. A unique feature is the nearly flat flow profile across the capillary diameter (see Figure 12) in contrast to the laminar flow in e.g. LC in consequence of the uniformly distributed driving force along the capillary. Hence the dispersion of the analytes is minor compared to a laminar flow.

As the EOF drags all analytes regardless of their charge, it is possible in CE to analyse cation and anions in a single run. The ions will be separated according to their μ_e . All neutrals are carried at the velocity of the EOF.

3.1.3. Injection of the sample

For sample injection in CE, one end of the capillary is temporary placed in a sample vial. The vial contains the analytes preferable dissolved in BGE. Either hydrodynamic or electrokinetic injection can be performed.

3.1.3.1. Hydrodynamic injection

For hydrodynamic injection a pressure difference between the two ends of the capillary is essential. This pressure difference can be obtained by application of pressure at the injection end or vacuum at the exit end of the capillary as well as having an elevation difference between the injection and exit reservoir. Latter is referred to as siphoning. The sample volume (V) for a given injection time (t) can be calculated using the Hagen-Poiseuille equation.

$$V = \frac{\Delta P d^4 t \pi}{128 L \eta} \quad \text{Equation 3.8}$$

Where ΔP is the pressure difference across the capillary, d the inner diameter of the capillary, η the viscosity of the BGE and L the total length of the capillary.

In case of siphoning ΔP can be calculated according to Equation 3.9.

$$\Delta P = \rho g \Delta h \quad \text{Equation 3.9}$$

Where ρ is the density of the BGE, g the gravitation constant and Δh the elevation difference of the two reservoirs.

3.1.3.2. Electrokinetic injection

For electrokinetic injection a voltage usually three to five times lower than the separation voltage is applied. In contrast to hydrodynamic injection, the amount of analyte injected for constant parameters is varying between the analytes since they show differences in μ_e . Additionally matrix effects appear, as changes of the resistance due to higher ion concentrations results in local differences in the electric field. In general electrokinetic injection is not as reproducible as hydrodynamic injection

3.1.4. Detection

UV absorption is the most common detection technique for CE because of its simplicity and flexibility. But also other detection methods such as mass

spectroscopy, Raman scattering, laser induced fluorescence and FTIR spectroscopy have been successfully demonstrated in combination with CE [27-29]. However these techniques are beyond the scope of this thesis. In the following section the on-line hyphenation of CE and IR detection will be described in detail as it is an essential part of this work.

3.1.4.1. Interface for online QCL detection in capillary electrophoresis

The challenging task in online hyphenation of QCL absorption measurements with CE is the interface since it has to fulfil several demands. The capillaries itself show high absorption of IR radiation in contrast to UV radiation. Measurements cannot be performed directly through the capillary. The interface must overcome this issue and hence be made of IR transparent materials [30]. The connection between the interface and the capillaries has to be tight and further isolated. Furthermore the electric field along the capillary shall not be affected by the interface. The interface should not change the performance of the CE separation in any way means e.g. no contribution to peak broadening. These considerations require a small inner volume of the interface. Because these demands are not fulfilled with commercial available flow cells as used for HPLC or FIA systems a new interface had to be developed. This interface was based on a recent development for FTIR detection in CE [18].

The interface consisted of an IR transparent flow cell and a cell holder designed to facilitate connection of the capillaries to the cell. A scheme of the cell is given in Figure 13. The cell is based on two CaF_2 plates. In a first step epoxy based photoresist SU 8 is applied on each disc, forming the flow channel of $150\mu\text{m}$ width and $60\mu\text{m}$ thickness. During a hard-bake process (200°C , 1h) the two discs are pressed together and bounded by SU 8 since the high temperature induces complete cross-linking. The areas outside the SU 8 streaks are filled with UV-curing epoxy adhesive. Finally on the top of the cell two pieces of aluminum foil were glued in order to form an optical aperture.

3 Concepts for quantitative QCL based analysis in aqueous phase

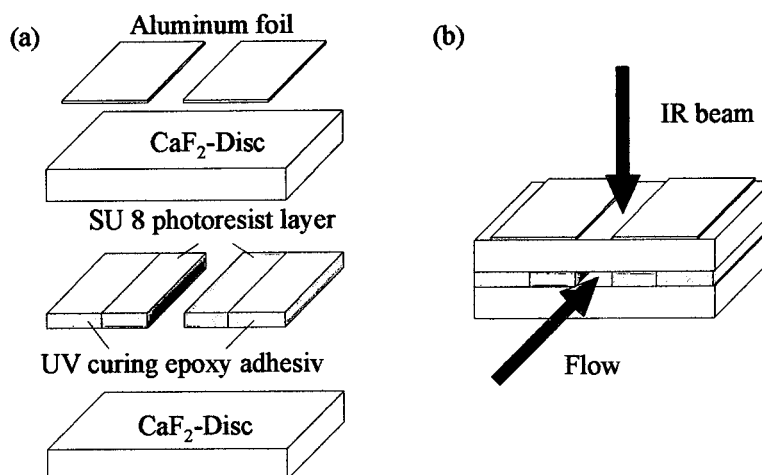


Figure 13: Schematic of the CE-IR cell: (a) components of the cell, (b) entire cell with indicated light path and flow channel.

To be able to connect the cell with the capillary and to ensure tightness a cell holder equipped with a movable sledge was constructed (see Figure 14a). That way the ends of the capillaries could be pressed to the flow channel. Commercially available o-rings were used to ensure a sealed connection (see Figure 14b).

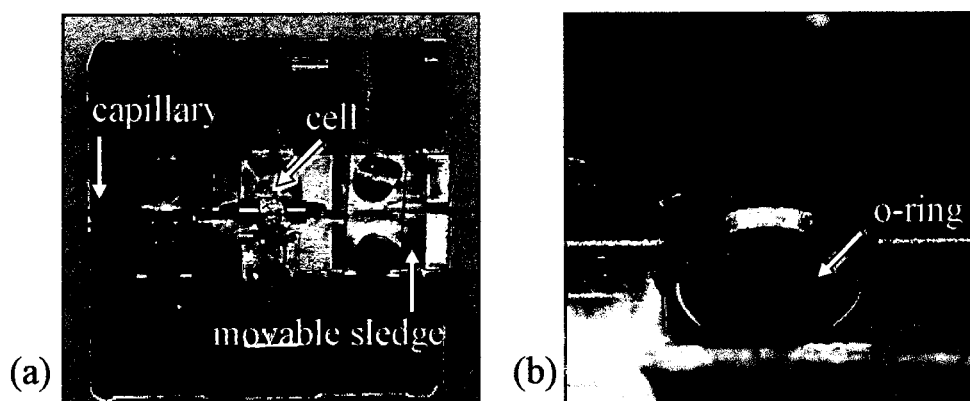


Figure 14: (a) Total view of the interface, (b) close-up of the cell holder showing the o-ring for tight connection between cell and capillary.

3.2. Flow injection analysis

The simplest FIA analyser [31] consists of a pump that generates the carrier stream, an injection valve for injecting a well-defined amount of sample into the carrier, a reaction coil in which the sample plug disperses and may react with the carrier, and a flow trough detector (see Figure 15). Such a simple flow injection manifold was used in **paper II**, where the sample did not undergo a chemical reaction. The system was used for reproducible injection of the sample

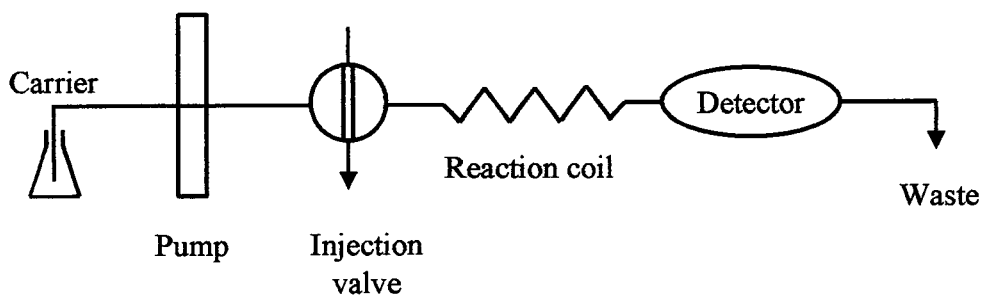


Figure 15: Single-line FIA manifold.

The shape of the recorded FIA peak is basically the result of two effects: on the one hand diffusion of the sample and on the other hand convection. The stronger effect is caused by the laminar flow and the therefore parabolic velocity profile found in FIA tubings. Assuming diffusion dominated distribution, a more or less Gaussian shape of the sample plug would be expected. The resulting changes of an initially square concentration profile at the injection zone to a concentration gradient at the detection zone of a typical FIA system is shown in Figure 16b, where Figure 16a shows the spatial distribution of the sample. The maximum concentration as well as the peak area of the read out are both related to the initial sample concentration.

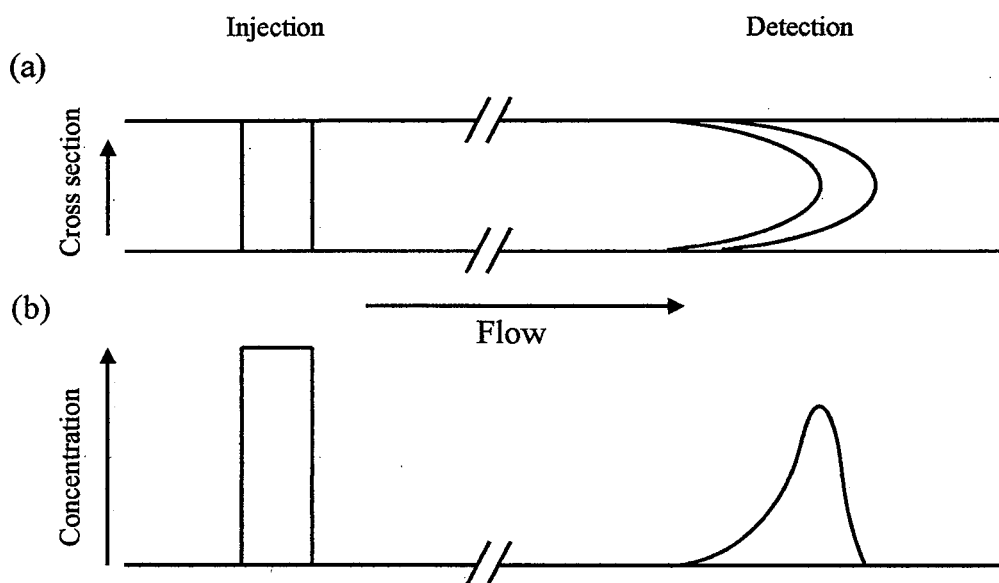


Figure 16: Conditions of sample distribution in a FIA system at the injection point (left) and detection point (right). (a) Spatial distribution of the sample inside the tubing. (b) Distribution of concentration along the tubing

One of the key features of a FIA system is its high degree of automation. The injection of the sample as well as its modulation is done in an automated way. The dispersion of the sample, chemical reaction or mixing with other flow streams is therefore highly reproducible. Features that are considered to be important for

conventional analytical techniques such as homogeneous mixing and complete reaction have lost their importance. Homogeneous mixing is never achieved in FIA and hardly any reaction is completed at the time the analyte passes the detector. But as all samples are treated in the same way and FIA systems show a high reproducibility of the dispersion profile and timing, same analyte concentration in different sample will generate the same signal.

3.3. Continuous on-line measurements

On-line measurements can be performed continuously or intermittently [24]. The frequency of measurement depends on the kinetic of the process expressed as the time constant. The time constant of a process (τ) can be described by two variables, the mean resident time in the reactor (τ_R) and the chemical reaction rate (k) using Equation 3.10.

$$\tau = \frac{\tau_R}{(1 + k \cdot \tau_R)} \quad \text{Equation 3.10}$$

To get the effective overall time constant (τ_{eff}) the equation has to be extended by the time response of the analytical measurement (T).

$$\tau_{eff} = \frac{\tau_R}{(1 + k \cdot \tau_R)} + T \quad \text{Equation 3.11}$$

The measurement interval should be significantly shorter compared to τ_{eff} . Using a running average of at least two measurements per time constant contributes to noise reduction. Typically four measurements per time constant are used.

3.4. Wavelength modulation of the QCL for background compensation.

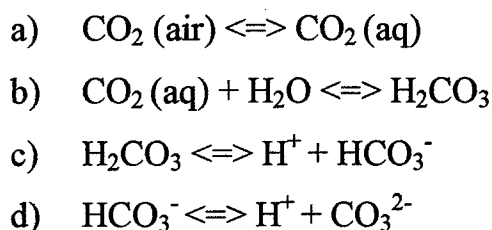
The aim of paper IV was to develop an analytical method for measuring CO₂ in beverages. As the pH has an influence on the CO₂ concentration, the pH-dependence of the inorganic carbon system in aqueous solution had to be investigated first. The next step was the examination of the influence of other constituents of beverages on the signal and the development of possible strategies to compensate this influence.

3.4.1. Investigation of the pH-dependent concentration of CO₂ (aq)

3.4.1.1. Motivation

The determination of carbon dioxide in aqueous samples is an industrially important task, especially for the beverage industry as carbon dioxide has a big influence on the taste of beverages. Current process analyzer for CO₂ expands the volume of a sample drawn from the process stream while stirring. The temperature and pressure of the generated gas phase are measured. These values are then related to the CO₂ concentration in the liquid via Henry's law.

CO₂ is not only dissolved in water, but undergoes a reaction with water to carbonic acid, which dissociates to hydrogen carbonate and carbonate. The reactions are given in Equation 3.12. All these species can be summarised as inorganic carbon.



Equation 3.12

But in beverages only a small part of the inorganic carbon is present as carbonic acid or one of its dissociation states [32]. For example in soft drinks like Cola with a pH value around 2,5 nearly 100% of the inorganic carbon is physically dissolved and forms a CO₂/H₂O cluster which structure is not completely elucidated [33]. In Beer that shows a pH value between 4 and 5 the percentage of physically dissolved inorganic carbon - CO₂ (aq) - is still more than 95%. For the beverage industry only the concentration of CO₂ (aq) is from interest. Because of the pH dependence of the dissociation the concentration of CO₂ (aq) shows also pH dependence. The aim of this experiment was to investigate the pH dependence of the signal obtained from IR absorption measurements of CO₂ (aq). This was done to get important information needed for the development of a new type of QCL based CO₂ analyzer.

3.4.1.2. *Experimental*

Chemicals

All chemicals were of analytical grade. Sodium hydrogen carbonate, acetic acid, sodium acetate trihydrate and potassium chloride were purchased from Merck. Trisodium citrate dihydrate, sodium hydroxid, sodium dihydrogen phosphate dihydrate and phosphoric acid were purchased from Fluka. Boric acid and citric acid were purchased from Sigma/Aldrich. Disodium hydrogen phosphate dihydrat was purchased from Riedel de Haen.

Different buffers of 100 mmol/L were prepared according to the instructions in Ref.[34]. The chosen buffer systems, the corresponding pKa values and the adjusted pH values are given in Table 6.

System	pKa	pH
Phosphoric acid (1 st dissociation)	(pKa1) 2,15	2.06
Citric acid (1 st dissociation)	(pKa1) 3.13	3.00
Acetic acid	4,76	4.01
Citric acid (2 nd dissociation)	(pKa2) 4.76	5.19
Citric acid (3 rd dissociation)	(pKa3) 6,40	6.21
Phosphoric acid (2 nd dissociation)	(pKa2) 7.20	7.20
Boric acid	9.23	9.30
Boric acid	9.23	10.08
Phosphoric acid (3 rd dissociation)	12.33	12.21
Sodium hydroxide	13.8	12.86

Table 6: Buffer systems, corresponding pKa values and adjusted pH values used in the experiment.

Instrumentation

All spectra were recorded on a portable Bruker Matrix-M spectrometer (Bruker Optik GmbH, Germany) equipped with a mercury cadmium telluride (MCT) detector. Each spectrum was a result of 128 co-added scans, recorded with 2 cm⁻¹ resolution, Blackman-Harris 3-term apodization and at 40 kHz scanning rate. The spectrometer was equipped with a home made flow cell, incorporating a horizontal ATR unit

(Durasample, SensIR II) [35]. In order to avoid background absorption of the gaseous CO_2 the spectrometer and the ATR compartment were purged with technical nitrogen. To adjust NaHCO_3 standards to different pH values a flow system was used. The flow system consisted of a peristaltic pump and two selection valves. All tubings were made of polytetrafluoroethane (PTFE) and had an inner diameter of 0.75 mm. The configuration of the flow system is shown in Figure 17.

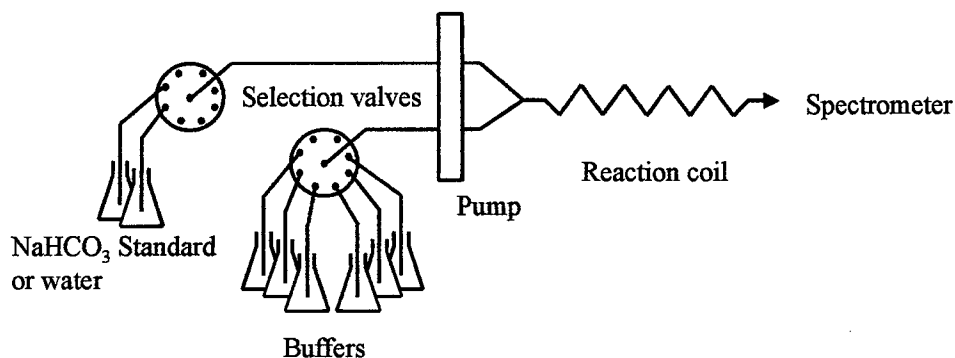


Figure 17: Schematically set-up of the flow system for preparing NaHCO_3 standards adjusted to different pH values.

The spectra were recorded during flow on. Water mixed with the particular buffer served as background. As the NaHCO_3 standard showed already a pH value of about 8.5 it was mixed with water instead of a buffer to obtain a spectrum in this pH region. After passing the flow cell fractions of the reaction mixtures were collected for determining the actual pH value.

3.4.1.3. Results and discussion

The obtained spectra were evaluated using the software OPUS 4.2. The area of the CO_2 absorption peak was integrated ($2337 - 2350 \text{ cm}^{-1}$) and normalized to the highest value and expressed in percentages. The theoretical $\text{pK}_{\text{a}1}$ value for carbonic acid is 6.35. According to this value the percentage of $\text{CO}_2 (\text{aq})$ in an inorganic carbon system for different pH values was calculated. Both – the calculated as well as the experimentally verified values – are plotted against the pH value in Figure 18.

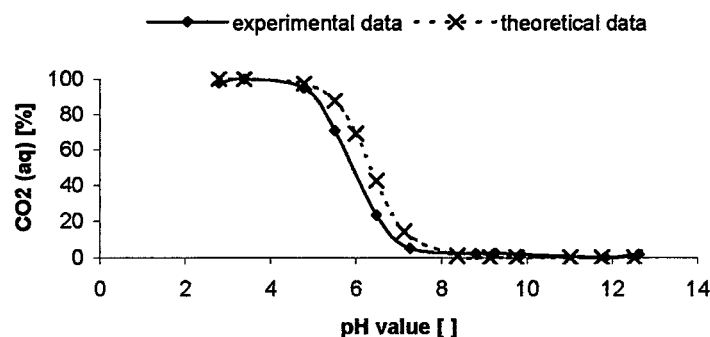


Figure 18: pH dependence of the CO₂ (aq) concentration in an inorganic carbon system, experimental vs. theoretical data.

As it can be seen there is a discrepancy between the experimental and the theoretical data. The reason for this can be found in the high ionic strength of the samples. This lowers the activity coefficients of the hydrogen carbonate and carbonate. As a consequence the equilibrium between the different species of inorganic carbon is effected and the concentration profiles are shifted to lower pH values.

For all further experiments different concentrations of CO₂ where produced by mixing NaHCO₃ standards with citric acid buffer of pH 3.13. This pH value guarantees high stability of the percentage of CO₂ (aq) close to 100% within the inorganic carbon system.

3.4.2. Investigation of water baseline changes due to relevant constituents of beverages

3.4.2.1. Motivation

In an ideal case the measurement of an analyte is selective and sensitive. This is generally the case in QCL based absorption measurements in the gas phase. In these applications the sharp laser lines match the rota-vibrational transitions present in gas phase. Therefor for each analyte isolated interference free absorption lines can be found. Analytes present in liquids generally show absorption bands significantly broader than QCL emission lines, especially when dealing with distributed feedback QCLs. Analytes dissolved in water often form broad absorption bands. Therefore in general it is not possible to find interference free, isolated absorption bands that can

be used for selective, quantitative analysis. Absorptions arising from other analytes or the matrix has to be determined and subtracted from the signal. This can be realised via application of more than one laser. The possibility of background compensation by measuring the absorption at two QCL wavelengths has been demonstrated by Martin et.al. [36] and for simultaneous measurements of interfering analytes in **paper II**.

Beside interferences of other analytes and matrix constituents, the background signal can also be influenced by changes in the water spectra itself. This can be easily understood as the main absorption of an aqueous sample arises from the strong water bands (see chapter 1.3). Every solute is surrounded by a hydration shell. Based on the interaction of the solute and the water molecules forming the hydration shell the absorption spectra of these water molecules is changed. Therefore different kinds of water with distinct IR spectra may be present in an aqueous system as demonstrated by Max et.al. [37]. In contrast to interfering species, changes in the water background may lead to negative absorption values. This is the case if the changes in the water background lead to a higher transparency at a given wavenumber.

The thematic of changes in the water background spectrum will be further discussed in the following section considering as an example the influence of glucose, fructose, sucrose and ethanol at $2000\text{-}2900\text{ cm}^{-1}$, a wavelength region where these substances do not absorb. The four chosen components are main ingredients of beverages and therefore of interest with respect to a QCL based analyser for CO_2 in beverages. The concept of QCL based CO_2 determination in water was already demonstrated [38], but measurements of real samples have not been reported until now.

3.4.2.2. Experimental

Chemicals

All chemicals were of analytical grade. Fructose, sucrose, sodium hydrogen carbonate and ethanol were purchased from Merck. Glucose and NaOH were purchased from Fluka and citric acid from Sigma/Aldrich.

Instrumentation

All spectra were taken with a Bruker IFS 88 spectrometer with a spectral resolution of 2 cm^{-1} . The spectrometer was equipped with a flow cell showing an optical path of 40

μm . In order to avoid background absorption of the gaseous CO_2 the dry air purge of the spectrometer was replaced by technical nitrogen gas.

To record spectra of standard solutions of glucose, fructose, sucrose and ethanol the samples were injected into the flow cell using a syringe. To record spectra of CO_2 standards containing different amounts of sugar a flow system was used. The flow system consisted of a peristaltic pump and two selection valves. All tubings were made of polytetrafluoroethane (PTFE) and had an inner diameter of 0.75 mm. The configuration of the flow system is shown in Figure 19. The system allowed the preparation of sodium hydrogen carbonate standards (1,932 g/l) containing sugars (glucose, fructose and sucrose at a ratio of 1:1:1) at different concentrations. By merging the NaHCO_3 stream with citric acid buffer (100 mMol, pH 3,13) the hydrogen carbonate was converted to carbonic acid that dissociated into CO_2 and water. As a consequence a defined amount of CO_2 (aq) was generated in-situ.

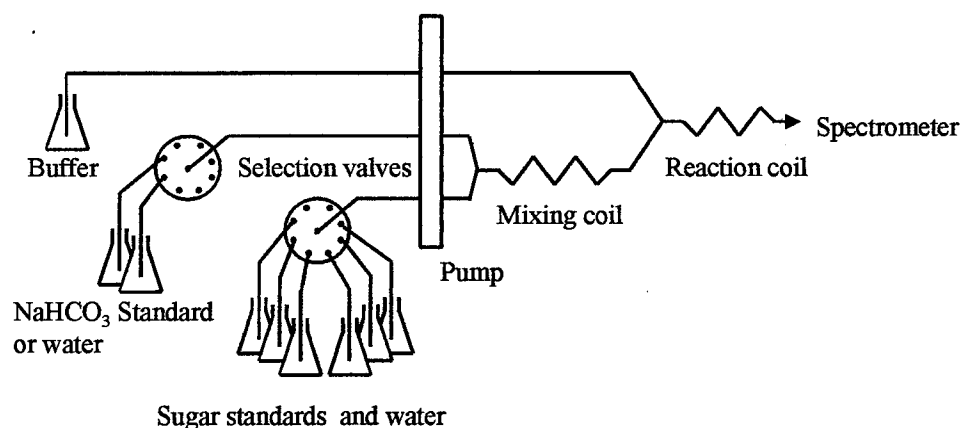


Figure 19: Schematical set-up of the flow system for preparing CO_2 standards with different amounts of sugars.

3.4.2.3. Results and discussion

In a first step the differences of background changes due to glucose, fructose, sucrose and ethanol have been investigated in order to get a clear picture of their individual effect on the water background. Figure 20 shows spectra of water containing different concentrations of glucose (a), fructose (b), sucrose (c) and ethanol (d) measured with a FTIR spectrometer with blank water serving as background. Figure 21 shows the corresponding single beam spectra.

3 Concepts for quantitative QCL based analysis in aqueous phase

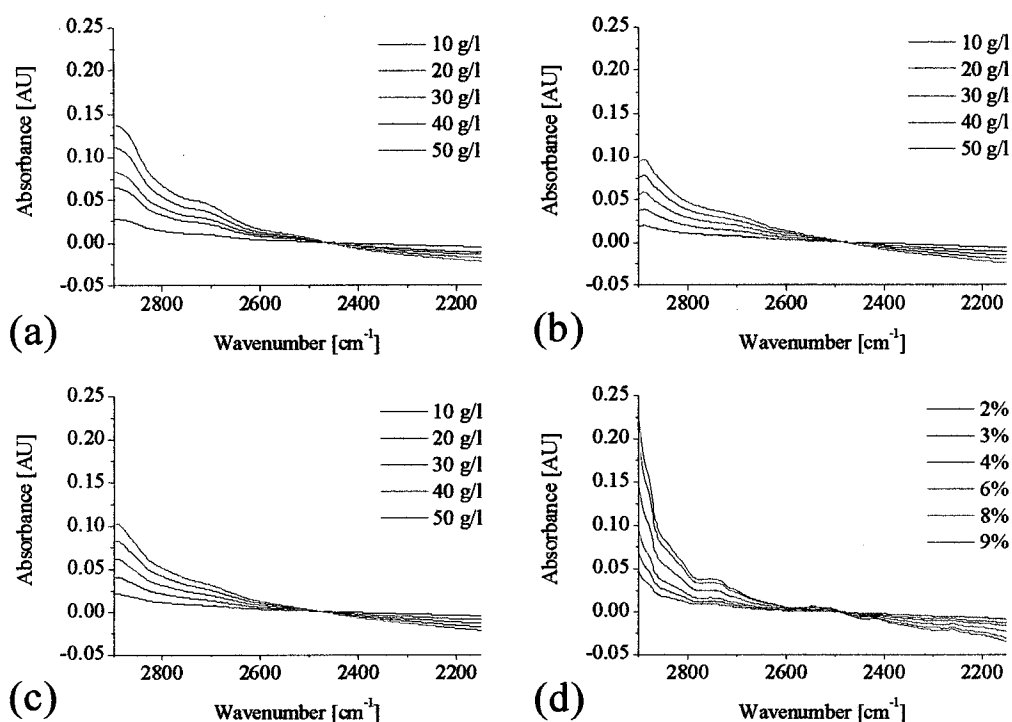


Figure 20: Absorption spectra of water containing different amounts of (a) glucose, (b) fructose, (c) sucrose and (d) ethanol.

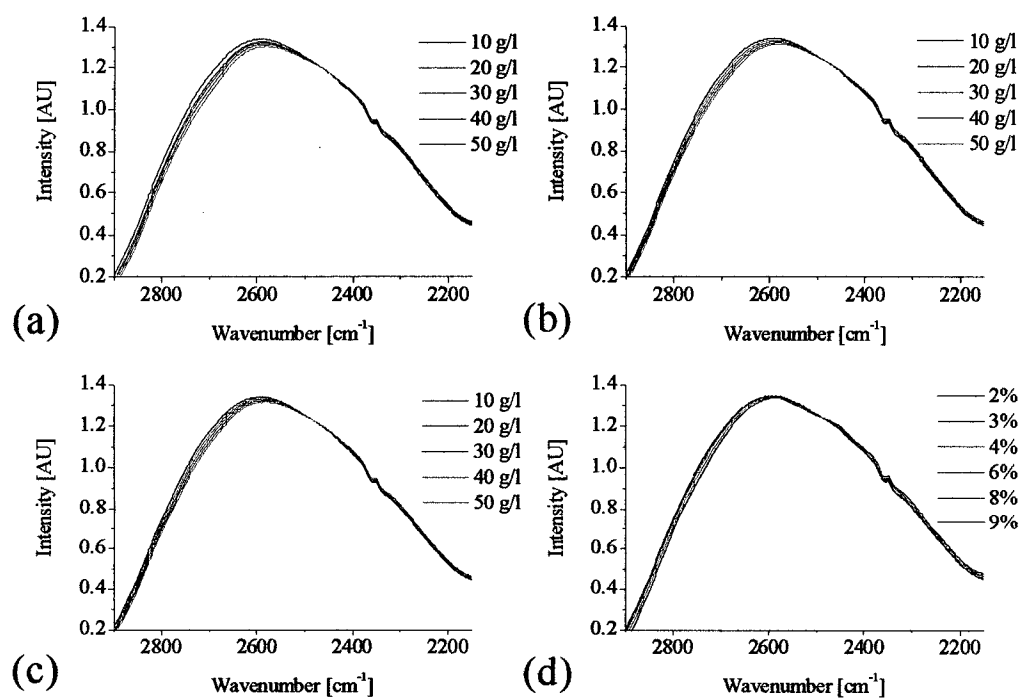


Figure 21: Single beam spectra of water containing different amounts of (a) glucose, (b) fructose, (c) sucrose and (d) ethanol.

Increased concentration of all interferents causes a sloping baseline. However there are differences in the influence on the water background. For this purpose one spectra of each analyte was normalized to the region of interest (2343 cm^{-1}). The normalized spectra in comparison with a spectrum of a CO_2 standard are given in Figure 22. For the whole region around the CO_2 absorption band the water background shows similar dependence on all of the solutes. Therefore the wavenumber for background compensation should be located between 2412 and 2385 cm^{-1} .

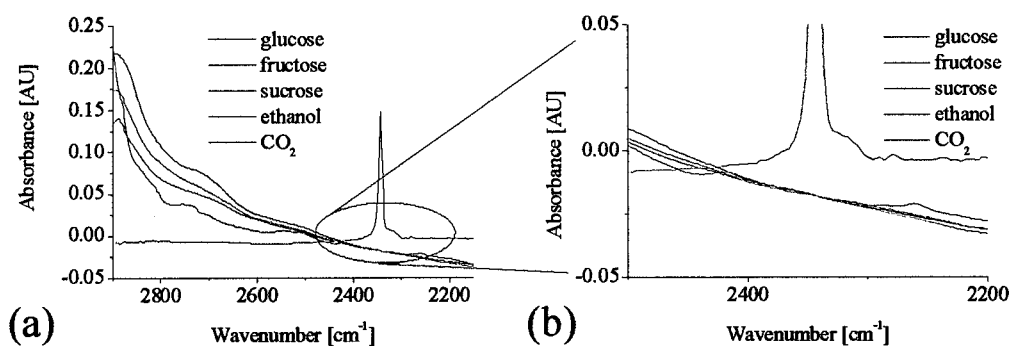


Figure 22: (a) Differences in the influence on the water background, (b) close up of the region of interest

Appropriate background spectra

CO_2 dissolved in water shows an absorption band with a maximum at 2343 cm^{-1} . The influence of a mixture of glucose, fructose and sucrose (1:1:1) on the absorption spectra in this region is shown in Figure 23a. The sample contained always the same amount of CO_2 but different amount of the sugar mixture. Buffer mixed with distilled water served as background. In contrast Figure 23b shows spectra of samples when the background spectra were taken from buffer mixed with distilled water containing a corresponding amount of the sugar mixture. It can be clearly seen that if information of the sugar content is present in both – the background as well as the sample spectra – the measured absorbance is only determined by the concentration of CO_2 . Normally this way of matrix compensation is not practicable as the analyte free background spectra are not available. For a practically relevant background compensation an approach based on the matrix-influenced spectra is required.

3 Concepts for quantitative QCL based analysis in aqueous phase

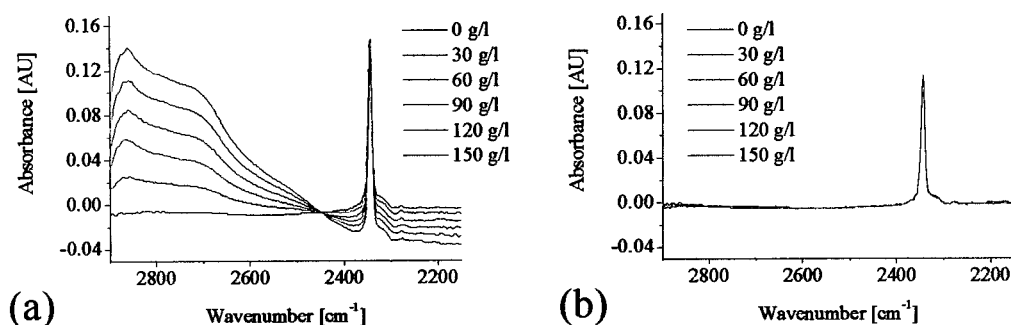


Figure 23: Spectra of a CO₂ standard (1,932 g/l) with different amounts of sugar: (a) measured against buffer mixed with blank water, (b) measured against buffer mixed with water containing a corresponding amount of sugar.

Baseline correction

In the case the whole FTIR spectrum is available a simple baseline correction may be performed. In that case a baseline is calculated at two wavenumbers at the edge of the CO₂ absorption band. The calculated peak areas with and without baseline correction for the data above are given in Figure 24. To be able to use this kind of evaluation for QCL absorption based measurements it would be necessary that the laser can be tuned across the whole absorption band of CO₂. As the absorption band is much broader than the tuning range of state of the art QCLs, this technique is currently not practicable.

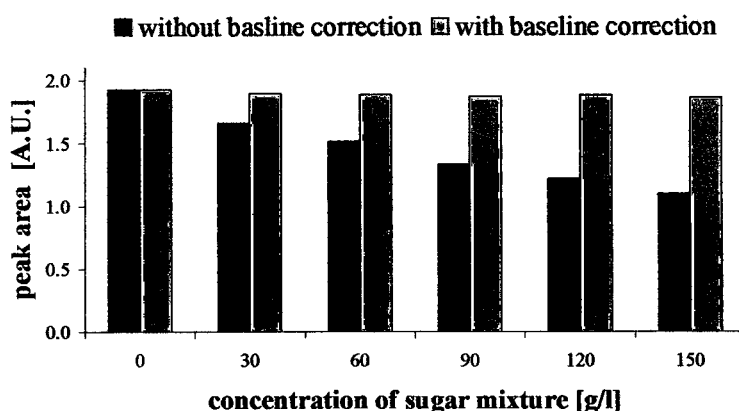


Figure 24: Calculated peak area of CO₂ standards with different amount of sugar for two evaluation methods.

Background compensation

Paper II introduced a second QCL as a reference measurement of the interfering analyte. This method can be also used for background compensation as shown in Ref.

[36], when the influence on the background is known. The adaptability of this principle for the determination of CO_2 will be discussed in the subsequent section.

The selection of the second wavelength underlies some requirements on sensitivity and precision. The highest sensitivity is achieved when the changes in the measured signal are maximized for changes in concentration. Additionally attention has to be paid that the precision of the measurement is high. For this reason it is recommended to evaluate wavelength regions that show minor changes in absorption for variations of the evaluated wavelength. That way inaccuracies arising from wavelength instabilities of the QCL play a minor roll. According to these requests a baseline correction based on the wavelength region around 2780 cm^{-1} was accomplished. Spectra of sugar solutions without CO_2 were taken and evaluated at both wavelength regions. A model describing the correlation between the baseline changes of both regions was created and applied for a background compensation on the spectra shown in Figure 23a. The results of this method can be seen in Figure 25. It demonstrates that for the measurement of CO_2 the application of a second QCL would enable an effective method to compensate background changes arising from other solutes.

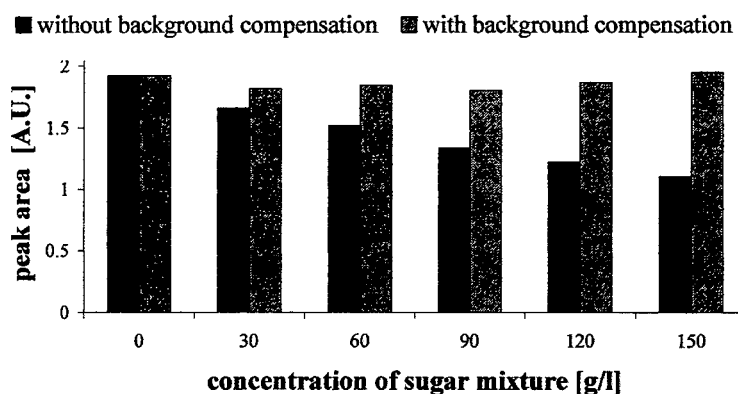


Figure 25: Calculated peak area of CO_2 standards with different amount of sugar. Evaluation of one wavelength region compared with an evaluation of an additional wavelength region for background compensation.

Additional to the already mentioned requirements on the reference wavenumber, the correction factor calculated from the reference measurement has to be independent from the interfering substance. That means that the ratio of the shifted absorption values of the baseline between the target wavenumber for the CO_2 measurement and

the wavenumber for the background compensation has to be the same for all substances. In other words: for a given background absorption at the target wavenumber all substances have to show the same background absorption at the wavenumber for the background compensation. Such a wavenumber had to be found. For this purpose one spectra of each analyte was normalized to the region of interest (2343 cm^{-1}). The normalized spectra in comparison with a spectrum of a CO_2 standard are given in Figure 26. For the region around the CO_2 absorption band the water background shows the same absorption values for all of the solutes. Therefore the wavenumber for background compensation should be located between 2412 and 2385 cm^{-1} .

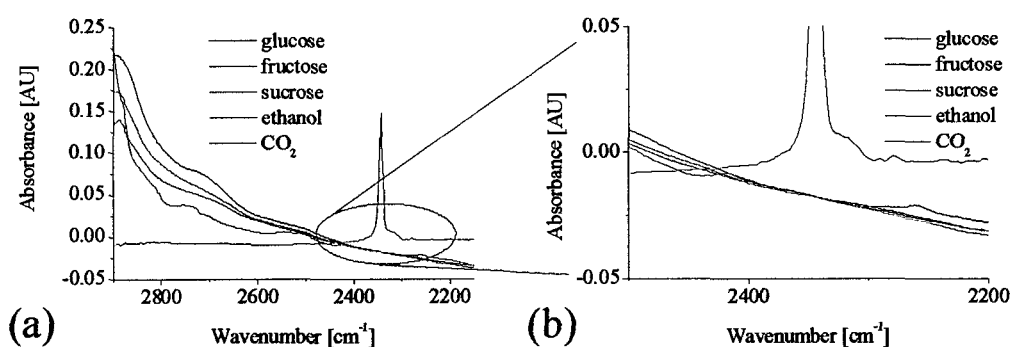


Figure 26: (a) Differences in the influence on the water background, (b) close up of the region of interest

First derivative spectra

A further possibility for compensation of baseline changes is the evaluation of the first derivative spectra instead of the original spectra. The first derivative represents the slope of a spectrum at each wavenumber and is independent from offsets arising from drifts or background changes. This technique was applied to the spectra presented already in Figure 23. The spectra together with the corresponding first derivatives are given in Figure 27.

3 Concepts for quantitative QCL based analysis in aqueous phase

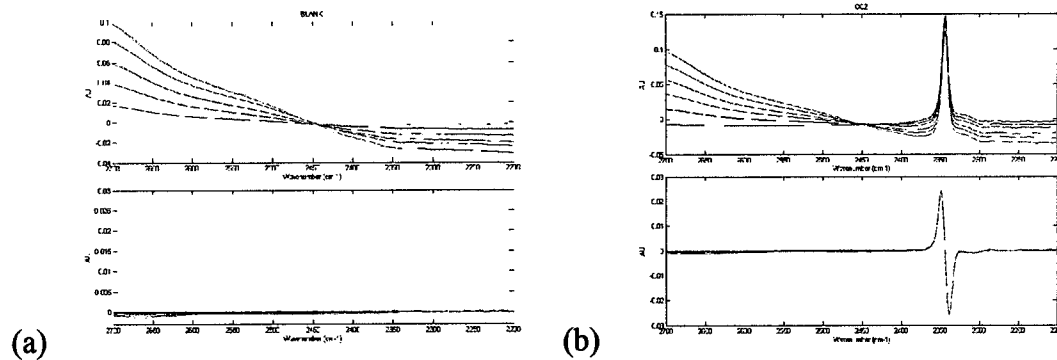


Figure 27: (a) Spectra of distilled water mixed with sugar standards and buffer solution (up) and the first derivatives (down), (b) Spectra of a sodium hydrogen carbonate standard mixed with sugar standards and buffer solution (up) and the first derivatives (down)

The absorbances of the original spectra as well as the one of the first derivative were evaluated for 2341.2 cm^{-1} . The results are given in Figure 28. For better visualisation the intensities are normalised to the one for 0 g/l of sugar.

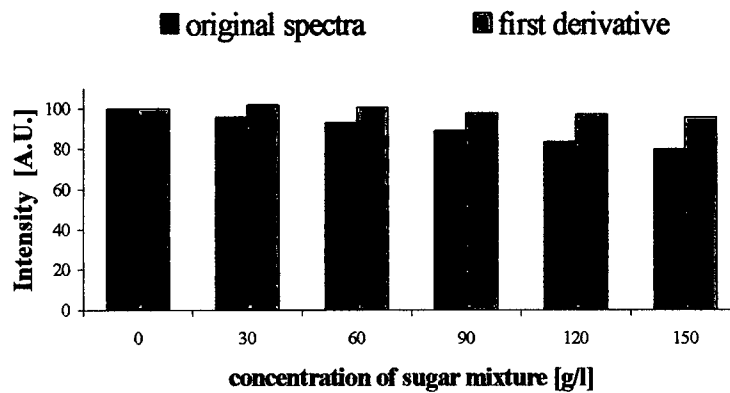


Figure 28: Normalised absorption of CO₂ standards (1,932 g/l) with different amounts of sugar. Evaluation of the original spectra compared to the evaluation of the first derivative spectre.

Using the first derivative compensates the influence of the sugar on the absorbance value. The same principle can be used in combination with laser absorption spectroscopy. But for calculating the first derivative or a proportional parameter it is essential to have a tunable laser to perform measurements at least at two neighboring wavelengths.

3.4.2.4. Conclusion

Different solutions for performing background compensation were discussed in the preceding chapter where not all of them are practicable for a QCL based process

analyzer. The analyte free sample matrix is hardly accessible for performing background measurements. The scanning across the whole absorption peak including measurements of the baseline before and after the peak would give enough information for a baseline corrected evaluation. State of the art QCLs show not sufficient tuning ranges for such a measurement. The application of a second QCL for determining the background signal was already proofed to be capable for other analytes. This principle could be also used for the determination of CO_2 (aq) in beverages. As QCLs offer the possibility of wavelength tuning, background compensation can also be performed by wavelength modulation of only one QCL. The gained information is equivalent to the information accessible using first derivative spectra. The optical as well as the electronically set-up for wavelength modulation is more simple than a set-up using two QCLs. For this reason the technique of wavelength modulation was exploited developing a QCL based system for analyzing CO_2 (aq). The results of the measurements are presented in **paper IV**.

4. Laser instrumentation and signal processing

All QCLs were mounted inside a laboratory laser housing (Alpes Lasers, Switzerland) on a Peltier element. The housing was equipped with a compartment for water cooling. Before closing all laser housings were purged with nitrogen and equipped with a bag filled with silica gel. The temperature of the QCL was regulated with a temperature controller unit TC-51 connected to the laser housing. The set point of the temperature was controlled with a front panel knob or via an external DC input signal (BNC connector). The temperature controller offered the possibility to monitor the actual temperature on the display as well as via a BNC connector delivering a DC voltage of 1 mV per 1°C.

For driving and controlling the lasers and processing the detector signal different devices were available. According to the special requirements of the particular experiment the devices were used in various configurations. In the next chapters the specifications of the devices are given, followed by a detailed description of the set-ups used for the papers I-IV.

4.1. General Devices

This chapter presents two devices - the function generator and the computer interface - that show a broad band of functions. Because of their flexibility these devices could be used for different tasks on key positions in the set-ups. The features/functions of both devices used for this thesis are explained here.

4.1.1. Function Generator

The function generator Model 33120A (Agilent Technologies, USA) delivered beside standard wave forms also the possibility to program any arbitrary wave form required for a particular application. The function generator has one output for the chosen function and a second one for a TTL trigger signal that allows synchronization with another device. Both outputs have a BNC connection.

4.1.2. Computer Interface

The computer interface (CI) module SR245 (Stanford Research Systems, USA) is equipped with 8 analog and 2 digital BNC connectors that can be either used as inputs or outputs. The analog connectors used for this work showed a range from -10 to $+10$ VDC and a resolution of 2.5 mV. The CI was linked to a PC via a RS232 connector. The connected PC software was determining the number of input and output channels as well as the delivered voltages of the output channels. In the used configuration connectors #1-3 were set as input and #4-8 as output channels. Detailed information about the function of the connectors is given in chapter 4.4.

4.2. Laser driving units

4.2.1. Alpes Lasers starter kit

Included in the Alpes Laser starter kit was a laser housing, the temperature control unit, that have already been described, the pulse generator TPG128, the laser diode driver - LDD100 as well as all the necessary connection cables.

The pulse generator defined the pulse duration and the pulse repetition rate of the QCL as preselected on the front panel. The pulse duration could be adjusted from 16 to 200 ns. The duration between the pulses could be set from 200 ns up to 105 μ s in 3 ranges. The pulse generator had two independent outputs for the pulses and one "Trigger OUT" output delivering a TTL signal for synchronization with other devices. The pulse generator included also a 12 V DC power supply needed by the laser diode driver.

The laser diode driver delivered negative current pulses that were led to the laser housing for driving the QCL. Information about pulse duration and the pulse repetition rate was received from the pulse generator. The voltage amplitude applied to the laser was determined via an external power supply that was connected to the laser diode driver. As different QCLs showed different values of resistance the resulting pulse current differed for all lasers if the same voltage amplitude was used. The current pulse was led to the laser housing via a low impedance line. The one originally included in the starter kit was considered to emit electromagnetic radiation that was effecting other devices, specially the units for evaluating the detector signal. Therefore a special shielded and shorter version (10 instead of 50 cm) of the low impedance line was used instead of the original one.

As an option the pulse generator could be replaced by the function generator. Therefore the function generator had to operate in a way that met the requirements of the laser diode driver and the used QCL. The function generator was operated with the parameters given in Table 7.

Main parameters of the function generator			Parameters for burst modulation	
Function:	Square Wave with Burst modulation		Burst counts	1
Frequency	990	kHz	Burst Rate	20.27 kHz
Amplitude	3.7	VPP	Burst Phase	0 deg.
Offset	+1.85	VDC	Burst source	intern
Duty cycle	20	%		

Table 7: Operation parameter of the function generator used to replace the pulse generator in the Alpes Lasers starter kit.

The parameters resulted in 100 ns long pulses of the QCL with a repetition rate of 20.27 kHz (NOTE: some of the parameters used represented the limits of the function generator). For most of the lasers distributed from Alpes Lasers 100 ns pulse duration exceeds the specifications, but as typical pulse frequencies lay around 400 kHz the specified duty cycle for the QCLs is not exceeded. Nevertheless until now only the QCL s1839a21 used in **paper I-III**, was driven with the function generator in combination with the Alpes Laser starter kit.

4.2.2. Quanta-BP

The Quanta-BP (Laser Components GmbH, Germany) was a specially modified laser pulser, dedicated to be attached to the laser housing from Alpes Lasers. The laser housing had to be equipped with 4 screws (M4) on which the Quanta-BP was mounted in a way that the pins on the back side of the housing could be connected with the socket board. The Quanta-BP showed one Sub-D connector (15-pin) and three SMB connectors. Via the Sub-D connector the Quanta-BP received the operating voltage of +12 VDC and two control voltages (nominal 0 to +5 VDC) controlling the pulse duration and the pulse amplitude. In contrast to the Laser diode driver from Alpes Lasers the Quanta-BP was delivering constant current pulses for a special adjustment instead of constant voltage pulses. An in-house made cable was used for all experiments splitting the Sub-D connector into two banana plugs for the

operating voltage and two BNC plugs for the control voltages for the pulse duration (marked in red) and the pulse amplitude (marked in blue).

The pulse frequency was defined via an external trigger signal fed to one of the SMB connectors. The trigger signal was either created by the function generator or the pulse generator. In both cases a connection cable switching from BNC to SMB had to be used. While triggering via the function generator the same operation parameter for the function generator were used than already described (see Table 7). The maximum allowed pulse frequency of the Quanta-BP was independent from the trigger source, but restricted by the maximum of the average current, being 24 mA. That means that the chosen pulse current and the pulse frequency have to result in an average current lower than 24 mA. The Quanta-BP offered the possibility to monitor the actual pulse current and pulse voltage using the particular SMB connectors.

An overview of the specifications of the two different driving equipments described above is given in Table 8.

	Starter Kit	Quanta-BP	Unit
Pulse Duration	16-200	20-300	ns
Pulse Frequency	0.65-5000	*	kHz
Amplitude of Pulse Current	0-30	0-9.5	A
Limitation of average Current	No	24	MA
Regulation of Current	No	Yes	
Regulation of Voltage	Yes	No	

* Maximum determined by the chosen pulse duration and pulse current

Table 8: Specifications of the Alpes Lasers starter kit and the Quanta-BP

4.3. Evaluation of the detector signal

For further processing of the detector signal boxcar averager modules SR250 from Stanford Research Systems were used. Beside the incoming signal the boxcar averagers needed a trigger signal to synchronize data evaluation with pulse frequency. The signal was evaluated using a gate of a minimum of 2 ns and a maximum of 15 μ s. By selecting a delay between the incoming trigger signal and the gate, the relative position of the gate to the signal was determined. The boxcar had also the possibility to select the delay of the gate via an external delay control input on the back panel. An offset of a maximum of ± 0.4 VDC was added to the input. The value of the signal

measured during the selected gate was provided as exponential moving averaged over a predetermined number of pulses. For all experiments this number was set to the maximum of 10000 pulses to average statistical fluctuations. The sensitivity of the boxcar could be set between 1 V/V to 1 V/5 mV (volts out/volts in). The calculated value was provided at the *average output* as a DC signal from -10 to +10 V.

4.4. Software

The QCL-Control software used to communicate with the computer interface and to store the signal from the boxcar averagers was a Microsoft Visual Basic 6.0 based program. It was developed in house. An overview about the most important features is given in this chapter. More details can be found in Ref. [39]. The Main Window of the software is given in Figure 29.

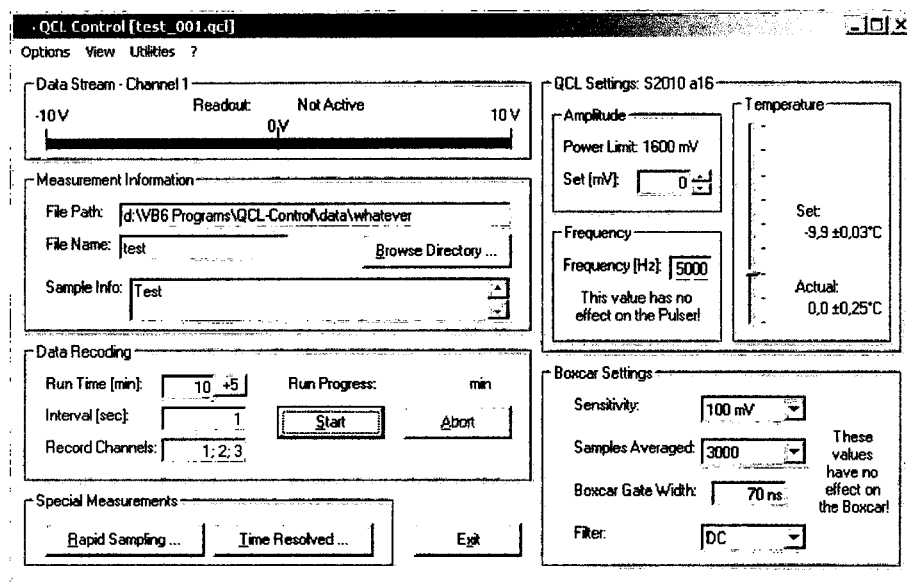


Figure 29: QCL-Control - Main Window

As mentioned in chapter 4.1.2 the software was determining the number of input and output channels as well as the delivered voltages of the output channels of the computer interface. The number of inputs was defined under the main window's menu "Options" and submenu "Setup". Input channels were always starting with channel #1. Channels not defined as input were automatically defined as output.

Using the *Measurement Information* frame specifications on the location and name of the file to be stored as well as any information that should be stored with the file was entered. The software used automatic filename incrementation based on the specified

filename followed by underscore, a changing three digit number and the extension “.qcl”.

With the *Data Recording* frame the duration of the recording, the interval between subsequent readout cycles and the input channels that were to be recorded could be defined. If more than one channel was entered they had to be separated by semicolon. The *Temperature* frame was dedicated to control and monitor the temperature of the QCL. For that purpose channel #2 (input) of the computer interface was connected with the temperature monitor output of the temperature controller and channel #7 (output) was connected with the external temperature control input of the temperature controller. The laser’s operating temperature was set with the help of the vertical sliding bar. The actual temperature was displayed if the data stream option in the “View” menu of the main window was on.

The *Amplitude* frame defined the DC voltage offered by channel #8 of the computer interface. For safety reasons a voltage maximum was defined using the main window’s menu “Options” and submenu “Setup”.

All parameters stated within the *Boxcar Settings* and *Frequency* frame did not effect the settings of possible hardware integrated in the set-up. Entries made here were merely added to the resulting measuring file as additional information.

4.5. Apparatus

4.5.1. Paper I

A schematically drawing of the set-up used in **paper I** is given in Figure 30.

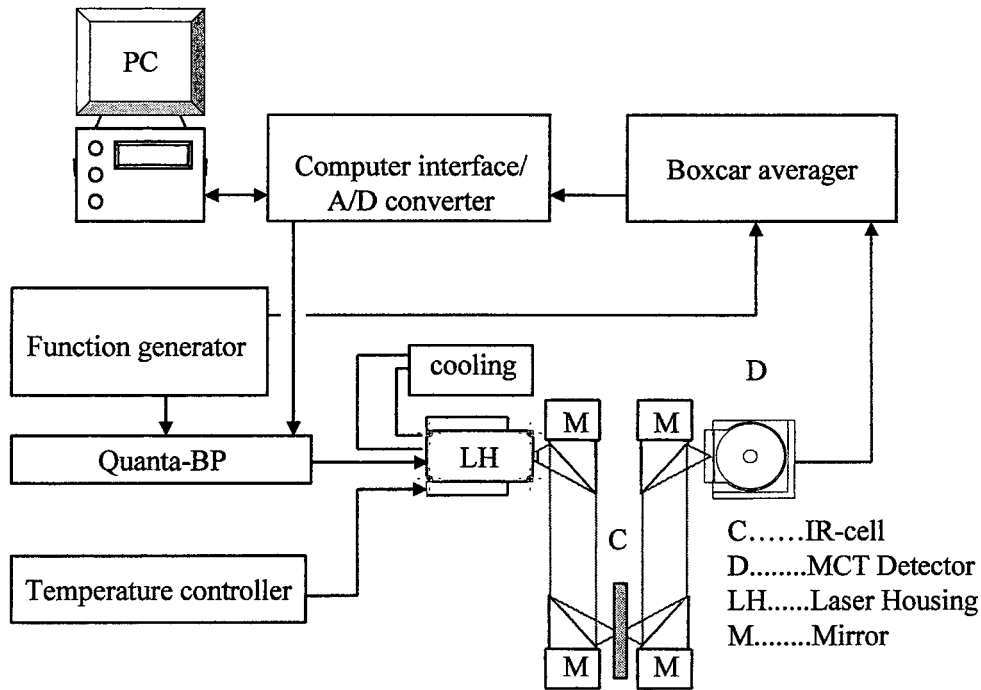


Figure 30: Schematically drawing of the set-up used in paper I.

The device used for driving the QCL was the Quanta-BP. The function generator was determining the pulse frequency (20.27 kHz) by triggering the function generator as well as the boxcar averager. The control voltages determining the pulse duration and pulse amplitude were provided by the computer interface, where the pulse amplitude was controlled via channel #8 and the pulse duration via channel #7. Channel #7 was originally dedicated to drive the temperature controller. Therefore it was not possible to enter directly the desired voltage. As described in chapter 4.4 via the software a temperature setting could be chosen that was corresponding to a particular voltage. It was necessary to evaluate the correlation between the temperature setting and the delivered voltage by means of a voltmeter.

The detector signal was further processed using the boxcar averager and recorded via channel #1 of the computer interface.

4.5.2. Paper II and III

Paper II and III were aiming at the simultaneous application of two QCLs. The electronic set-up was identical. The optical set-up differed in the position of the MCT detector and its preceding mirror in respect to the beam splitter. Differences can be

found in the choice of analytes, the flow system and the dynamic of the chemical system.

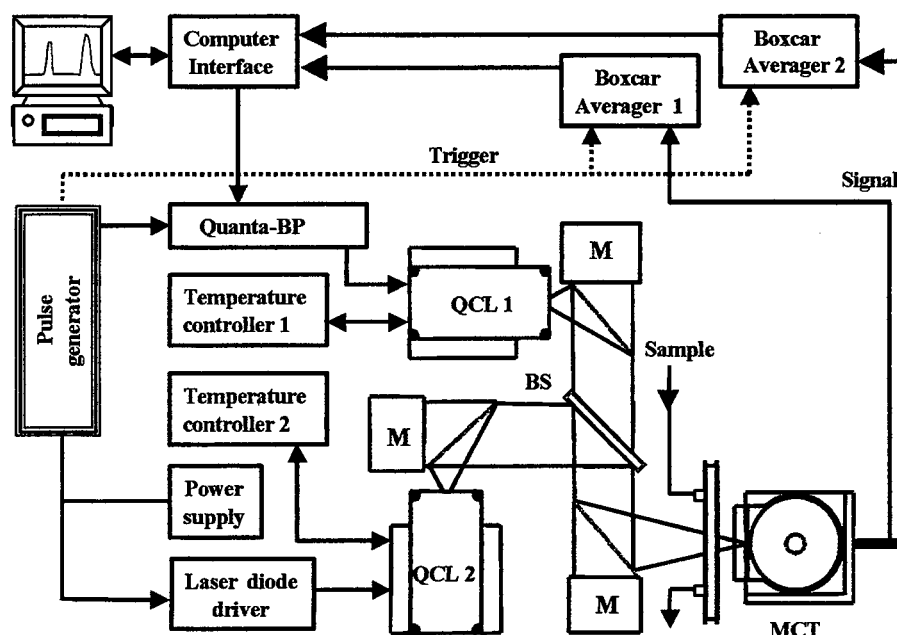


Figure 31: Schematically drawing of the set-up used in **paper II** and **III**. For **paper III** the position of the MCT detector and its preceding mirror was changed to the free side of the beam splitter. M: mirror, MCT: mercury cadmium telluride detector. BS: beam splitter

The pulse generator controlled the timing and synchronisation of the whole system. The *Trigger OUT* signal was split using a T-piece in order to trigger the Quanta-BP and the corresponding boxcar averager. The Quanta-BP was driving QCL1. The pulse duration and pulse amplitude were determined as described for **paper I**. The laser diode driver was driving QCL2. The pulse duration and pulse frequency were determined by the pulse generator via the pulse output *out 2*. The corresponding boxcar averager for QCL2 was triggered by the pulse generator via the pulse output *out 1*. The detector signal was split using a T-piece, further processed with both boxcar averagers and recorded via channel #1 and #3 of the computer interface. Each boxcar averager was processing the pulses of one QCL.

4.5.3. Paper IV

Paper IV aimed at the modulation of the emission wavelength of a QCL. Therefore the pulse amplitude of the QCL had to be modulated. A schematically drawing of the set-up is given in Figure 32.

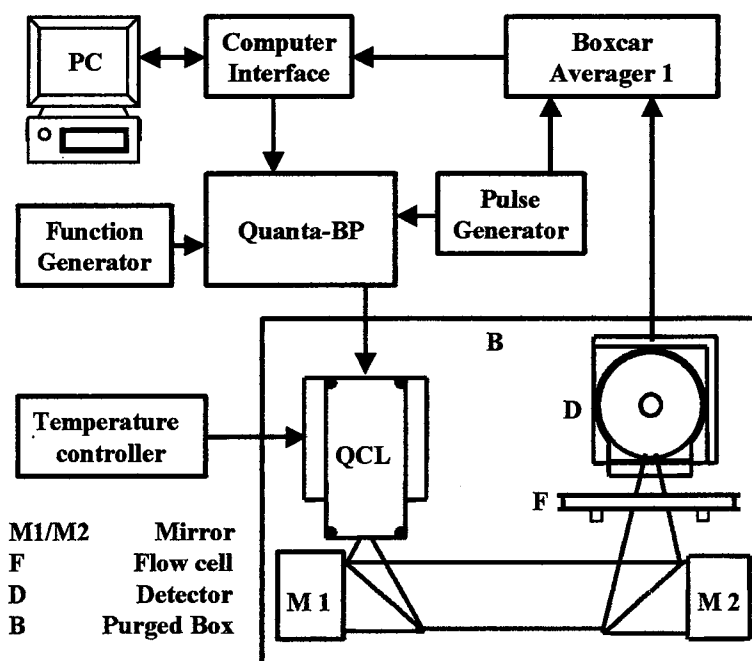


Figure 32: Schematically drawing of the set-up used in paper IV

The Quanta-BP was driving the QCL. The function generator was determining the pulse frequency (247.5 kHz) by triggering the function generator as well as the boxcar averager. Tuning of a QCL is more efficient using higher duty cycles as the cavity is effected more by the generated heat [40]. Therefore the pulse frequency was set to the maximum that was limited by the maximum allowed average current of 24 mA determined by the Quanta-BP. As the maximum trigger rate of the boxcar averager was 20 kHz, only 8% of the generated pulses were processed. The pulse duration was determined as described for paper I.

The function generator determined the pulse amplitude. It was oscillating between two DC values with a frequency of 50 mHz. This resulted in a modulation of the pulse amplitude and therefore also in a modulation of the QCL emission wavelength. The frequency of 50 mHz was necessary as it took around 2 seconds after the pulse amplitude of the QCL was changed until the exponential moving average provided by the boxcar averager showed a stable signal. The operation parameters of the function generator are given in Table 9.

Main Settings of the Function generator		Settings for Arbitrary wave form	
Funktion:	Arbitrary wave form	Number of Points	10000
Frequency	50 mHz	Point 0-4999	100 %
Amplitude	70.03 mVPP	Point 5000-10000	50 %
Offset	+70.00 mVDC		

Table 9: Operation parameters of the function generator for wavelength modulation of the QCL

The output of the function generator showed an impedance of $50\ \Omega$ and was designed to end in an impedance of $50\ \Omega$. The Quanta-BP showed an impedance of $1\ \text{M}\Omega$. Therefore the effective voltage applied to the Quanta-BP was higher than the adjusted value. To display the effective voltage, the output of the function generator was monitored using a voltmeter, or an Oscilloscope with an impedance of $1\ \text{M}\Omega$.

The target analyte of this paper was CO_2 dissolved in water. Gaseous CO_2 shows absorption at the same wavelength. As a consequence the optical part of the set-up was covered with an acrylic plastic box, purged at 15 l/min with nitrogen so that the optics was free from gaseous CO_2 . The detector signal was further processed using the boxcar averager and recorded via channel #1 of the computer interface.

5. References

1. http://www.physik.tu-cottbus.de/physik/ap2/ausstattung/hp_ausst_fir.htm. 2006.

Ref Type: Internet Communication

2. <http://www.chemguide.co.uk/analysis/ir/fingerprint.html>. 2006.

Ref Type: Internet Communication

3. M. Kansiz, J. R. Gapes, D. McNaughton, B. Lendl, and K. C. Schuster, "Mid-infrared spectroscopy coupled to sequential injection analysis for the on-line monitoring of the acetone-butanol fermentation process," *Analytica Chimica Acta* **438**, 175-186 (2001).
 4. V. N. Korolev, A. V. Marugin, and V. B. Tsaregradskii, "Estimation of the Petroleum Product Knock Rating by Regression Analysis of Near-Infrared Absorption Spectra," *Technical Physics* **45**, 1177-1181 (2000).
 5. J. J. Kelly, C. H. Barlow, T. M. Jinguji, and J. B. Callis, "Prediction of gasoline octane numbers from near-infrared spectral features in the range 660-1215 nm," *Analytical Chemistry* **61**, 313-320 (1989).
 6. <http://www.sbu.ac.uk/water/vibrat.html>. 2006.
- Ref Type: Internet Communication
7. P. R. Griffiths and J. deHaseth, *Fourier Transform Infrared Spectrometry*, (John Wiley & Sons, New York, 1986).
 8. J. Faist, F. Capasso, D. L. Sivco, C. Sirtori, A. L. Hutchinson, and A. Y. Cho, "Quantum cascade laser," *Science* **264**, 553-556 (1994).
 9. R. F. Kazarinov and R. A. Suris, "Possible amplification of electromagnetic waves in a semiconductor with a superlattice," *Fizika i Tekhnika Poluprovodnikov* **5**, 797-800 (1971).
 10. J. Faist, C. Gmachl, F. Capasso, C. Sirtori, D. L. Sivco, J. N. Baillargeon, and A. Y. Cho, "Distributed feedback quantum cascade lasers," *Applied Physical Letters* **70**, 2670-2672 (1997).
 11. A. A. Kosterev and F. K. Tittel, "Chemical sensors based on quantum cascade lasers," *Ieee Journal of Quantum Electronics* **38**, 582-591 (2002).
 12. B. A. Paldus, C. C. Harb, T. G. Spence, R. N. Zare, C. Gmachl, F. Capasso, D. L. Sivco, J. N. Baillargeon, A. L. Hutchinson, and A. Y. Cho, "Cavity ringdown spectroscopy using mid-infrared quantum-cascade lasers," *Optics Letters* **25**, 666-668 (2000).
 13. A. A. Kosterev, A. L. Malinovsky, F. K. Tittel, C. Gmachl, F. Capasso, D. L. Sivco, J. N. Baillargeon, A. L. Hutchinson, and A. Y. Cho, "Cavity ringdown

- spectroscopic detection of nitric oxide with a continuous-wave quantum-cascade laser," *Applied Optics* **40**, 5522-5529 (2001).
14. Y. A. Bakirkin, A. A. Kosterev, C. Roller, R. F. Curl, and F. K. Tittel, "Mid-infrared quantum cascade laser based off-axis integrated cavity output spectroscopy for biogenic nitric oxide detection," *Applied Optics* **43**, 2257-2266 (2004).
 15. M. G. da Silva, H. Vargas, A. Miklos, and P. Hess, "Photoacoustic detection of ozone using a quantum cascade laser," *Applied Physics B-Lasers and Optics* **78**, 677-680 (2004).
 16. A. A. Kosterev, Y. A. Bakirkin, F. K. Tittel, S. Blaser, Y. Bonetti, and L. Hvozdar, "Photoacoustic phase shift as a chemically selective spectroscopic parameter," *Applied Physics B-Lasers and Optics* **78**, 673-676 (2004).
 17. H. Ganser, M. Horstjann, C. V. Suschek, P. Hering, and M. Murtz, "Online monitoring of biogenic nitric oxide with a QC laser-based Faraday modulation technique," *Applied Physics B-Lasers and Optics* **78**, 513-517 (2004).
 18. M. Kölhed, P. Hinsmann, P. Svasek, J. Frank, B. Karlberg, and B. Lendl, "On-Line Fourier Transform Infrared Detection in Capillary Electrophoresis," *Analytical Chemistry* **74**, 3843-3848 (2002).
 19. M. Kölhed, P. Hinsmann, B. Lendl, and B. Karlberg, "Micellar electrokinetic chromatography with on-line Fourier transform infrared detection," *Electrophoresis* **24**, 687-692 (2003).
 20. M. Kölhed, M. Haberkorn, V. Pustogov, B. Mizaikoff, J. Frank, B. Karlberg, and B. Lendl, "Assessment of quantum cascade lasers as mid infrared light sources for measurement of aqueous samples," *Vibrational Spectroscopy* **29**, 283-289 (2002).
 21. B. Lendl, J. Frank, R. Schindler, A. Muller, M. Beck, and J. Faist, "Mid-infrared quantum cascade lasers for flow injection analysis," *Analytical Chemistry* **72**, 1645-1648 (2000).
 22. A. Edelmann, C. Ruzicka, J. Frank, B. Lendl, W. Schrenk, E. Gornik, and G. Strasser, "Towards functional group-specific detection in high-performance liquid chromatography using mid-infrared quantum cascade lasers," *Journal of Chromatography A* **934**, 123-128 (2001).
 23. D. R. Mattson, "Sensitivity of a Fourier transform infrared spectrometer," *Applied Spectroscopy* **32**, 335-338 (1978).
 24. R. Kellner, J. M. Mermet, M. Otto, and H. M. Widmer, *Analytical Chemistry*, (WILEY-VCH Verlag GmbH, Weinheim, 1998).
 25. J. Ruzicka, "The second coming of flow-injection analysis," *Analytica Chimica Acta* **261**, 3-10 (1992).

26. D. Heiger, *An introduction: High performance capillary electrophoresis*, (Agilent Technologies, 2000).
27. K. Swinney and D. J. Bornhop, "Detection in Capillary Electrophoresis," *Electrophoresis* **21**, 1239-1250 (2000).
28. K. Swinney and D. Bornhop, "A Review of CE detection methodologies," *Critical Reviews Analytical Chemistry* **30**, 1-30 (2000).
29. A. von Brocke, G. Nicholson, and E. Bayer, "Recent advances in capillary electrophoresis / electrospray-mass spectrometry," *Electrophoresis* **22**, 1251-1266 (2001).
30. P. Hinsmann, "Novel microfluidic chips with Fourier transform infrared spectroscopic detection for reaction and separation monitoring in miniaturised analysis systems," 2002).
31. J. Ruzicka and E. H. Hansen, *Flow Injection Analysis*, (John Wiley & sons, New York, 1988).
32. <http://www.roempp.com/prod/index1.html> (searching for keyword "Kohlensäure"). 2006.
Ref Type: Internet Communication
33. <http://www.sbu.ac.uk/water/co2.html>. 2006.
Ref Type: Internet Communication
34. D. D. Perrin and B. Dempsey, *Buffers for pH and Metal Ion Control*, (Chapman and Hall, London, 1974).
35. J. Schnöller, "Development and Application of a Portable FTIR Analyzer for On-Line Monitoring of Micro-Organism During Bioprocesses," 2006).
36. Martin W.B., Mirov S., and Venugopalan R, "Middle Infrared, Quantum Cascade Laser Optoelectronic Absorption System For Monitoring Glucose in Serum," *Applied Spectroscopy* **59**, 881-884 (2005).
37. J. J. Max and C. Chapados, "Infrared Spectroscopy of Aqueous Carboxylic Acids: Malic Acid," *Journal of Physical Chemistry A* **106**, 6452-6461 (2002).
38. S. Schaden, M. Haberkorn, J. Frank, J. R. Baena, and B. Lendl, "Direct determination of carbon dioxide in aqueous solution using mid-infrared quantum cascade lasers," *Applied Spectroscopy* **58**, 667-670 (2004).
39. M. Haberkorn, "Development and Implementation of novel Interfaces for Miniaturized Analysis Systems with Vibrational Spectroscopic Detection," 2003).
40. A. A. Kosterev, R. F. Curl, F. K. Tittel, M. Rochat, M. Beck, D. Hofstetter, and J. Faist, "Chemical sensing with pulsed QC-DFB lasers operating at 15.6 μm ," *Applied Physics B-Lasers and Optics* **75**, 351-357 (2002).

6. Appendix

PAPER I

On-line hyphenation of quantum cascade laser and capillary electrophoresis

Malin Kölhed^a, Stefan Schaden^b, Bo Karlberg^{a,*}, Bernhard Lendl^b

^a Department of Analytical Chemistry, Stockholm University, SE-106 91 Stockholm, Sweden

^b Institute of Chemical Technologies and Analytics, Vienna University of Technology, Getreidemarkt 9/164, A-1060 Vienna, Austria

Received 29 March 2005; received in revised form 30 May 2005; accepted 8 June 2005

Abstract

We report the first successful hyphenation of a Fabry Pérot quantum cascade (QC) laser to a capillary electrophoresis system. This involved use of a dedicated IR-transparent flow cell, made of CaF₂, constructed by means of SU-8 based lithography and low temperature wafer bonding techniques. Adenosine, guanosine, xanthosine and adenosine-5'-monophosphate were separated in a borate-containing separation electrolyte (10 mM, pH 9.3). Functional group (carbohydrate) detection was accomplished by use of the 1080 cm⁻¹ emission line of the available QC-laser. The assessable optical path length could be increased, from the normally available 10–15 µm in CE-FTIR analyses, to 60 µm using this powerful mid-infrared laser and aqueous solutions.

© 2005 Elsevier B.V. All rights reserved.

Keywords: Quantum cascade laser; Capillary electrophoresis; Mid-infrared detection; On-line hyphenation; Aqueous samples

1. Introduction

Rapidly growing interest in chemical separation research is focused on micro-scale techniques such as capillary liquid chromatography (LC) and capillary electrophoresis (CE). The popularity of CE arises from its ability to separate a wide range of substance, including compounds with similar functional groups, efficiently and rapidly. CE is an electrically driven separation process generally performed in fused silica capillaries (i.d. in the range 20–100 µm) using aqueous buffers. CE has been adapted for the separation of an immense range of compounds, including small inorganic ions and large proteins and peptides. Laser-induced fluorescence (LIF) spectroscopy is currently the most sensitive technique for detecting CE-separated compounds [1], although UV detection systems are most commonly used.

In the mid-infrared region almost all organic compounds exhibit characteristic vibrational patterns, thus providing a sensitive means of fingerprint identification and quantification. However, nearly all compounds absorb in the mid-IR region, which may be disadvantageous when working with complex mixtures. Thus, hyphenation with a separation system prior to mid-IR detection is often necessary for the determination of specific organic compounds in mixtures. Hyphenation may be performed either off-line, employing sophisticated solvent elimination approaches, or on-line, utilising short optical path lengths [2,3]. A frequently cited shortcoming of on-line hyphenation is that a shorter optical path length will inevitably lead to lower sensitivity according to Lambert–Beer's law. When applying mid-IR light with aqueous, biologically interesting compounds the intense water absorption may hamper its use, predominantly due to the strong absorption arising from the O–H bending vibration of water around 1640 cm⁻¹. With respect to these shortcomings, quantum cascade (QC) laser technology offers significant improvements. QC-lasers are powerful, mid-IR light sources, providing the ability to increase the optical path length,

* Corresponding author. Tel.: +46 8164316; fax: +46 8156391.

E-mail address: bo.karlberg@anchem.su.se (B. Karlberg).

and hence improve sensitivity [4,5]. In QC-lasers photon emission occurs within the conducting band via intersubband transitions, in contrast to normal semi-conducting diode lasers where photon emission is due to the recombination of electrons and holes in *p-n* junctions. These intersubband transitions can be controlled by careful bandstructure engineering at monomolecular resolution, thereby forming an artificial semi-conducting crystal with a heterostructure of alternating “well” and “barrier” layers, grown by molecular beam epitaxy (MBE) techniques. Faist et al. presented the first quantum cascade laser in [6]. The intersubband nature of the optical transitions has several key advantages. First, the laser emission wavelength is primarily a function of the thickness of the quantum well (QW) layers. Hence, the wavelength can be tailored over a wide spectral region, essentially the entire mid-IR and into the far-IR, using the same semi-conducting material, in contrast to normal lasers, where the chemical characteristics of the active material determine the emission wavelength. Secondly, the multistage cascade nature of the QW permits electrons to be recycled as they remain inside the conducting band, contributing in every cycle to the gain and photon emissions. Consequently, each injected electron above the laser threshold value can, in principle, generate n_p photons, where n_p is the number of active regions in the laser. This leads to very high quantum efficiencies and optical power, both of which are proportional to n_p . Rapid progress in heterostructure semi-conducting research soon led to the development of QC-lasers that can function in continuing mode (cw) at cryogenic temperatures as well as at room temperature in pulsed mode, covering the mid- to far-IR region [7,8]. The research focus then shifted to the development of new laser waveguide designs allowing cw-operation at room temperature [9,10] and different heterostructure materials providing shorter wavelengths and multiple cascade operation [11,12]. Within a decade of their invention QC-lasers started to become commercially available [13].

QC-lasers have primarily been adapted for use as chemical gas sensors for detecting and monitoring toxic and dangerous compounds, including various pollutants and exhaust emissions [14]. Their potential utility as powerful light sources in the condensed phase has only recently been demonstrated [5,15].

In this study the on-line hyphenation of a QC-laser to a CE separation system is presented for the first time. Functional group detection of carbohydrate-containing analytes, dissolved in the separation electrolyte solution, was achieved utilizing a custom-built IR-transparent flow cell, with an optical path length of 60 μm , and a Fabry P  rot QC-laser emitting light at 1080 cm^{-1} .

2. Experimental

The entire experimental set-up, including the QC-laser system, the data acquisition system and the CE system are schematically illustrated in Fig. 1.

2.1. Quantum cascade laser system

A Fabry P  rot QC-Laser (S1839a21, Alpes Lasers, Neuch  tel, Switzerland) with an emission maximum at 1080 cm^{-1} was used throughout the experiments. The laser was placed in a dedicated laser housing (Alpes Lasers) equipped with an air- or water-cooled Peltier element. Before it was sealed, the laser housing was filled with dry nitrogen gas and silica gel pads. A temperature controller (TC51, Alpes Lasers) was included to allow precise monitoring of the laser's temperature. The laser operation was controlled by a specially fabricated laser driver (QUANTA-BP, Laser Components GmbH, Olching, Germany), triggered by a function generator (Model 33120A, Agilent Technologies, Palo Alto, California, USA). The laser was operated at -30°C with a pulse current of 4.5 V, a pulse frequency of 20 kHz and a pulse duration of 50 ns. With the selected operating conditions and according to the specification of Alpes Lasers, a peak power of 1 W is obtained which results in an emitted average power of 1 mW. A home-made software package (Sagittarius v. 3.0) [16] was developed enabling, in combination with a computer interface, control of the pulse duration and amplitude as well as the A/D conversion of the laser signal.

2.2. Data acquisition system

The light from the laser was collimated and focused by means of two gold-coated parabolic mirrors (focal length: 43 mm) onto the developed IR-transparent flow cell (see Fig. 1). Subsequently, using the same type of mirrors, the remaining light was collimated and focused onto a photovoltaic mercury cadmium telluride (MCT) detector element (KMPV12-0.1-J1/100 MHz Kolmar Technologies, Newburyport, MA, USA). The detector signal was processed using a Boxcar Averager (SR250, Stanford Research Systems, Sunnyvale, California, USA). Ten thousand pulses, triggered by the function generator, were averaged within a 10 ns gate window in the laser pulse. Using this system a new value could be recorded and stored every second.

2.3. Capillary electrophoresis system

The CE system was constructed in-house, consisting of untreated fused-silica capillaries (i.d. 50 μm , o.d. 375 μm , Polymicro Technologies, Phoenix, Arizona, USA), a high voltage power supply (Brandenburg, Thornton Heath, UK) and two platinum electrodes. The total capillary length was 51 cm, with the IR detection cell 30 cm from the injection end. The applied voltage at the injection end of the capillary was +16 kV, resulting in currents of around 54 μA . The surface of new capillaries was activated by rinsing with 1 M NaOH, 0.1 M NaOH, distilled water (each for 5 min) and electrolyte solution (10 min). The capillary was washed between runs, when necessary, using 0.1 M NaOH, distilled water and electrolyte solution (each for 3 min). Hydrodynamic sample

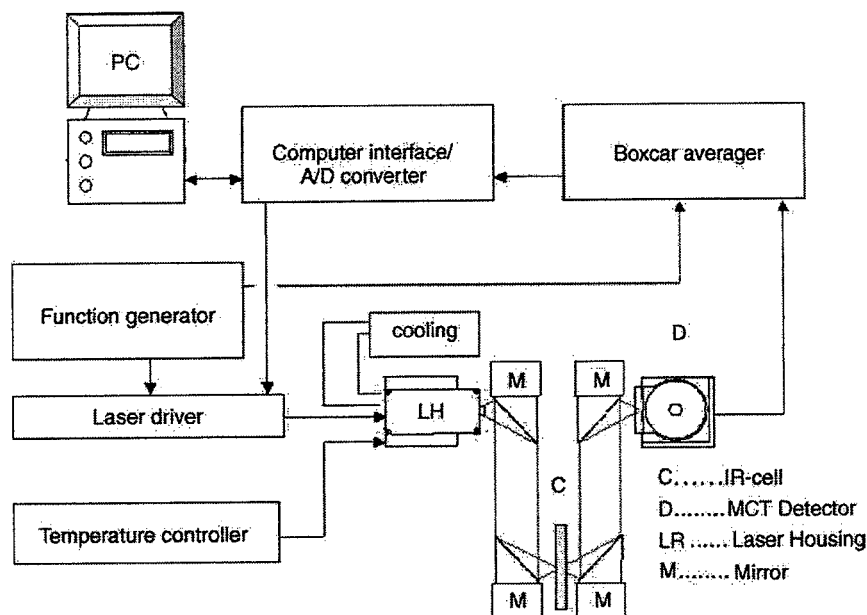


Fig. 1. Schematic view of the experimental set-up including the optical, separation and data acquisition systems.

injection was accomplished by manually elevating the inlet side of the capillary 23 cm for 20 s.

2.4. The flow cell unit

The production of the IR-transparent CaF_2 flow cells has been described in detail elsewhere [17], but a number of modifications to the published procedure were introduced, and are briefly described here. The flow channel was formed by two streaks (100 μm wide and $\sim 30 \mu\text{m}$ thick) of epoxy-based SU-8 photoresist (Microchem Corp., Newton, MA, USA) on each CaF_2 disc, producing a 150 μm wide channel with an optical path length of 60 μm . Aluminium foil was glued to the top-surface of the flow cell, providing an optical aperture. The fused silica capillary was carefully cut to ensure that the terminus of the capillary was perpendicular to its axis and that the surrounding polymer was not frayed. The flow cell was placed in a cell-holder and commercially available o-rings (1.10 mm \times 0.5 mm \times 0.30 mm, Rudolf Flume Technik GmbH, Essen, Germany) were used to ensure a tight connection between the flow cell and the cut capillary ends. Fig. 2 shows a microscopic view of the cell in the cell-holder.

2.5. Chemicals

Adenosine (>99%), guanosine (>98%), and adenosine-5'-monophosphate disodium salt (>99%) were purchased from Fluka (Buchs, Switzerland) and xanthosine (>99%) from Sigma-Aldrich (St. Louis, MO, USA). The separation electrolyte consisted of 10 mM borate (pH 9.3) dissolved in 0.2- μm filtered HPLC water (Fluka, Buchs, Switzerland). Five millimolar stock-solutions of the individual analytes were prepared and dissolved in the separation electrolyte. Before

introduction into the CE system, all solutions were degassed for 15 min in an ultrasonic bath.

2.6. Reference measurements

Reference FTIR spectra of all analytes dissolved in the separation electrolyte were obtained by a Bruker IFS 88 spectrometer (Bruker Optik GmbH, Germany) equipped with a MCT detector (J-15D16 Judson, Montgomeryville, PA, USA) and a commercially available CaF_2 flow cell based on transmission with a 44 μm optical path length. The spectra were recorded, with the separation electrolyte serving as background, between 4000 and 700 cm^{-1} , at 8 cm^{-1} spectral resolution, with 500 co-additions and applying a Blackman-Harris 3-Term apodization function.

The emission wavelength of the QC-laser was experimentally verified. For this purpose the black body radiation source of a Bruker Equinox 55 spectrometer (Bruker Optik GmbH, Germany) was substituted for the QC-laser. The spectra were recorded between 1400 and 900 cm^{-1} with a spectral resolution of 2 cm^{-1} using an MCT detector (KMPV11-1-LJ2/239 Kolmar Technologies, Newburyport, MA, USA). One hundred twenty-eight scans were co-added and a Blackman-Harris 3-Term apodization function was applied.

An Ultimate fiber optic UV-Detector (Dionex, Sunnyvale, California, USA) set at 210 nm and an ELDS Pro 1.0 laboratory data system (Chromatography Data systems, Kungshög, Sweden) were used to register the UV electropherograms. On-line UV detection was achieved by removing the polyimide coating from a short segment of the fused silica capillary and placing it in the optical path of the UV detector. The UV reference measurements were performed under the

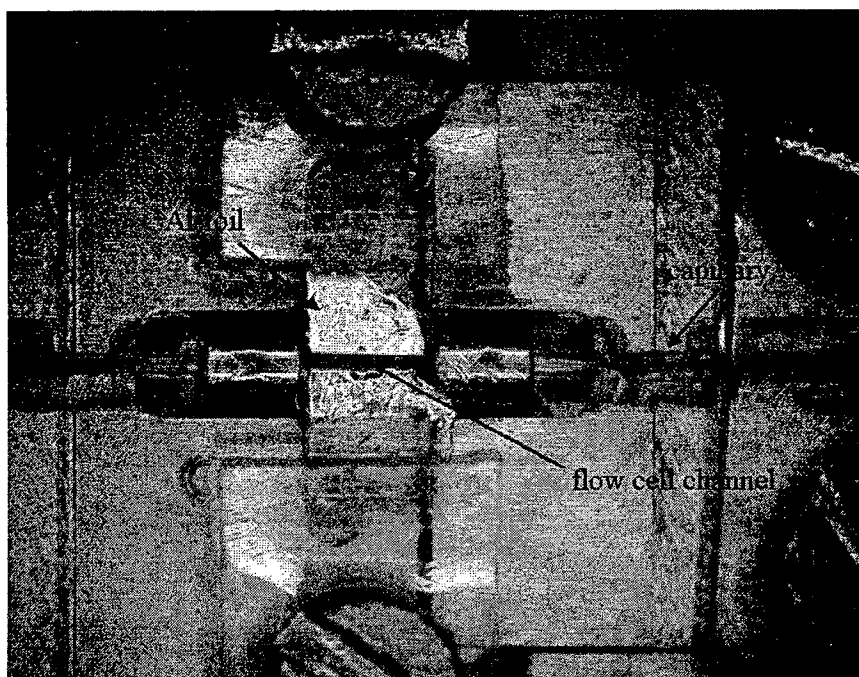


Fig. 2. Microscopic view of the custom-built IR-transparent flow cell and cell-holder.

same experimental conditions as those used when the QC-laser provided the light source.

3. Results and discussion

3.1. CE-QCL recordings

Fig. 3 shows a typical electropherogram illustrating the on-line, real-time registration from a CE separation utilizing

a QC-laser as a light source for mid-IR detection. The analytes separated were adenosine, guanosine, xanthosine and adenosine-5'-monophosphate (AMP), each with a concentration of 5 mM. The signal from the bulk sample, i.e. the electroosmotic flow, is easily detected as a sharp negative peak in the electropherogram. Also included in this figure is the electropherogram from a CE separation, recorded under similar separation conditions, but with the QC-laser exchanged for a UV detection light source. Both detectors give comparable electrophoretic peak shapes, although the

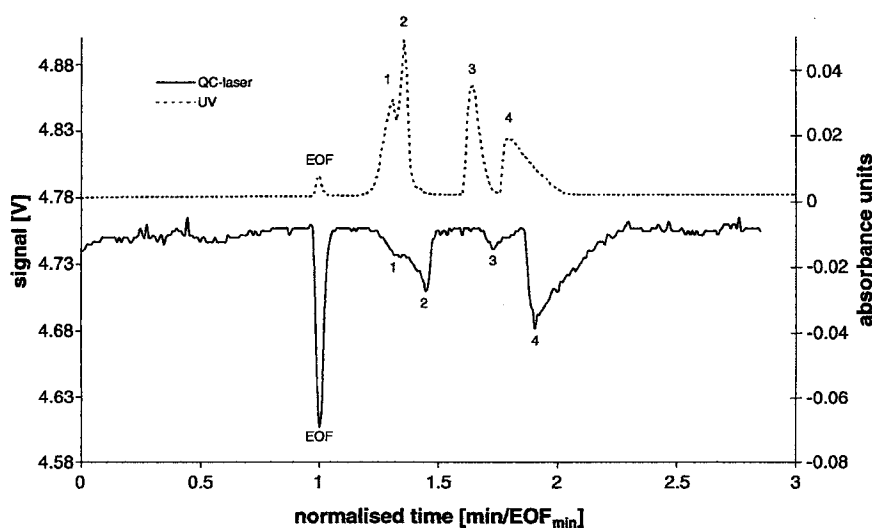


Fig. 3. On-line CE-QCL electropherogram (solid line) and a CE-UV electropherogram (dotted line), recorded under similar conditions, of (1) adenosine, (2) guanosine (3) xanthosine and (4) AMP each with a concentration of 5 mM separated with CE. Applied voltage, 310 V cm^{-1} ; capillary inner diameter, $50 \text{ }\mu\text{m}$; length to the detection point, 30 cm ; separation electrolyte, 10 mM borate buffer at pH 9.3; hydrodynamic injection by manual elevation.

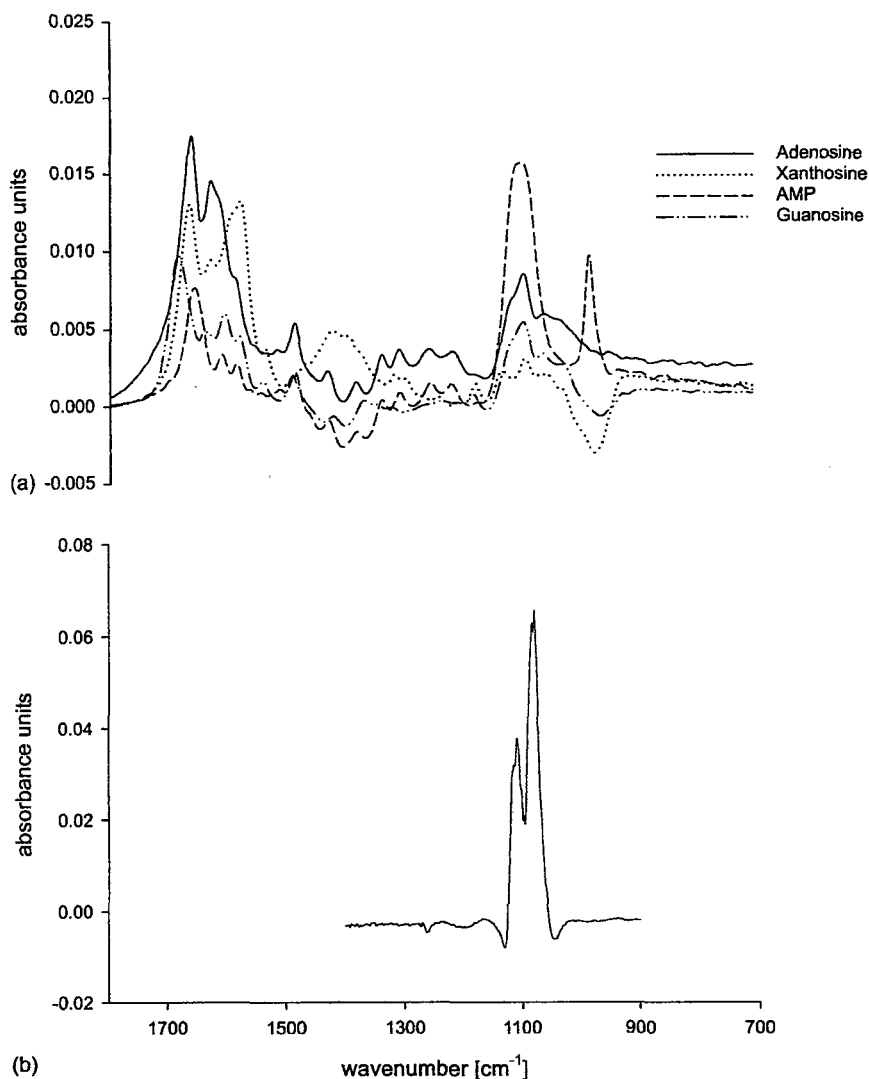


Fig. 4. (a) FTIR reference spectrum ($1800\text{--}700\text{ cm}^{-1}$) of adenosine (solid line), guanosine (dashed-dotted line), xanthosine (dotted line) and AMP (dashed line), each at a concentration of 5 mM with the separation electrolyte serving as background. Spectral resolution, 8 cm^{-1} ; 500 co-additions. (b) QC-laser emission spectrum recorded between 1400 and 900 cm^{-1} with a spectral resolution of 2 cm^{-1} ; 128 co-additions and applying a Blackman-Harris 3-Term apodization function.

QC-laser and UV-detector provide transmission peaks and absorption peaks, respectively.

3.2. Functional group detection

Fig. 4a presents reference FTIR spectra of the analytes in the region between 1800 and 700 cm^{-1} . All four analytes contain a furanose ring-structure, absorbing in both the UV and IR regions, as well as a carbohydrate group that only absorbs light in the IR. The absorptivities differ, but all analytes absorb light at around 1080 cm^{-1} , primarily due to the C–O–H motions of the carbohydrate group. In addition to the carbohydrate, the AMP also contains a phosphate group, absorbing at around 980 cm^{-1} . Fig. 4b shows the emission spectrum of the QC-laser. The QC-laser emission has a broad peak between 1055 and 1127 cm^{-1} , hence it is suitable for

the naturally large, condensed-phase absorption peaks. Consequently, a specific functional group (the carbohydrate) of the carbohydrate-containing analytes separated by the CE system can be detected using the available QC-laser.

3.3. Estimation of the signal-to-noise ratio

The signals from the four CE-separated analytes were investigated with respect to their signal-to-noise (S/N) ratios, calculated from the baseline noise and their respective peak heights. The results are presented in Table 1. For comparison, the same concentration of the individual analytes was measured in a FTIR spectrometer using a commercial flow cell with an optical path length of $44\text{ }\mu\text{m}$. The analytes were dissolved in the electrolyte solution and the background spectrum was obtained from the electrolyte solution. The highest

Table 1
Signal-to-noise estimates

Analyte	QCL	FTIR
Adenosine	2.4	9.5
Guanosine	4.4	6.0
Xanthosine	1.8	3.4
AMP	6.6	17.6

Table 2
Linear regression data

Analyte	Slope (mAU mM ⁻¹)	Intercept (mAU)	r ²
Adenosine	0.342	0.475	0.96
Guanosine	0.744	0.240	0.96
Xanthosine	0.284	0.170	0.91
AMP	0.931	1.126	0.99

r² = regression coefficient, number of calibration points = 5.

peak in the region between 995 and 1150 cm⁻¹, i.e. the region where the laser emission occurs, was compared to a reference background spectrum in the same region. Again, the S/N ratios were calculated from the baseline noise and respective peak heights. The results are included in Table 1.

As recently reported [18], the commercially available electronic systems (i.e. the laser starter kit from Alpes laser) generate a significant amount of electronic noise and, consequently, the operating conditions for the QC-laser were not entirely satisfactory. However, modifications allowing 50-fold improvements in S/N ratios have been reported recently for the detection of phosphate [5] using a home-made and no longer available set-up, and the authors see no reason why similar improvements should not be possible for determining the analytes determined here when the commercially available electronic systems become more stable.

3.4. Quantification

To obtain figures of merit for the calibration of the presented method the concentration of the injected sample was varied between 2 and 5 mM for adenosine (0.53–1.34 g L⁻¹), guanosine (0.57–1.42 g L⁻¹), xanthosine (0.57–1.42 g L⁻¹) and AMP (0.69–1.74 g L⁻¹). Exceeding these upper concentration regions resulted in overload in the CE system. The resulting transmission peaks were recorded as functions of time. After conversion into absorbance units, the peak heights were measured and the linearity of their relationship with the concentration of the corresponding analytes was calculated by regression analysis.

The results are presented in Table 2.

4. Conclusions

The first preliminary results obtained utilizing a Fabry Péro QC-laser as a powerful, mid-IR light source in a CE

separation system are presented. The on-line hyphenation maintains the spatial profile acquired in the CE separations. The poor signal-to-noise ratio obtained is primarily a result of electrical noise arising in the laser housing. When the connection between the QC-laser and the electrical contact is improved by the manufacturers we are convinced that the S/N will increase sharply. Nevertheless, the results achieved indicate the potential utility of QC-lasers, as tuneable, tailored mid-IR light sources, providing new detection opportunities in capillary electrophoresis. When production costs are reduced the scope for deploying arrays of QC-lasers or QC-lasers with multiple cascade operation will further boost interest in this field and the authors are convinced that research into and the application of QC-lasers will continue apace.


Acknowledgements

S.S. and B.L. are grateful for the financial support received within the project No. 15531 of the Austrian Science Fund (FWF). Foss Analytical is acknowledged for financial support.

References

- [1] T. Li, R.T. Kennedy, *Trends Anal. Chem.* 17 (1998) 484.
- [2] P.R. Griffiths, S.L. Pentoney, A. Giorgetti, K.H. Shafer, *Anal. Chem.* 58 (1986) 1349A.
- [3] M. Kölhed, B. Lendl, B. Karlberg, *Analyst* 128 (2003) 2.
- [4] M. Kölhed, M. Haberkorn, V. Pustogov, B. Mizaikoff, J. Frank, B. Karlberg, B. Lendl, *Vib. Spectrosc.* 29 (2002) 283.
- [5] B. Lendl, J. Frank, R. Schindler, A. Müller, M. Beck, J. Faist, *Anal. Chem.* 72 (2000) 1645.
- [6] J. Faist, F. Capasso, D.L. Sivco, C. Sirtori, A.L. Hutchinson, A.Y. Cho, *Science* 264 (1994) 553.
- [7] F. Capasso, C. Gmachl, D.L. Sivco, A.Y. Cho, *Phys. Today* 55 (2002) 34.
- [8] C. Sirtori, J. Nagle, *Comptes Rendus Physique* 4 (2003) 639.
- [9] D. Hofstetter, M. Beck, T. Aellen, J. Faist, *Appl. Phys. Lett.* 78 (2001) 396.
- [10] M. Beck, D. Hofstetter, T. Aellen, S. Blaser, J. Faist, U. Oesterle, E. Gini, *J. Cryst. Growth* 251 (2003) 697.
- [11] C. Sirtori, P. Kruck, S. Barbieri, P. Collot, J. Nagle, M. Beck, J. Faist, U. Oesterle, *Appl. Phys. Lett.* 73 (1998) 3486.
- [12] C. Gmachl, D.L. Sivco, J.N. Baillargeon, A.L. Hutchinson, F. Capasso, A.Y. Cho, *Appl. Phys. Lett.* 79 (2001) 572.
- [13] L. Mechold, J. Kunsch, *Laser Focus World* 40 (2004) 88.
- [14] A.A. Kosterev, F.K. Tittel, *IEEE J. Quantum Electron.* 38 (2002) 582.
- [15] A. Edelmann, C. Ruzicka, J. Frank, B. Lendl, W. Schrenk, E. Gornik, G. Strasser, *J. Chromatogr. A* 934 (2001) 123.
- [16] M. Haberkorn, Ph.D. thesis, Vienna University of Technology, Vienna, Austria, 2003.
- [17] M. Kölhed, P. Hinsmann, P. Svasek, J. Frank, B. Karlberg, B. Lendl, *Anal. Chem.* 74 (2002) 3843.
- [18] S. Schaden, M. Haberkorn, J. Frank, J.R. Baena, B. Lendl, *Appl. Spectrosc.* 58 (2004) 667.

PAPER II

S. SCHADEN
A. DOMÍNGUEZ-VIDAL
B. LENDL 

Simultaneous measurement of two compounds in aqueous solution with dual quantum cascade laser absorption spectroscopy

Institute of Chemical Technologies and Analytics, Vienna University of Technology,
Getreidemarkt 9/164AC, 1060 Vienna, Austria

Received: 6 October 2005/Revised version: 20 December 2005

Published online: 4 February 2006 • © Springer-Verlag 2006

ABSTRACT Two pulsed Fabry–Pérot quantum cascade lasers (QCL) have been employed for the simultaneous measurement of two analytes in aqueous solutions. Two laser beams (1393 and 1080 cm^{-1}) were combined by an optical system of parabolic mirrors and a ZnSe-beam splitter. Measurements were made in transmission using a $41\text{ }\mu\text{m}$ CaF_2 -flow cell and a mercury-cadmium-telluride (MCT) detector. Using glucose and sodium acetate as model analytes, the measurements show the potential of dual QCL absorption spectroscopy for analyte specific detection and background compensation. The use of the two lasers gives quantitative information about the analytes, even when they show overlapping absorption bands typically found in condensed phase.

PACS 42.55.Px; 42.62.Fi


1 Introduction

Quantum cascade lasers (QCL) have become a powerful light source for use in vibrational spectroscopy. The most attractive features for analytical applications are high spectral power density, small size, and operation without cryogenic cooling. QCLs are unipolar semiconductor lasers that differ in a fundamental way from diode lasers [1]. In QCLs the transition of electrons takes place between conduction band states arising from size quantization in semiconductor hetero structures, rather than from recombination of conduction electrons and band holes. The design of the hetero structure determines the emission wavelengths of the QCL. This design allows QCLs to cover a spectral region from $3.2\text{ }\mu\text{m}$ to far infrared (terahertz region). Applications based on QCLs take advantage of the high absorption coefficients of fundamental vibrations present in the middleinfrared, which are significantly higher than those of the corresponding overtones found in the near infrared (NIR) spectral region.

The application of QCLs for laser spectroscopy in the gas phase has already been demonstrated for several techniques such as direct absorption spectroscopy [2, 3], cavity ring down spectroscopy [4, 5], photo acoustic spectroscopy [6–8] or Faraday modulation spectroscopy [9, 10].

QCLs are not only interesting for gas phase measurements, but they are also attractive tools for measurements in condensed phase [11]. The high emission power compared to conventional infrared sources used in Fourier transform infrared (FTIR) spectrometers allows extension of the optical path for transmission measurements of aqueous samples, from typically $8\text{--}30\text{ }\mu\text{m}$ for FTIR-spectroscopy to about $120\text{--}250\text{ }\mu\text{m}$ [12]. But unlike in the gas phase, analytes dissolved in water show much broader absorption lines, often forming broad absorption bands. Therefore, it is almost impossible to find interference free, isolated absorption bands that can be used for selective quantitative analysis. One possible strategy to deal with this handicap is the use of a separation technique prior to detection for the purpose of separation of the analytes from the matrix, and to detect them one after the other as they pass the detector. This principle has been demonstrated for high performance liquid chromatography (HPLC) [13] and capillary electrophoresis (CE) [14]. Alternatively a selected chemical reaction that induces traceable changes in analyte absorption bands can also be used to enhance selectivity [11]. If separation of the analytes or selective reactions cannot be performed other strategies to measure interfering analytes have to be developed. A possible solution is the application of more than one laser. The possibility of background compensation by measuring the absorption at two QCL wavelengths has been recently demonstrated [15]. But until now such measurements had to be carried out sequentially by replacing the laser for each measurement. This is time consuming and requires higher sample volumes. With the system presented in this work, information on two different wavelength regions can be obtained simultaneously. The availability of quantitative information from an additional laser line significantly increases selectivity and robustness of the measurement system. Apart from background correction in direct sample measurements the simultaneous detection of different functional groups [13] would also be possible when the system is used as a detector in separation techniques (HPLC, CE). In addition dual QCL absorption spectroscopy also provides a route to obtain more structural information on the analytes under investigation.

For gas phase absorption measurements Barren et al. [16] recently used four QCLs and multiple pass cells. However, such an attempt for quantitative analysis in the liquid phase has not been reported so far.

 Fax: +43-1-58801-15199, E-mail: blendl@mail.zserv.tuwien.ac.at

2 Experimental

2.1 Chemicals

D(+)-Glucose monohydrate (> 99%) and sodium acetate trihydrate (> 99%) were purchased from Fluka. Stock solutions containing 50 g/l of each one of the analytes were prepared in distilled water. By further diluting, standards containing 37.5, 25, 12.5 and 1 g/l were prepared as well as mixtures of both analytes with different concentration ratios. In order to get the equilibrium alpha-beta glucose in aqueous solution, samples were prepared at least 1 h before analyzing. All solutions were also degassed for 10 min in an ultrasonic bath.

2.2 Reference spectra of the analytes

Reference FTIR spectra of standards containing 25 g/l of glucose and sodium acetate dissolved in distilled water were obtained (Fig. 1) employing a Bruker IFS 88 spectrometer (Bruker Optik) equipped with a mercury-cadmium-telluride (MCT) detector (J-15D16 Judson) and by use of a commercially available flow cell with a 25 μm optical path length. The spectra were recorded, with distilled water serving as the background, between 3000 and 700 cm^{-1} , with 4 cm^{-1} as the spectral resolution, 128 co-additions and performing a Blackman-Harris 3-Term apodization function.

2.3 Quantum cascade laser system

For the experiments two different Fabry-Pérot (FP) lasers were used, both purchased from Alpes Lasers. They show multimode emission where the intensity profile depends on the operation parameters. One showed emission at around 1393 cm^{-1} (QCL1) with a pulse power of 400 mW (n121b17) the other one at around 1080 cm^{-1} (QCL2) with a pulse power of 1000 mW (S1839a21). Both lasers were mounted in laser housings, which were filled with nitrogen and closed. The housings were also provided with silica gel pads, a Peltier element and a compartment allowing water-cooling.

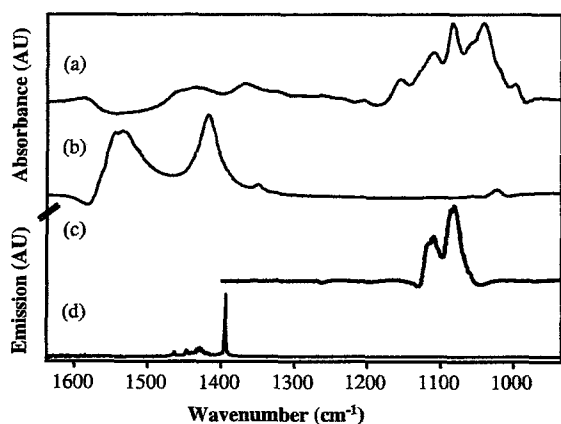


FIGURE 1 Absorption spectra of glucose (a) (25 g/l) and sodium acetate (b) (25 g/l), measured with a FTIR spectrometer in a flow cell with 25 μm optical path against water, in comparison with the emission spectra of the QCL1 (d) and 2 (c)

2.3.1 Characterization of the lasers. The emission wavelength of the QCLs under different operating conditions, especially different pulse amplitudes and operating temperatures, was first experimentally verified. For this purpose the globar light source of a Bruker Equinox 55 FTIR-spectrometer was replaced by the quantum cascade laser. This technique has already proved to be successful in former works [17]. Figure 1 shows also the emission spectra for the finally chosen parameters compared to the absorption spectra of the analytes.

2.3.2 Experimental setup. Figure 2 shows the experimental setup used for the dual QCL absorption spectroscopy. Sample handling was performed by a flow injection system (Fig. 2a). The solutions were pumped at a flow rate of 1.95 ml/min by a Gilson Minipuls3 peristaltic pump (Villiers le Bell). A Valco injection valve (Houston, TX, USA) with 340 μl as the sample loop, was used to insert the sample into the carrier stream (distilled water). Tubings were made of polytetrafluoroethane (PTFE) and of 0.75 mm i.d. Upon injection the sample was transported to the detector where a flow injection peak was recorded as the dispersed sample plug passed the flow cell. Dispersion of the system was determined [18] to be 1.03 and the distance between injection point and detection point was 52 cm. The flow cell was purchased from Perkin

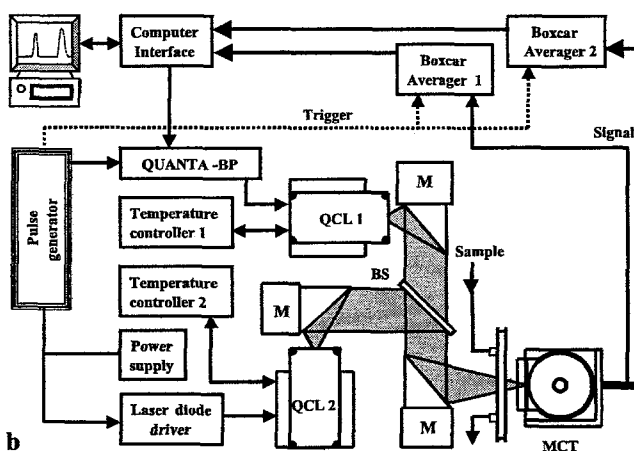
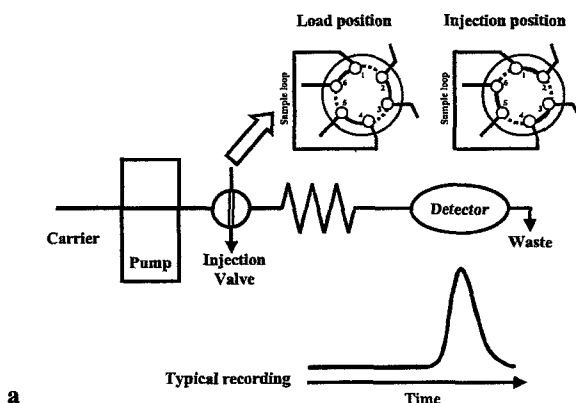


FIGURE 2 Experimental setup. (a) Scheme of the flow injection system used with typical flow injection peak as analytical readout detail: injection valve in load and inject position. (b) QCLs system, BS: beam splitter, MCT: mercury cadmium telluride detector, M: parabolic mirror

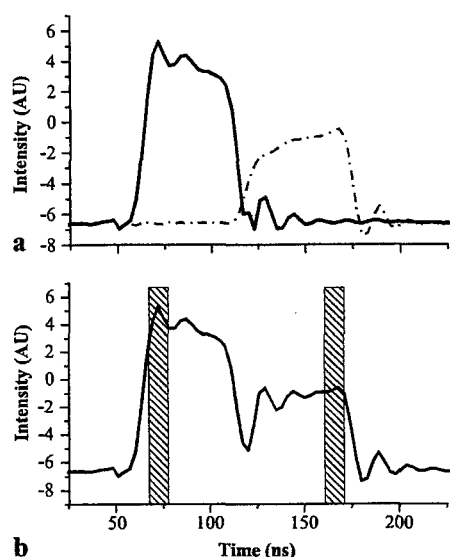


FIGURE 3 Recording of the pulse shapes using the time resolved detector signal. (a) Individual pulse shapes for QCL1 at 1393 cm^{-1} (solid line) and for QCL2 at 1080 cm^{-1} (dash-dotted line); (b) signal if both QCLs are active, including markers for the evaluated signal intervals

Elmer (Wellesley, MA, USA), equipped with CaF_2 windows of 2 mm of width and a spacer forming an optical path of 41 μm .

The QCL system has two major parts: the optical system and the combined laser control-signal processing system (Fig. 2b).

Manufacturer specifications claim divergence of around 60° in the vertical axis and about 40° in the horizontal axis of the QCL beams; so for each laser a parabolic mirror was used to generate a parallel beam. These mirrors were made of aluminum with a gold-coated surface and they have a focal length of 43.1 mm and 44 mm in diameter. The beams of both lasers were sent with a 45° angle, with one on each side of a beam splitter to combine them through the flow cell. The beam splitter was made of a ZnSe plate of 3 mm thickness. The transmitted beam of the QCL1 and the reflected beam of the QCL2 were collimated with a parabolic mirror similar to that previously described, but with a focal distance of 69 mm. The longer focal distance resulted in a smaller aperture angle that made it possible to place the flow cell between the mirror and its focus. In this way both beams were focused through the flow cell on the detector element of an MCT detector KMPV12-0,1-J1/100MHZ (Kolmar Technologies).

The QCLs were operated with two different driving equipments: the Alpes Lasers starter kit and a specially fabricated laser driver from Laser Components (QUANTA-BP), which

needs a trigger input as information for the pulse repetition rate and two direct current control voltages for the pulse length and for the pulse amplitude. As already described in previous works [17], the low impedance line cable from the starter kit was exchanged to a special shielded version to reduce pick-up noise in the electronic system.

A working temperature of -30°C and pulse duration of 50 ns with a repetition frequency of 20 kHz were set as the operating parameters, resulting in a duty cycle of 0.1% and an average power of 0.4 (QCL1) and 1 mW (QCL2). The pulse currents used for driving the lasers were 2.4 A and 4.1 A, for QCL1 and QCL2 respectively. These values mean, in both cases, around 95% of the maximum specified by the producers. Custom software was used to control the pulse duration and pulse amplitude of the QCL1 via a computer interface and the laser driver (QUANTA-BP). The pulse generator of the starter kit acted as the central device for timing and synchronization of the whole system. It was used to drive the QCL2 via the laser diode driver (LDD) unit and to trigger the laser driver controlling the QCL1 too. Figure 3a shows that the instrumentation specific delay between the trigger signal for the QUANTA-BP and the pulse output for the LDD unit resulted in a spacing between the two laser pulses of approximately 55 ns, which allows for their simultaneous detection.

The detector signal was split and processed using two Boxcar Averagers Model SR250 (Stanford Research Systems) where each one was used to evaluate one QCL signal by averaging the value of 10 000 pulses within a 10 ns gate. The location of the gates within the QCL pulses can be seen in Fig. 3b. The analog output signals of the boxcar averagers were converted into a digital signal using a computer interface model SR245 (Stanford Research Systems). The signal from both QCLs was recorded using custom software. A new value was recorded and stored every second.

3 Data analysis

The recorded data were further evaluated using a spreadsheet software program. The recorded transmission was first calculated into absorbance values. Low frequency drifts appearing during the measurements were eliminated using baseline subtraction. The flow injection peaks of each injected standard as well as from the sample mixtures were evaluated based on the calculated peak areas.

4 Results

Calibration curves were established for both analytes. For this purpose, standards and their mixtures were injected into the flow system and the resulting flow injection peaks recorded. The recording following the absorption

Analyte	Wavenumber (cm^{-1})	Slope ($\text{AU}/(\text{g/l})$)	Intercept (AU)	r^2	s_{x0} (g/l)
Sodium Acetate	1393	8.5×10^{-3}	4.1×10^{-3}	0.9932	1.54
Glucose	1393	1.7×10^{-3}	4.0×10^{-4}	0.9934	1.53
Glucose	1080	8.9×10^{-3}	6.7×10^{-3}	0.9989	0.61

s_{x0} : standard deviation of the method according to ISO: 8466-1

TABLE 1 Linear regression data of the calibration lines for both QCLs

TABLE 2 Recovery values of four samples containing both analytes. Real concentrations are also given

Glucose (at 1080 cm ⁻¹)	Sample 1	Sample 2	Sample 3	Sample 4
Real concentration (g/l)	40	30	20	10
Recovery (%)	97.6 ± 1.9	96.5 ± 2.2	94.1 ± 1.7	89.1 ± 5.0
Sodium Acetate (at 1393 cm ⁻¹)	Sample 1	Sample 2	Sample 3	Sample 4
Real concentration (g/l)	10	20	30	40
Recovery without correction (%)	187.2 ± 8.8	133.6 ± 2.7	118.8 ± 3.3	107.7 ± 6.7
Recovery with correction (%)	109.0 ± 10.2	104.6 ± 3.2	106.2 ± 3.3	103.3 ± 6.8

at 1393 cm⁻¹ was used for sodium acetate, and at 1393 cm⁻¹ as well as at 1080 cm⁻¹ for glucose. Measurements were made in triplicate. The analytical parameters are given in Table 1. Figure 4 shows as an example, a complete run of measurements, consisting of pure standards followed by the four samples containing both analytes at different concentrations. The gained calibration was used to determine the amount of glucose and sodium acetate contained in the sample mixtures. Glucose concentration could be obtained directly from the absorption at 1080 cm⁻¹ but it showed strong interference at 1393 cm⁻¹ used for determination of sodium acetate. To remove this interference the contribution in absorption of glucose at 1393 cm⁻¹ was calculated considering the simultaneously recorded values at 1080 cm⁻¹ and subtracted from the measured values at 1393 cm⁻¹. In this way interference from glucose in the determination of acetate could be avoided. Table 2 shows the obtained results. Without the correction of the absorption values using the information of the second laser line, the recoveries percentages of sodium acetate were higher, coming from a wrong estimation of the concentration of acetate due to the influence of glucose in the signal. Nevertheless it has to be men-

tioned that the standard error in determination of the glucose concentration is propagated into the calculation of the corrected sodium acetate values. Therefore, the corrected values show a higher standard deviation than the uncorrected ones.

The application of a beam splitter in the setup leads to a loss in intensity of the QCL beams probing the flow cell. However, the reflected beam that is so far not used, could be recorded to correct for pulse-to-pulse fluctuations in the emitted laser power. This would enhance the analytical figures of merit of the proposed method. Further improvements are seen in the use of driving electronics allowing a higher time delay between the pulses of the two QCLs, which in turn would allow the use of a detector with a lower time constant but higher sensitivity.

In the experimental set up both lasers are operated quasi simultaneously with one data point recorded per laser and second. Considering the typical dwell times of a flow injection or chromatographic experiment, sufficient data points are recorded to accurately measure the passage of the sample through the cell. Measurement of the laser emission lines before and after the measurement campaign confirmed constant laser emission characteristics. Due to the small laser sizes and thermoelectric temperature control, efficient miniaturization of the experimental set-up is possible, opening the path for application on-line or in-line measurement of liquid process streams.

5 Conclusions

Combinations of quantum cascade laser beams for quantitative studies in condensed phase is a very promising concept in analytical chemistry. We have demonstrated the feasibility of simultaneous absorption measurements with two Fabry-Pérot QCLs in aqueous solutions. Selective measurements of the two analytes (glucose and acetate) present at the same time were performed by using information on the absorption at two different wavelengths (1393 cm⁻¹, 1080 cm⁻¹). Overlapping absorption bands at 1393 cm⁻¹ could be evaluated by compensation measurements of the specific absorption band of only one analyte (glucose) at 1080 cm⁻¹. This technique allows not only simultaneous determination of two analytes but also a background compensation for determination in changing matrices. Additionally dual QCL spectroscopy can be used for group specific detection of analytes in combination with a separation technique prior to detection.

ACKNOWLEDGEMENTS Financial support received from the Austrian Science Fund within the project FWF I5531 is acknowledged. A.D. is also grateful for a postdoctoral grant from the Ministerio de Educación y Ciencia, Secretaría de Estado de Universidades e Investigación (Spain).

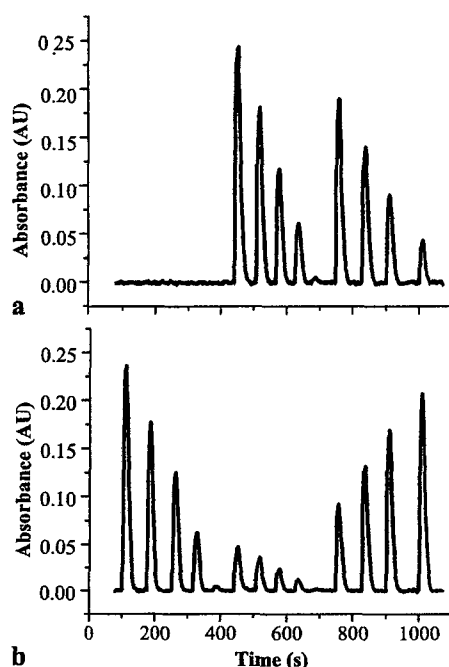


FIGURE 4 Simultaneously measured absorptions at two different wavelengths: (a) 1080 cm⁻¹, (b) 1393 cm⁻¹. Order of injections: sodium acetate standards (50, 37.5, 25, 12.5 and 1 g/l), glucose standards (50, 37.5, 25, 12.5 and 1 g/l) and mixtures of both analytes (sodium acetate + glucose: 10 + 40, 20 + 30, 30 + 20 and 40 + 10 g/l)

REFERENCES

- 1 J. Faist, F. Capasso, D.L. Sivco, C. Sirtori, A.L. Hutchinson, A.Y. Cho, *Science* **264**, 553 (1994)
- 2 D.D. Nelson, B. McManus, S. Urbanski, S. Herndon, M.S. Zahniser, *Spectrochim. Acta A* **60**, 3325 (2004)
- 3 G. Wysocki, A.A. Kosterev, F.K. Tittel, *Appl. Phys. B* **80**, 617 (2005)
- 4 B.A. Paldus, C.C. Harb, T.G. Spence, R.N. Zare, C. Gmachl, F. Capasso, D.L. Sivco, J.N. Baillargeon, A.L. Hutchinson, A.Y. Cho, *Opt. Lett.* **25**, 666 (2000)
- 5 A.A. Kosterev, A.L. Malinovsky, F.K. Tittel, C. Gmachl, F. Capasso, D.L. Sivco, J.N. Baillargeon, A.L. Hutchinson, A.Y. Cho, *Appl. Opt.* **40**, 5522 (2001)
- 6 B.A. Paldus, T.G. Spence, R.N. Zare, J. Oomens, F.J.M. Harren, D.H. Parker, C. Gmachl, F. Capasso, D.L. Sivco, J.N. Baillargeon, A.L. Hutchinson, A.Y. Cho, *Opt. Lett.* **24**, 178 (1999)
- 7 M.G. da Silva, H. Vargas, A. Miklos, P. Hess, *Appl. Phys. B* **78**, 677 (2004)
- 8 A.A. Kosterev, Y.A. Bakhrkin, F.K. Tittel, *Appl. Phys. B* **80**, 133 (2005)
- 9 H. Ganser, W. Urban, A.M. Brown, *Mol. Phys.* **101**, 545 (2003)
- 10 H. Ganser, M. Horstjann, C.V. Suschek, P. Hering, M. Murtz, *Appl. Phys. B* **78**, 513 (2004)
- 11 B. Lendl, J. Frank, R. Schindler, A. Muller, M. Beck, J. Faist, *Anal. Chem.* **72**, 1645 (2000)
- 12 M. Kolhed, M. Haberkorn, V. Pustogov, B. Mizaikoff, J. Frank, B. Karlberg, B. Lendl, *Vibrational Spectrosc.* **29**, 283 (2002)
- 13 A. Edelmann, C. Ruzicka, J. Frank, B. Lendl, W. Schrenk, E. Gornik, G. Strasser, *J. Chromatography A* **934**, 123 (2001)
- 14 M. Kolhed, S. Schaden, B. Karlberg, B. Lendl, *J. Chromatography A* **1083**, 199 (2005)
- 15 W.B. Martin, S. Mirov, R. Venugopalan, *Appl. Spectrosc.* **59**, 881 (2005)
- 16 R.E. Baren, M.E. Parrish, K.H. Shafer, C.N. Harward, S. Quan, D.D. Nelson, J.B. McManus, M.S. Zahniser, *Spectrochim. Acta A* **60**, 3437 (2004)
- 17 S. Schaden, M. Haberkorn, J. Frank, J.R. Baena, B. Lendl, *Appl. Spectrosc.* **58**, 667 (2004)
- 18 J. Ruzicka, E.H. Hansen, *Flow Injection Analysis* (Wiley, New York 1988)

PAPER III

Online reaction monitoring in liquid phase using two mid-IR quantum cascade lasers simultaneously

Stefan Schaden, Ana Domínguez-Vidal and Bernhard Lendl*

Institute of Chemical Technologies and Analytics, Vienna University of Technology,
Getreidemarkt 9/164AC A-1060, Vienna, Austria.

*Author to whom correspondence should be sent: blendl@mail.zserv.tuwien.ac.at

ABSTRACT

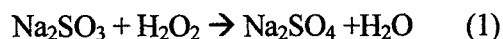
Online Monitoring of a model reaction was performed by employing two pulsed mid-IR Fabry P  rot Quantum cascade lasers (QCL). The emission maxima of the QCLs were located at 1393 and 1080 cm^{-1} . An optical system of parabolic mirrors and a ZnSe-beam splitter combined the two laser beams and allowed to probe a transmission cell with both QCLs simultaneously. The reaction mixture was pumped continuously through a cell that had an optical path of 48 μm . This dual QCL system allowed fast absorption measurements of the reaction mixture at two distinct wavenumbers. The reaction under study was the oxidation of sulphite to sulphate with hydrogen peroxide acting as oxidant. On-line measurements of the chemical reaction allowed direct, real-time monitoring of sulphate formation and hydrogen peroxide depletion.

Index Headings: Quantum cascade laser; MID-IR, online monitoring, sulfit oxidation

INTRODUCTION

Quantum cascade lasers¹ (QCL) have become a powerful light source for use in vibrational spectroscopy. Most attractive features for analytical applications are room temperature or near room temperature operation, high spectral power density and small size. The wavelength of QCLs can be tailored by micro-machining technology providing access to almost any wavelength in the mid-IR spectral region. Due to their characteristics, QCLs hold promise to be used in robust and compact sensing devices. So far QCLs have predominantly been used for gas phase monitoring^{2,3} using different spectroscopic methods^{4,5,6,7}. In these applications the match between sharp laser lines and the rotational-vibrational transitions present in gas phase made high selective and sensitive measurements possible. Analytes present in liquids generally show absorptions significantly broader than QCL emission lines, especially when dealing with distributed feedback QCLs⁸. However, for liquid phase analysis a new generation of chemical process analysers can be conceived due to the possibilities offered by developing QCL technology^{9,10}. Based on the high spectral power density of QCLs, longer paths for transmission measurements than possible with FT-IR based analysers can be realized with positive impact on sensitivity and robustness of measurements¹¹. Other strategies are the application of waveguides or fibers for evanescent field measurements as recently demonstrated^{12,13}. Also, to assure long term stability of QCL based analyzers, a reference wavelength would be highly desirable. However, contrary to the gas phase¹⁴ only one quantum cascade laser at a time has been used in liquid phase analysis so far^{11,15}. Measurements at different wavenumbers had to be performed consecutively, which made it impossible to follow dynamic systems such as chemical reactions at two distinct wavenumbers.

In this study we present a system that is capable to operate and to record the signal of two Fabry Pérot QCLs simultaneously, one with an emission maxima located at 1393 cm^{-1} and the other one with the maxima located at 1080 cm^{-1} . The chemical system chosen to demonstrate simultaneous online measurements with two QCLs in aqueous solutions was the oxidation of sulphite to sulphate with hydrogen peroxide as described in eqn. (1):



METHODOLOGY

Reagents and Instrumentation

Sodium sulphate and sodium sulphite were purchased by Fluka (Buchs, Switzerland). Hydrogen peroxide (30% mass) was obtained from Merck (Darmstadt, Germany). Stock solutions of the analytes were prepared in distilled water.

The whole set up is shown in Fig. 1. The optical system consists of parabolic mirrors for collecting the emitted laser radiation, a beam splitter for combining the two QCL beams and one parabolic mirror located behind the beam splitter for focusing the beams through a flow cell on a liquid nitrogen cooled photovoltaic MCT detector (Kolmar Technologies, Newburyport, MA, USA), located behind the flow cell. The optical path of the cell was determined to be $48\text{ }\mu\text{m}$. For the experiments two different Fabry Pérot (FP) Lasers were used, both purchased from Alpes Lasers (Neuchâtel, Switzerland). They were operated with two different driving equipments: one with the Alpes Lasers starter kit and the other one with a specially fabricated laser driver QUANTA-BP (Laser Components, Olching, Germany) that can be attached to the laser housing from Alpes Lasers. The instrumentation specific delay in the time response of the two devices to the synchronic trigger input resulted in a spacing between the two laser pulses of approximately 55 ns,

which allows for their simultaneous detection. Using the same driving equipment for both QCLs would demand a more sophisticated trigger unit to do so. In both cases the operation parameters were set as follows: heat sink temperature -30°C , pulse frequency 20 kHz, pulse duration 50 ns and pulse amplitude of about 95% of the specified maximum. For timing and synchronization of the whole system, a pulse generator (Alpes Lasers) acted as the central device. The QCLs were operated with a time delay of 55 ns. The detector signal was split and processed with two boxcar averagers (Stanford Research Systems, Sunnyvale, California, USA) where each QCL signal was evaluated separately by averaging the value of 10,000 pulses within a 10 ns gate. With the data acquisition software (Sagittarius, vs. 3.0) a new value for each QCL signal could be stored every second. To get the offset of the detector signal, the beam line was interrupted.

Experimental procedure

The reaction was performed in a 250 ml three-necked flask, equipped with a 25ml tap funnel and a thermometer. The reaction mixture was magnetically stirred. A peristaltic pump was used to establish a continuous flow (2 ml/min) of the reaction mixture through the cell and back into the flask. The time required for pumping the solution from the flask into the cell was 30 seconds. In order to prevent decomposition of the hydrogen peroxide prior to reaction, the flask was cooled with a mixture of water and ice (resulting temperature of the reaction mixture: $2-3^{\circ}\text{C}$).

In all experiments the flask contained 85 ml of an aqueous solution A, where 25 ml of an aqueous solution B were added during 7 minutes. Two different types of experiments were carried out. First the flask contained 1.28 g of hydrogen peroxide (solution A). The

experiment was repeated with different amounts of sodium sulphite (1-4 g) dissolved in solution B.

In a second experiment sodium sulphite was placed in the reaction flask (solution A) and 1.28 g hydrogen peroxide in 25 ml distilled water (solution B) was added over a period of 7 min. This experiment was also repeated with different amounts of sodium sulphite (1-4g) dissolved in solution A.

RESULTS AND DISCUSSION

The absorption spectra of all three substances as well as the emission spectra of both QCLs are shown in Fig. 2. The chosen concentrations for the spectra of sulphate (a) and sulphite (b) were 47 g/L which corresponds to the sulphite concentration at the beginning of the reaction. Also for the spectra of hydrogen peroxide (c) the initial concentration was chosen (15 g/L). Hydrogen peroxide shows weak and broad absorption around the emission of QCL1 (1393 cm^{-1}). The sulphite ion shows a weak absorption band at the emission of QCL2. Sulphate shows approximately nine times higher absorption at the emission of QCL2 than sulphite.

Changes in absorbance when sulphite was added to the peroxide solution are displayed in Fig. 3. The intensity recorded with QCL1 and QCL2 prior to addition of sulphite was used as background for calculating the absorbance values during the reaction. The absorption value for QCL2 is clearly increasing during the addition of sulphite as a result of the ongoing sulphate formation. On the other hand hydrogen peroxide consumption took place that led to a decreasing absorption for QCL1. Sulphite absorption is not observed as the excess of hydrogen peroxide directly oxidizes it to sulphate. Also well visible is the dependence of both absorptions on the initial sulphite concentration.

The resulting changes of the absorption values shown in Fig. 4 correspond to the experiment where peroxide was added to sulphite solutions. The signal intensities recorded for QCL1 and QCL2 at the beginning of the experiment were again taken as background.

The absorptions for QCL2 show similar characteristics as obtained in the antecedent experiment. However a difference is observable close to the end of the hydrogen peroxide addition. In the moment the whole amount of sulphite had been oxidised, the absorption is slightly decreasing again. This can be explained by dilution caused by the excess of added hydrogen peroxide solution. The absorption profile for the QCL1 shows a more complex behaviour since two substances – sulphite as well as hydrogen peroxide – contribute to the signal. At higher sulphite concentrations a decrease of the absorption can be noticed at the beginning of the hydrogen peroxide addition. Close to the end the hydrogen peroxide concentration in the reaction mixture is rising and so does the absorption. At lower sulphite concentration the effect of decreasing sulphite absorption and increasing hydrogen peroxide absorption are overlapping. Nevertheless a relation between the sulphite concentration and the hydrogen peroxide conversion is also visible in this experiment.

For a first estimation of the limits of detection of the system, the absorption values of the analytes with distilled water serving as background were determined. Sulphite and hydrogen peroxide concentrations corresponding to the initial levels of the reaction and a sulphate concentration corresponding to the end level of the reaction were measured for one minute. According to three times the noise, limits of detection were calculated (Table 1).

CONCLUSIONS

The developed experiments have proven the capability of the dual quantum cascade laser set up to directly measure increase and decrease of the concentration of the different molecules in aqueous solutions. This concept can in principle be extended to multiple QCLs. In the conceived process analyzers these different wavelengths may also be integrated in one laser unit, which thus would substantially reduce the size of the experimental set-up. Apart from multianalyte determination capability, the advantage of dual or multi-QCL detection is seen in improved long term stability of the sensor systems because of possible background compensations.

ACKNOWLEDGEMENTS

Financial support received from the Austrian Science Fund within the project FWF 15531 is acknowledged. A.D. is also grateful for a postdoctoral grant from the *Ministerio de Educación y Ciencia*, Secretaría de Estado de Universidades e Investigación (Spain).

Reference List

1. J. Faist, F. Capasso, D.L. Sivco, C. Sirtori, A.L. Hutchinson, A.Y. Cho, *Science* **264**, 553 (1994)
2. A.A. Kosterev, F.K. Tittel, *Ieee Journal of Quantum Electronics* **38**, 582 (2002)
3. F.K. Tittel, D. Richter, A. Fried, *Solid-State Mid-Infrared Laser Sources* **89**, 445 (2003)
4. B.A. Paldus, C.C. Harb, T.G. Spence, R.N. Zare, C. Gmachl, F. Capasso, D.L. Sivco, J.N. Baillargeon, A.L. Hutchinson, A.Y. Cho, *Optics Letters* **25**, 666 (2000)
5. Y.A. Bakhirkin, A.A. Kosterev, C. Roller, R.F. Curl, F.K. Tittel, *Applied Optics* **43**, 2257 (2004)
6. A.A. Kosterev, Y.A. Bakhirkin, F.K. Tittel, *Applied Physics B-Lasers and Optics* **80**, 133 (2005)
7. H. Ganser, M. Horstjann, C.V. Suschek, P. Hering, M. Murtz, *Applied Physics B-Lasers and Optics* **78**, 513 (2004)
8. J. Faist, C. Gmachl, F. Capasso, C. Sirtori, D.L. Sivco, J.N. Baillargeon, A.Y. Cho, *Applied Physical Letters* **70**, 2670 (1997)
9. B. Lendl, J. Frank, R. Schindler, A. Muller, M. Beck, J. Faist, *Analytical Chemistry* **72**, 1645 (2000)

10. S. Schaden, M. Haberkorn, J. Frank, J.R. Baena, B. Lendl, *Applied Spectroscopy* **58**, 667 (2004)
11. M. Kolhed, M. Haberkorn, V. Pustogov, B. Mizaikoff, J. Frank, B. Karlberg, B. Lendl, *Vibrational Spectroscopy* **29**, 283 (2002)
12. C. Charlton, A. Katzir, B. Mizaikoff, *Analytical Chemistry* **77**, 4398 (2005)
13. J.Z. Chen, Z. Liu, C.F. Gmachl, *optics express* **13**, 5953 (2005)
14. R.E. Baren, M.E. Parrish, K.H. Shafer, C.N. Harward, S. Quan, D.D. Nelson, J.B. McManus, M.S. Zahniser, *Spectrochimica Acta Part A-Molecular and Biomolecular Spectroscopy* **60**, 3437 (2004)
15. Martin W.B., Mirov S., Venugopalan R, *Applied Spectroscopy* **59**, 881 (2005)

FIGURE CAPTIONS

Fig. 1. Schematic of the experimental setup. BS: beam splitter, MCT: Mercury Cadmium Telluric detector, M: Mirror, QCL: Quantum cascade laser, T: Thermometer

Fig. 2. Absorption spectra of sodium sulphate 374 mM (a), sodium sulphite 374 mM (b), hydrogen peroxide 568 mM (c) and emission spectra of the quantum cascade lasers QCL1 (d) and QCL2 (e).

Fig. 3. Recorded absorptions for QCL2 around 1080 cm^{-1} (a) and QCL1 around 1393 cm^{-1} (b). Different amounts of sodium sulphite dissolved in 25 ml distilled water were added to 1.28g hydrogen peroxide dissolved in 85 ml distilled water.

Fig. 4. Recorded absorptions of QCL2 around 1080 cm^{-1} (a) and QCL1 around 1393 cm^{-1} (b). 1.28 g hydrogen peroxide dissolved in 25 ml distilled water was added to different amounts of sodium sulphite dissolved in 85 ml distilled water.

Figure 1

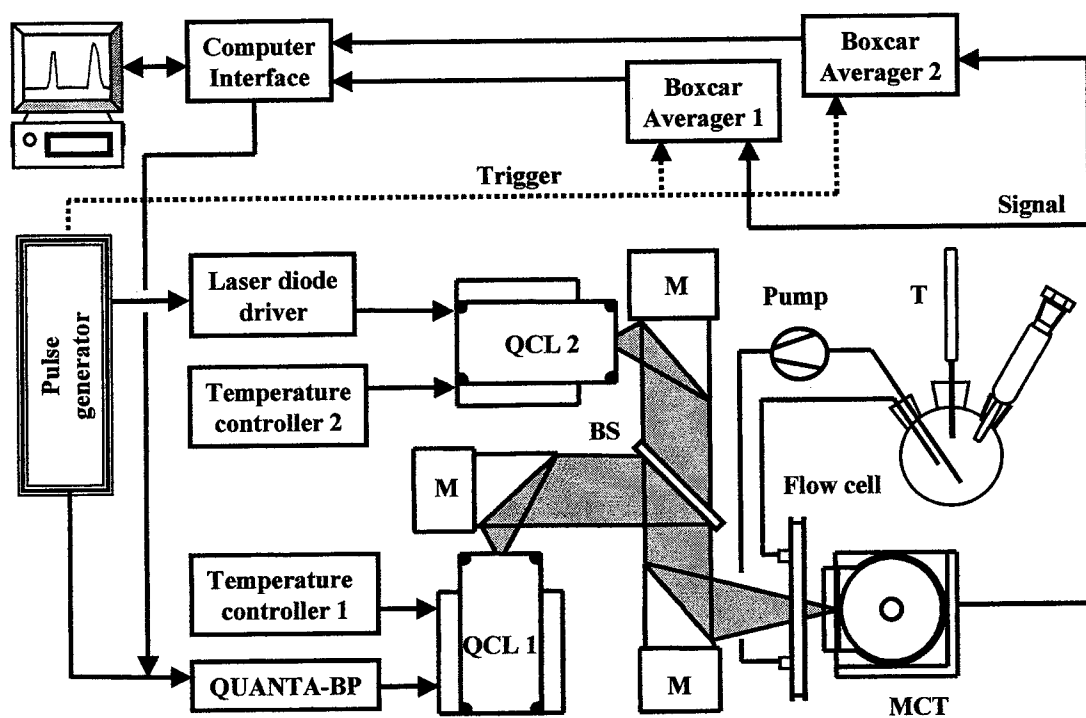


Figure 2

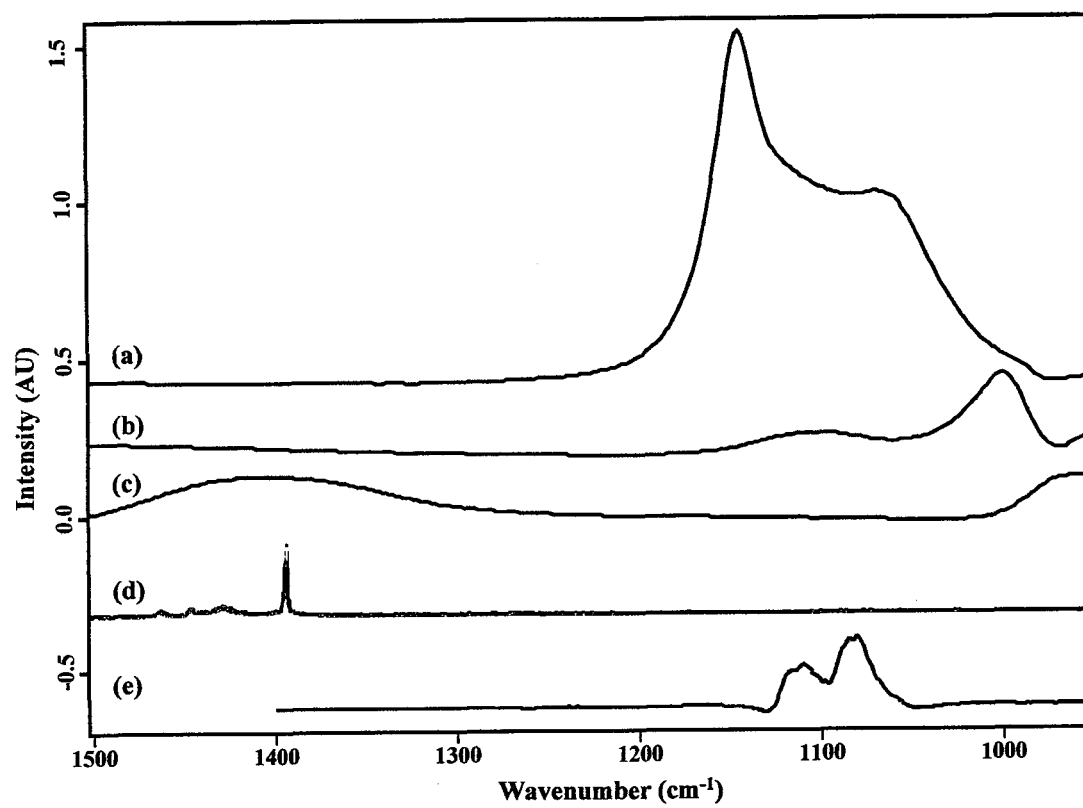


Figure 3

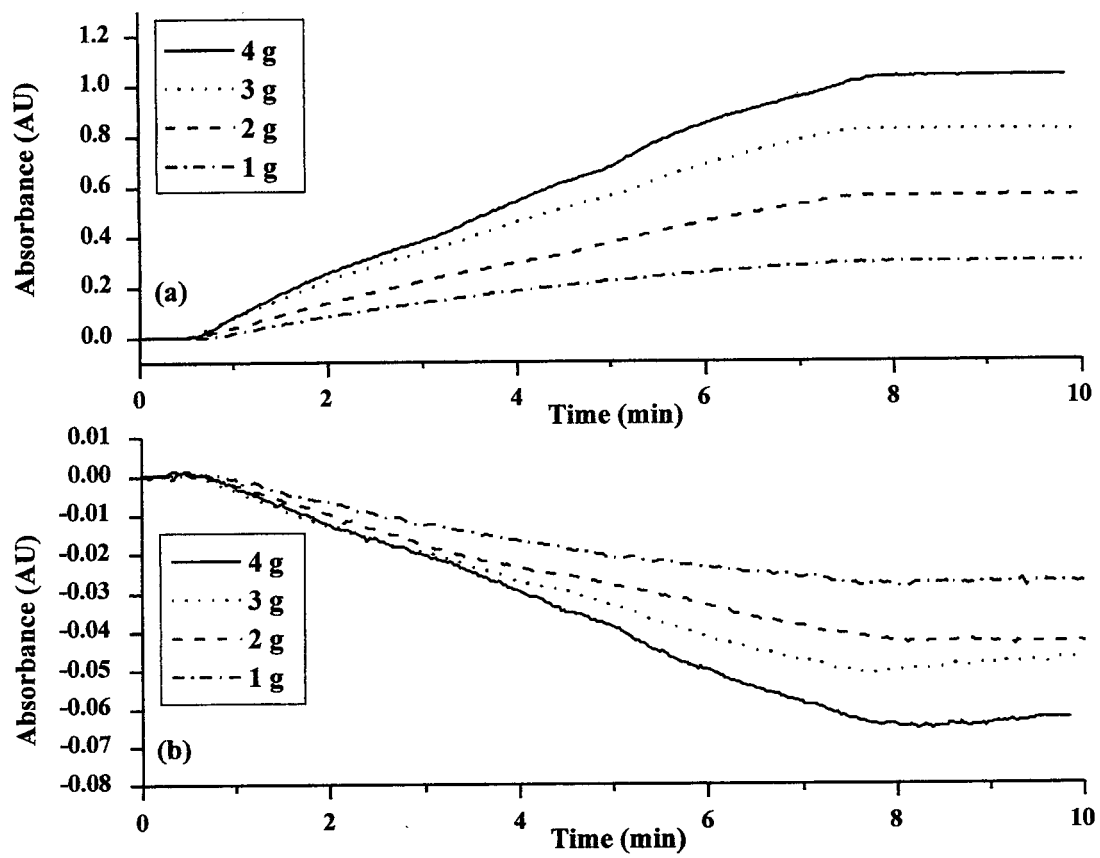


Figure 4

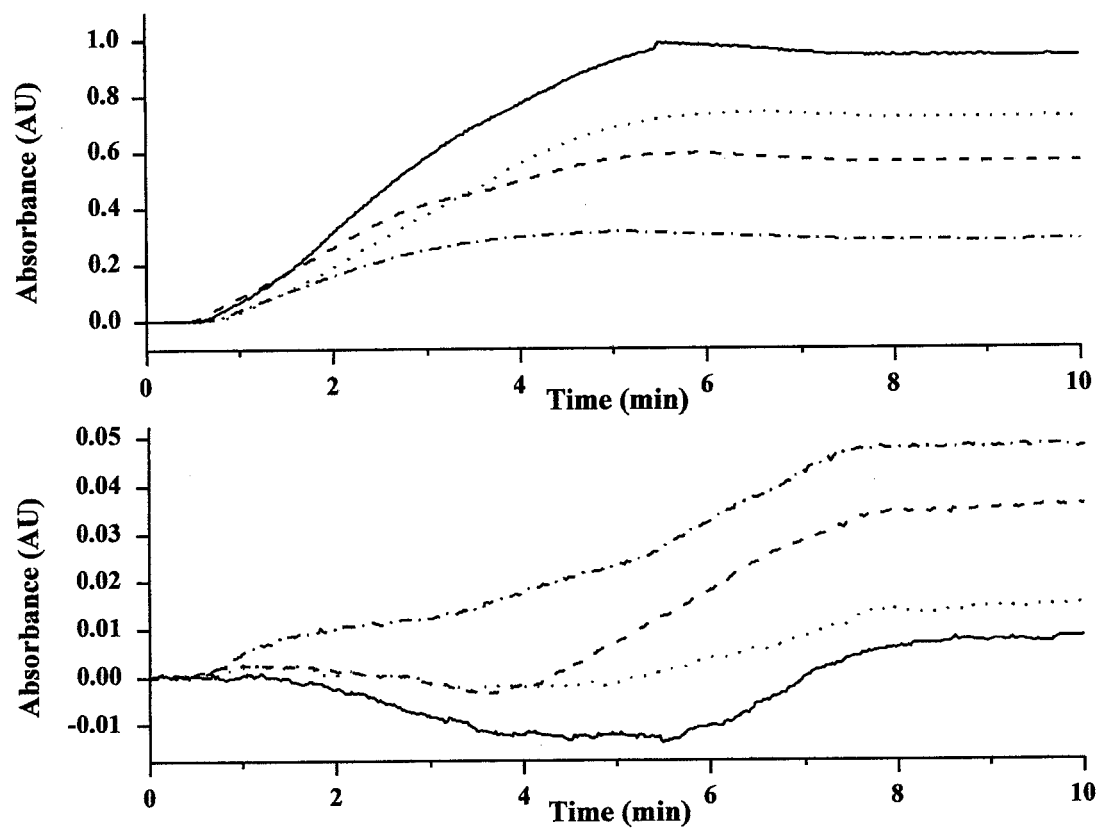


Table 1. Estimation of the limits of detection

Analyte	Limits of detection (mM) measured at	
	1393 cm^{-1}	1080 cm^{-1}
Hydrogen peroxide	9.61	-----
Sulphite	65.69	12.91
Sulphate	-----	3.66

PAPER IV

Quantum cascade laser modulation for correction of matrix induced background changes in aqueous samples

S. Schaden, A. Domínguez-Vidal, and B. Lendl^a

Institute of Chemical Technologies and Analytics, Vienna University of Technology,

Getreidemarkt 9/164AC, A-1060 Vienna, Austria

^aCorresponding author. FAX: +43 1 58801 15199; Phone: +43 1 58801 15140

E-mail: blendl@mail.zserv.tuwien.ac.at

Running title: Quantum cascade laser modulation for correction of matrix induced background changes in aqueous samples

Abstract

A robust method for the determination of carbon dioxide in sugar containing solutions using a single distributed feedback quantum cascade laser (QCL) has been developed. By switching the driving current between two selected values, 1.6 and 1 A, emission wavelengths at 2341.4 and 2341.6 cm⁻¹ could be achieved.

The method is based on absorbance measurements in transmission and the calculation of the absorbance differences between both wavenumbers. This allows the elimination of indirect matrix interference produced on carbon dioxide measurements with increasing sugar concentrations. A flow injection setup was employed to in situ produce carbon dioxide standards from a series of bicarbonate solutions (0-3 g/l) by adjusting the pH with a sodium hydroxide/citric acid buffer solution to pH 3.13. Different concentrations (0-

90g/l) of sugar were also mixed on line with the analyte to study their influence on carbon dioxide measurement. As the difference in the two evaluated wavelengths is small compared to the absorption peak of CO₂, the analytical readout of the QCL modulation can be seen as a proportional parameter to the first derivative of FTIR spectra in this spectral region.

PACS

42.55.Px (Semiconductor lasers; laser diodes); 42.62.Fi (Laser spectroscopy)

1 Introduction

Mid Infrared Laser Spectroscopy is a powerful tool for many sensing applications[1,2]. Most molecules exhibit their fundamental vibrations in the mid-infrared region showing higher absorption coefficients than the overtones in the near infrared. Compared to broadband emitters, laser light sources provide increased spectral power densities enabling to improve signal to noise ratios and hence reduced detection limits. The demands on the laser source[1] are a compact design, a narrow line width and preferable room temperature or near room temperature operation. Ideally, the wavelength should be tuneable across absorption lines of one or more analytes. Quantum cascade lasers (QCLs) are semiconductor lasers that can easily fulfill these demands in gas sensing applications. The light generation in QCLs is based on intersubband transition within the conduction band [3]. The electron states arise from size quantisation in semiconductor heterostructures. The wavelength can be tailored by bandstructure engineering over a

wide spectral region and to the particular need of a given application. The distributed feed back [4] (DFB) design ensures narrow line width. Most application of QCLs aim at the detection of trace gases [5-10] with various techniques. In the gas phase mostly - with some exceptions [11] - it is usually possible to find background free, isolated absorption lines that can be used for sensitive and selective measurements.

However, absorption bands in condensed phase are much broader than in gas phase and spectral overlapping is commonly frequent. For some applications in liquid phase it is advisable to apply more than one laser to explore an extended wavelength region. Martin et al. [12] demonstrated this for the monitoring of glucose in serum by performing subsequent measurements at 1036 and 1194 cm^{-1} on the same sample. An improved setup allowing for quasi simultaneous measurements using two Fabry-Pérot QCLs (1393 and 1080 cm^{-1}) has recently been reported by Schaden et al. and applied to the simultaneous measurement of glucose and sodium acetate [13] as well as sulfite/sulfate and peroxide [14]. Separation of the analytes from interfering matrix molecules prior to the detection as well as a chemical modulation to induce analyte characteristic spectral changes are alternative strategies to increase selectivity in liquid phase. This was demonstrated for QCL absorption spectroscopy in combination with high performance liquid chromatography [15], capillary electrophoresis [16] and flow injection analysis [17].

The high spectral power density of QCLs as compared to thermal light sources brings also substantial advantages for liquid phase measurement. In this context the possibility of increasing the employed optical path for transmission measurements from typically 8-30 μm as used in FTIR-Spectroscopy to about 120-150 μm [18] must be mentioned.

Beside spectral overlapping of the analytes and strong solvent absorption FTIR spectroscopy in aqueous phase is often made difficult by changes in the water background absorption arising from pH changes [19] or changing concentrations of solutes [20-22]. As a consequence baseline changes are often observed in the analyte spectra. Calculation of first derivative spectra is a common approach to compensate for baseline drifts arising from these effects. To apply this concept to QCL spectroscopy it becomes essential to perform measurements at least at two neighboring wavelengths. Evaluation of the recordable absorbance differences is thus a promising approach for robust QCL absorption spectroscopy in liquid phase.

In this paper we used the above outlined concept for the first time to compensate for matrix interferences in the determination of CO₂ due to changing sugar concentrations. The possibility of a QCL based measurement of dissolved CO₂ has been demonstrated previously using a single wavelength for analysis [23]. However, further studies showed that for the realization of a robust QCL based process analyzer for CO₂ means to correct changes in the water background absorption due to the presence of other constituents in beverages had to be found.

2 Experimental

2.1 Chemicals

All used chemicals were of analytical grade. Fructose, sucrose and sodium hydrogen carbonate (NaHCO₃) were purchased from Merck. Glucose and sodium hydroxide (NaOH) were purchased from Fluka and citric acid from Sigma/Aldrich. All solutions were prepared in distilled water. The buffer solution (100mM) was prepared by

dissolving citric acid crystals in distilled water and adjusting the pH value to 3.13 with a 1 M NaOH solution.

2.2 Flow system setup and procedure

The manifold (Fig.1a) consisted of a Gilson Minipuls 3 peristaltic pump (Gilson S.A., Villiers Le Bel, France) and two multi-port selection valves (Valco Instruments, Houston, TX). All tubings were made of polytetrafluoroethane (PTFE) and had an inner diameter of 0.75 mm. The flow rates used were 2.0 mL/min for the buffer, 1.8 mL/min for the NaHCO₃ standards and 1.9 mL/min for the sugar solutions.

A series of bicarbonate standards is mixed on line with the buffer solution. In this way, acidic pH shifts the reaction equilibrium (eq. 1, pKa=3.6) to produce in situ carbonic acid. Carbonic acid is present in equilibrium with its hydrated anhydride (CO₂ aq). As this equilibrium (eq. 2, pKa=2.77), is strongly on the side of CO₂ aq, this species needs to be monitored.



NaHCO₃ standards (0, 1, 2 and 3 g/l) were used to obtain a defined concentration of aqueous CO₂ (0, 165, 331 and 496 mg/l) in the cell. Common used sugars, sucrose, fructose and glucose as well as mixtures (1:1:1) showed similar influence on the water background in the region where our measurements are made (Fig. 2). Therefore, to study the influence of the sugars in the signal, sucrose was chosen to act as modeling substance. For that, different solutions of sucrose (0, 30, 60 and 90 g/l) were mixed on-line with the NaHCO₃ standards previously to the mixing with the buffer resulting in sucrose concentrations of 0, 10, 20 and 30 g/l in the cell. Each sample (combination of hydrogen

carbonate standards and sucrose) was pumped for 4 minutes through the flow cell while measurements are performed.

2.3 FT-IR system

A Bruker IFS 88 spectrometer (Bruker Optik GmbH, Karlsruhe, Germany) with a mercury cadmium telluride (MCT) detector was used to record the spectra. For the measurements a flow cell with CaF_2 windows (Perkin Elmer, Wellesley, MA, USA) and a spacer generating an optical path of $30\mu\text{m}$ were used. Each spectrum was a result of 128 co-added scans, recorded with 2 cm^{-1} resolution, Blackman-Harris three-term apodization and at 100 kHz scanning rate. In order to avoid background absorption of the gaseous CO_2 , the spectrometer was purged with technical nitrogen.

2.4 Quantum cascade laser system

For all experiments a distributed feed back QCL (sb78, Alpes Lasers, Neuchatel, Switerland) placed in a laser housing equipped with a Peltier element, a compartment for water-cooling and a silica gel pad was used. Before closing, the laser housing was filled with technical nitrogen. The emission wavelength of the QCL under different operating conditions, especially different pulse amplitudes, operation temperatures and frequencies, was experimentally verified. For this purpose the globar light source of a Bruker Equinox 55 FTIR-spectrometer was replaced by the quantum cascade laser.

The specified maximum pulse power of the QCL was 50 mW. The QCL was operated at a temperature of -30°C controlled via TC-51 unit (Alpes Lasers, Neuchatel, Switerland). The pulse frequency has an influence on the emission wavelength [24] and also on the accessible tuning range. Tuning a QCL is more efficient using higher duty cycles as the

cavity is effected more by the generated heat. According to the datasheet provided by the producer this QCL show a maximal tuning range of 1.3 cm^{-1} at -30°C using 400 KHz and 1 and 1.6 A. In our experiments the operation frequency was limited by the laser driver QUANTA-BP (Laser Components, Olching, Germany) so the QCL was operated at the maximum possible frequency of 247.5 kHz. The control voltage needed by the laser driver for determining the pulse amplitude was delivered by the Function generator 33120A (Agilent Technologies, Palo Alto, California). The function generator was programmed to deliver a square wave function. That way the pulse amplitude of the QCL was modulated with a frequency of 50 mHz. The two alternating pulse amplitudes of 1 and 1.6 A levels were determined by the extreme values possible for the laser and resulted in a maximum of the emission spectra of 2341.6 cm^{-1} and 2341.4 cm^{-1} respectively (see Fig. 4a). Using these operating parameters the wavelength shift in the emission was 0.2 cm^{-1} . Pulse duration was fixed at 50 ns. However, according to the manufacturer of the laser pulser, the pulse amplitude of 1.0 A is already in a range in which the real pulse shape can differ from the adjusted parameters. This can be seen in Figure 3, where the pulse at 1 A has shorter duration than 50 ns and also starts later than the corresponding to 1.6 A. The gate was selected at 10 ns and located taking the maximum signal for the less intense pulse.

The used optical setup is given in Fig. 1b. The QCL beam was collected using an off axis parabolic mirror (focal length 43.1 mm) and focused through the flow cell (same as for the FT-IR experiments but with a $120\mu\text{m}$ spacer) on a photovoltaic MCT detector KMPV12-0,1-J1/100MHZ (Kolmar Technologies, Newburyport, MA, USA) using a second off axis parabolic mirror (focal length 69 mm). The whole optical part of the set-

up was covered with an acrylic plastic box, which was purged at 15 l/min with technical nitrogen to avoid background absorption of the gaseous CO₂. The detector signal was processed using a Boxcar Averagers Model SR250 (Stanford Research Systems, Sunnyvale, California, USA) by averaging the value of 10,000 pulses.

The maximum working frequency of the boxcar averager was 20 kHz. Hence only 8% of the generated pulses were processed. The analog output signal of the boxcar averager was converted into a digital signal using a computer interface model SR245 (Stanford Research Systems, Sunnyvale, California, USA). The QCL signal was recorded using custom software (Fig. 4b). A new value was recorded and stored every second. The function generator modulated the emission of the QCL automatically while the samples were passing the flow cell.

3 Data analysis

3.1 FT-IR Data

FTIR spectra were treated in Matlab 7.0 (The Math Works Inc., Natick, MA, 1999). A Savitsky-Golay smoothing and differentiation was performed obtaining the first-derivative row vectors resulting from a 7-point first order Savitzky-Golay smooth of each row of the matrix composed by all the spectra.

3.2 QCL Data

The recorded data were further evaluated using a spreadsheet software program. From the recorded intensities, absorbance value was calculated using the transmission obtained for distilled water as background. For both wavelengths and each combination of CO₂ with a sugar standard the corresponding absorption values were determined.

4 Results and discussion

4.1 FT-IR Spectra

Fig. 5a shows how the spectra of increasing concentrations of sugar mixtures (1:1:1) measured against distilled water caused an increasing sloping baseline with an isosbestic point at 2450 cm^{-1} . The same baseline shift can be observed in the presence of a constant carbon dioxide concentration (Fig. 5b). If quantification of the CO_2 would be based on the measurement of the absorption at a single wavenumber changing sugar concentration would significantly influence the result. First derivative spectra were calculated from these spectra (blank and CO_2 solutions with different sugar concentrations). From Figures 5c and 5d, it can be seen that the influence of the changing sugar concentration is negligible and the first derivative of the absorption band of CO_2 is not influenced by the changing sugar concentration. Calculation of the first derivative is thus, an appropriate means to correct baseline shifts due to the presence of sugars in the matrix.

4.2 QCL modulation measurements

The absorption values of CO_2 at 2341.6 cm^{-1} , measured with different concentrations of sucrose were used to determine the influence of sucrose on the measured CO_2 concentration. Evaluating one wavelength, sucrose concentrations above 9.46 g/l led to an underestimation of the CO_2 concentration. An increase of the sucrose concentration of 10 g/l in the sample results in a decrease of the measured CO_2 concentration of 11.9 mg/l . To avoid this influence, absorption values at both wavenumbers, 2341.6 cm^{-1} and 2341.4 cm^{-1} were calculated for all combinations of CO_2 and sucrose concentrations and subtracted, obtaining absorption differences. These values are proportional to the first

derivative spectra and are only hardly influenced by changes in the sucrose concentration. Table 1 resumes the results; carbon dioxide calibration (0-496 mg/l) was performed for different sucrose concentrations ranging from 0 to 30 g/l. When analyzing just one wavelength the intercepts of the regression equations when sucrose concentration is increasing were decreasing while they remained almost constant when the modulation method was applied. The absorption values of the modulation method when sucrose was present were within the standard deviation of the values when no sucrose was present. The analytical parameters for the calibration using these values were a regression coefficient R^2 of 0.9964, a standard deviation, according to ISO 8466-1, s_{ox} of 11.3 mg/l CO_2 and a detection limit of 33.9 mg/l CO_2 . Standard deviation is smaller than the decrease in the absorption values for CO_2 that occurs when sucrose is present.

The evaluation of only one wavelength (namely at 2341.6 cm^{-1}) shows an approximately 3.2 times lower standard deviation and therefore better limit of detection compared to the evaluation of the absorbance difference. But both methods show a better performance compared to previously reported works, where a standard deviation of 19.4 mg/l CO_2 has been reported. The main reason for the lower standard deviation can be found in the better match between the absorption line of the analyte and the emission line of the used QCL. Nevertheless, for the quasi first derivative spectra better results could be achieved with a higher tuning range of the QCL. An enhanced spectral difference between the two evaluated wavenumbers would result in bigger differences of the absorption values of these wavenumbers and therefore also in a higher signal of the analytical signal.

5 Conclusions

Wavelength tuning of a QCL was successfully applied in liquid phase spectroscopy as a promising tool for compensating background changes. Even if the tuning range of the used QCL was essentially smaller than the absorption band of the analyte, the gained information of two neighboring wavenumbers was sufficient to compensate changes in the water background arising from variations in the matrix. We demonstrated the feasibility of measuring carbon dioxide dissolved in water independently of the sugar concentration. The evaluation of only one wave number showed a negative correlation with the sucrose concentration that was successfully eliminated by evaluation of the absorbance difference at two wavenumbers. We therefore report this method highly promising for the development of a robust QCL based CO₂ sensor for different kind of liquid samples.

6 Acknowledgement

Financial support received from the Austrian Science Fund within the project FWF 15531 is acknowledged. A.D.V. is also grateful for a postdoctoral grant from the *Ministerio de Educación y Ciencia*, Secretaría de Estado de Universidades e Investigación (Spain).

REFERENCES

1. A. A. Kosterev and F. K. Tittel, *Ieee Journal of Quantum Electronics* **38**,582 (2002).
2. J. Wagner, C. Mann, M. Rattunde, and G. Weimann, *Applied Physics A-Materials Science & Processing* **78**,505 (2004).
3. J. Faist, F. Capasso, D. L. Sivco, C. Sirtori, A. L. Hutchinson, and A. Y. Cho, *Science* **264**,553 (1994).
4. J. Faist, C. Gmachl, F. Capasso, C. Sirtori, D. L. Sivco, J. N. Baillargeon, and A. Y. Cho, *Applied Physical Letters* **70**,2670 (1997).
5. D. Weidmann, F. K. Tittel, T. Aellen, M. Beck, D. Hofstetter, J. Faist, and S. Blaser, *Applied Physics B-Lasers and Optics* **79**,907 (2004).
6. Q. Shi, D. D. Nelson, J. B. McManus, M. S. Zahniser, M. E. Parrish, R. E. Baren, K. H. Shafer, and C. N. Harward, *Analytical Chemistry* **75**,5180 (2003).
7. M. Nagele, D. Hofstetter, J. Faist, and M. W. Sigrist, *Analytical Sciences* **17**,S497 (2001).
8. G. Wysocki, M. McCurdy, S. So, D. Weidmann, C. Roller, R. F. Curl, and F. K. Tittel, *Applied Optics* **43**,6040 (2004).
9. B. A. Paldus, C. C. Harb, T. G. Spence, R. N. Zare, C. Gmachl, F. Capasso, D. L. Sivco, J. N. Baillargeon, A. L. Hutchinson, and A. Y. Cho, *Optics Letters* **25**,666 (2000).
10. H. Ganser, M. Horstjann, C. V. Suschek, P. Hering, and M. Murtz, *Applied Physics B-Lasers and Optics* **78**,513 (2004).
11. A. A. Kosterev, Y. A. Bakhirkin, F. K. Tittel, S. Blaser, Y. Bonetti, and L. Hvozdar, *Applied Physics B-Lasers and Optics* **78**,673 (2004).
12. Martin W.B., Mirov S., and Venugopalan R, *Applied Spectroscopy* **59**,881 (2005).
13. S. Schaden, A. Domínguez-Vidal, and B. Lendl, *Applied Physics B: Lasers and Optics* **83**,135 (2006).
14. S. Schaden, A. Dominguez-Vidal, and B. Lendl, *Applied Spectroscopy* **60**, (2006) in press.
15. A. Edelmann, C. Ruzicka, J. Frank, B. Lendl, W. Schrenk, E. Gornik, and G. Strasser, *Journal of Chromatography A* **934**,123 (2001).

16. M. Kölhed, S. Schaden, B. Karlberg, and B. Lendl, *Journal of Chromatography A* **1083**,199 (2005).
17. B. Lendl, J. Frank, R. Schindler, A. Muller, M. Beck, and J. Faist, *Analytical Chemistry* **72**,1645 (2000).
18. M. Kolhed, M. Haberkorn, V. Pustogov, B. Mizaikoff, J. Frank, B. Karlberg, and B. Lendl, *Vibrational Spectroscopy* **29**,283 (2002).
19. J. J. Max and C. Chapados, *Journal of Physical Chemistry A* **106**,6452 (2002).
20. N. Kaun, J. R. Baena, D. Newnham, and B. Lendl, *Applied Spectroscopy* **59**,505 (2005).
21. K. A. Sharp, B. Madan, E. Manas, and J. M. Vanderkooi, *Journal of Chemical Physics* **114**,1791 (2001).
22. J. B. Brubach, A. Mermet, A. Filabozzi, A. Gerschel, D. Lairez, M. P. Krafft, and P. Roy, *Journal of Physical Chemistry B* **105**,430 (2001).
23. S. Schaden, M. Haberkorn, J. Frank, J. R. Baena, and B. Lendl, *Applied Spectroscopy* **58**,667 (2004).
24. A. A. Kosterev, R. F. Curl, F. K. Tittel, M. Rochat, M. Beck, D. Hofstetter, and J. Faist, *Applied Physics B-Lasers and Optics* **75**,351 (2002).

Tables

Table 1

sucrose [g/l]	d [AU]	k [AU/(g/l)]
2341.6 cm⁻¹		
0	-0.0008	0.5945
10	-0.0055	0.5945
20	-0.0123	0.6041
30	-0.0191	0.6172
Absorbance differences		
0	-0.00005	0.1098
10	0.00121	0.1037
20	0.00005	0.1078
30	-0.00085	0.1112

Figure captions

Figure 1. Experimental setup. (a) Flow system (b) QCL system (M, Mirror; F, Flow Cell; D, Detector; B, Purged Box).

Figure 2. FTIR spectra normalized on the target wavenumber of 2341.6 cm^{-1} for sucrose (solid line), fructose (dashed line) and glucose (dotted line) Concentration is in all cases was 30g/l.

Figure 3. Pulse shapes obtained using a pulse amplitude of 1.6 A (solid line, 2341.4 cm^{-1}) and 1.0 A (dotted line, 2341.6 cm^{-1}). Location of 10 ns gate is also shown.

Figure 4. (a) Normalized QCL emission spectra (left scale) for pulse amplitudes of 1.0 A (solid line) and 1.6 A (dashed line). In the right scale, absorption spectra (dash-dot line) of aqueous carbon dioxide (spectra of water was taken as background) is shown.

(b) Recorded signal of a CO_2 standard (165 mg/l) with different amounts of sucrose. The higher intensities correspond to pulse amplitude of 1.6 A (2341.4 cm^{-1}), lower intensities correspond to the emission with 1.0 A (2341.6 cm^{-1}). Increasing sugar concentrations led for both wavelengths to higher detector signals and therefore decreasing absorption values.

Figure 5. Original FT-IR spectra of (a) water and (b) a carbon dioxide solution (331 mg/l) in the presence of increasing concentrations of sugars. First derivative spectra from the same experiments respectively (c) and (d).

Figures

Figure 1

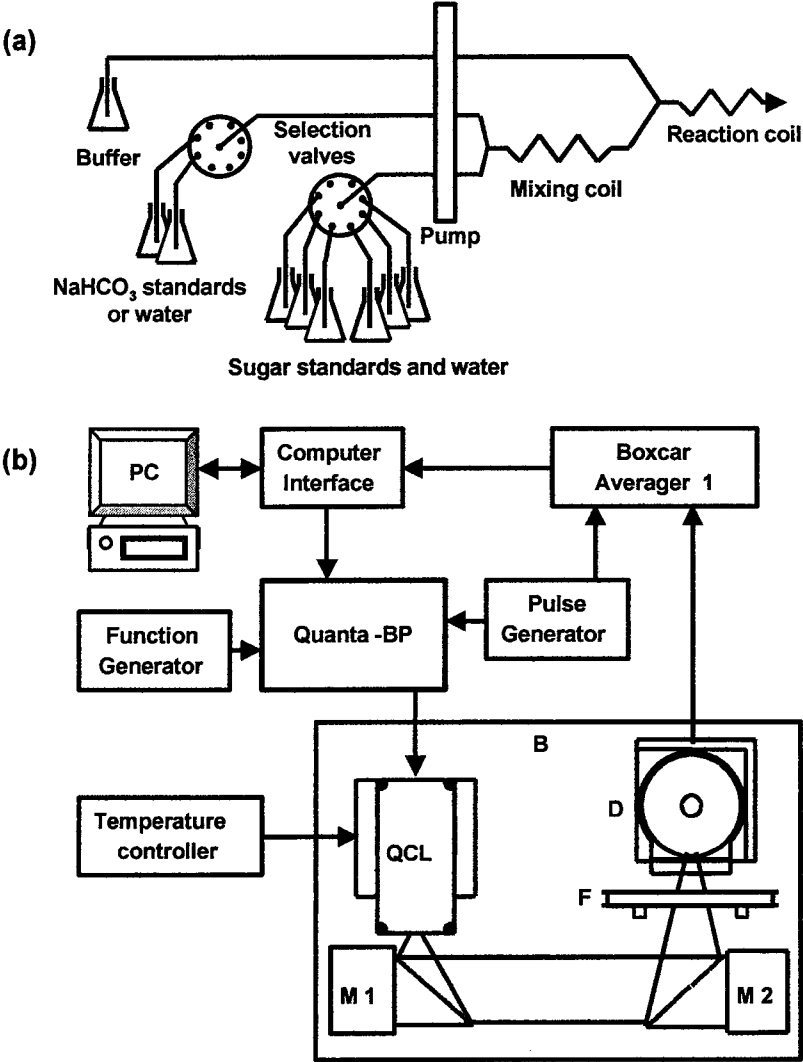


Figure 2

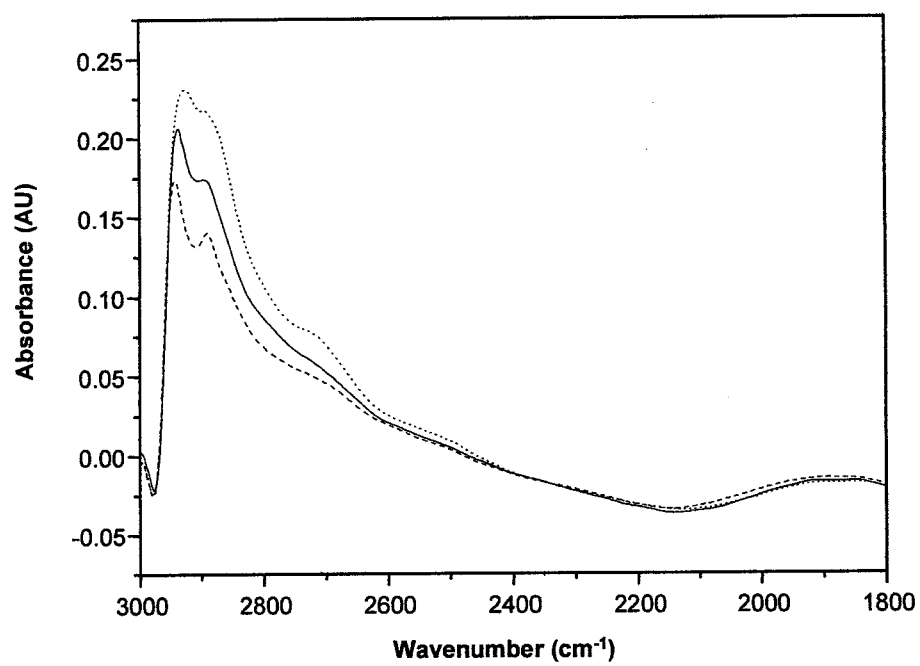


Figure 3

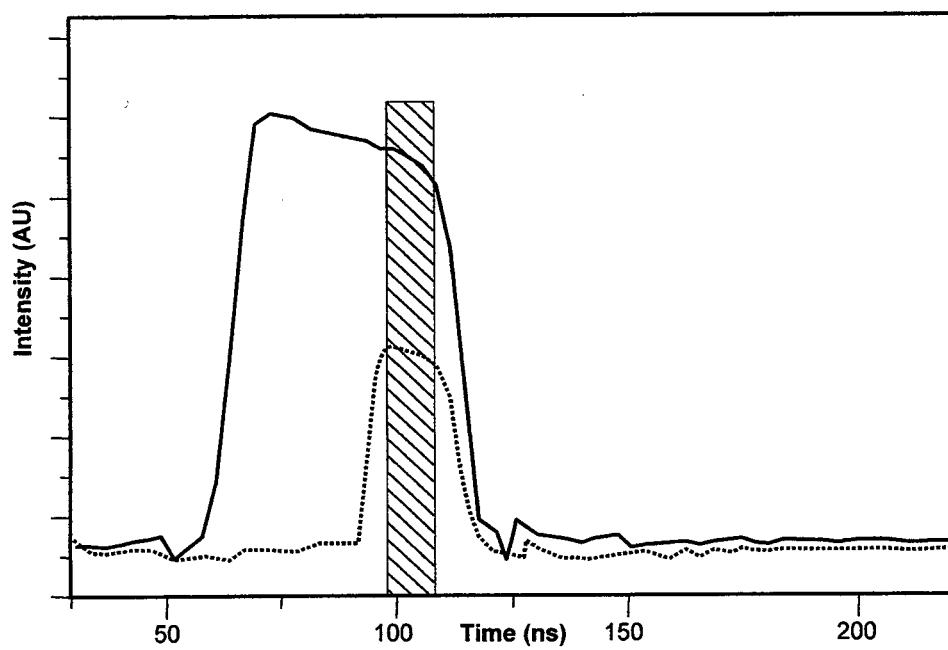


Figure 4

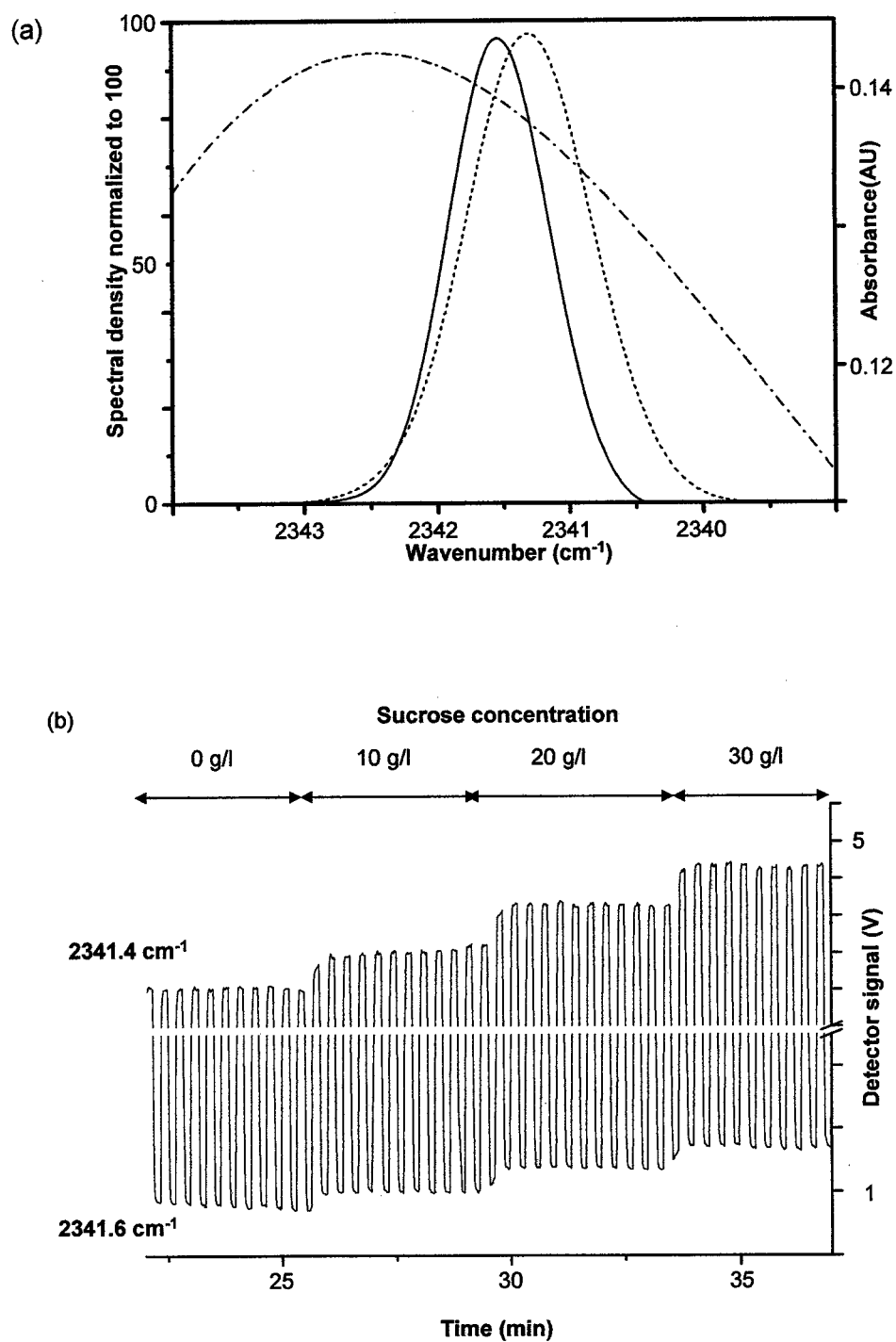
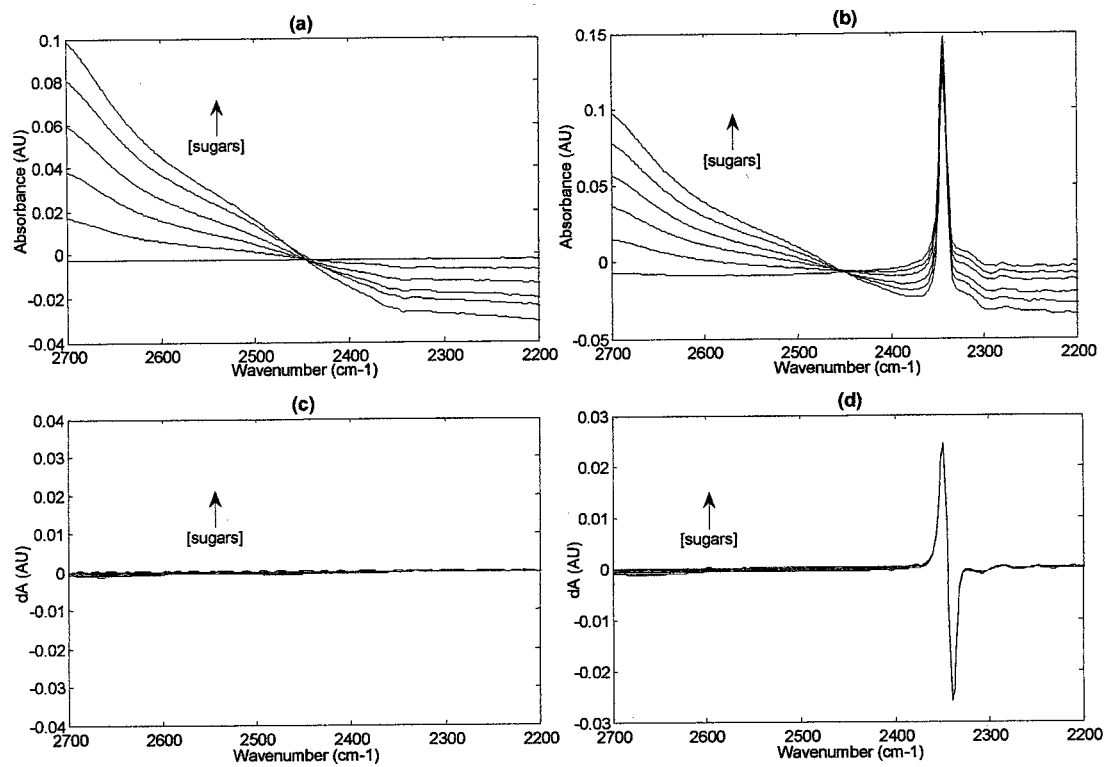


Figure 5



PAPER V

QUANTUM CASCADE LASERS: A PROMISING LIGHT SOURCE FOR VIBRATIONAL SPECTROSCOPY

S. Schaden¹, L. Hvozda², A. Müller² B. Lendl^{1*}

¹ Institute of Chemical Technologies and Analytics, Vienna University of Technology, Getreidemarkt
9/164AC A-1060 Vienna, Austria

² Alpes Lasers S.A., Passage Maximilien de Meuron 1-3, 2000 Neuchâtel, Switzerland

* Corresponding author. FAX: +43 1 58801 15199; Phone: +43 1 58801 15140

1	Quantum Cascade Lasers	3
1.1	Solid state physics and technological fundamentals.....	3
1.2	QCL Design.....	4
1.3	Laser fabrication – or why are the lasers not so easy to obtain.	5
1.4	Properties of the QCLs.....	5
1.5	Sources of the lasers and the future prospect.....	6
2	Spectroscopic Techniques.....	7
2.1	Wavelength tuning	7
2.2	Determination of laser emission wavelengths	8
2.3	Absorption measurements	9
2.3.1	Direct absorption measurements.....	9
2.3.1.1	Gas Phase	9
2.3.1.2	Measurements in liquid phase	10
2.3.1.3	Imaging using QCL.....	11
2.3.2	Absorption measurements using high-finesse optical cavity	12
2.3.2.1	Cavity ring down Spectroscopy (CRDS)	13
2.3.2.2	Integrated Cavity Output Spectroscopy / Cavity Enhanced Spectroscopy.....	13
2.4	Photoacoustic spectroscopy.....	14
2.5	Faraday modulation spectroscopy	16
3	Applications.....	17
3.1	Atmospheric trace gas	17
3.2	Traffic and combustion.....	20
3.3	Medical and biological applications	22
3.4	Spectroscopic studies	24
3.5	Process monitoring	25
3.6	Applications in the liquid phase	26
4	References.....	29

Advances in spectroscopy can often be traced back to the advent of new technologies. Such stages of development usually allow to conceive new measurement concepts which provide more elegant or practical useful solutions to a given analytical problem. Frequently such stages of development also allow to address analytical challenges for the first time. Important landmark developments in vibrational spectroscopy which represent such stages are the development of the Fourier transform spectrometers, availability of fiber optics, the advent of array detectors and in case of Raman spectroscopy the development of high quality lasers. The evident success of lasers in Raman spectroscopy is based on the high performance that has been achieved for various types of lasers emitting in the UV, visible and near infrared region. A further important issue, which facilitated the implementation of lasers in Raman spectrometers is the fact that only one laser line is required for acquisition of a full Raman spectrum. Spectral resolution and bandwidth in Raman spectrometry is determined by components and not by the light source itself. Concerning the perspectives of laser technology for recording full mid-infrared spectra the panorama is much more demanding. Instead of a few high performing laser lines as in the case of Raman spectrometers widely tunable IR lasers or IR laser arrays would be required. For applications where a reduced spectral bandwidth is sufficient to solve a given problem this condition is relaxed. A typical example would be gas phase spectroscopy where selective measurements are possible by probing narrow rota-vibrational lines of the target molecule. However, still technologies or materials different from those employed in UV, visible or NIR lasers are needed to achieve emission in the mid-infrared spectral region. It was realized already long ago that in case such lasers would be available a tremendous gain in sensitivity and selectivity especially for gas phase spectroscopy would be possible due to the possible match of narrow and strong fundamental transitions with mid-infrared lasers. Driven by these expectations and first results using cryogenically cooled mid-infrared lasers, the advent of mid-IR lasers has been announced repeatedly during the last decades. Lead salt lasers and fiber lasers have been developed and also commercialized. Fueled by first promising results reported in research publications high expectation with regard to performance and possible application in dedicated analyzers or general purpose spectrometer systems had arose in the scientific community. However, these high expectations have not been met yet. Limited spectral coverage, frequent need for liquid nitrogen cooling, emission power remaining in the hundreds of μW , together with high price have probably hindered the spread and thus the full development of these types of lasers.

The advent of quantum cascade laser technology has now resurged expectations in mid-infrared lasers for use in vibrational spectroscopy in general and in sensor development in especial. It is the aim of this article to provide an introduction to the principles of QCL technology, to review most relevant experimental setups as well as to cover applications in the field of atmospheric trace gas detection, medical diagnostics, industrial process control, liquid phase measurements as well as spectroscopic studies.

1 Quantum Cascade Lasers

1.1 Solid state physics and technological fundamentals

Every solid can be assigned an energetic diagram, showing the energies allowed for the charge carriers (electrons) present in it. A group of (mostly) covalent crystals, which exhibit electrical conductivity only under certain conditions (doping, illumination, elevated temperature) are referred to as semiconductors¹. Searching for the understanding of this behavior it was proved, that a band of energies, forbidden for the electrons is present in their energetic diagrams. It is referred to as band gap – E_g . The band gap is embedded between the edges of the conduction band E_c and the valence band E_v (fig. 1a). The width of the band gap is typically in the range of up to several electron-volts, where $1\text{eV} = 1.602 \cdot 10^{-19}$ Joule. Each semiconductor material exhibits a different width of the band gap.

If a crystal consisting of two different semiconductor materials is grown, the edges of E_v and E_c will line up, forming an abrupt step in the band structure (fig. 1b). We speak from heterostructure - in this case from a quantum step (fig. 1b). A heterostructure composed of one narrow-gap semiconductor layer, embedded between two layers of semiconductor with a broader gap constitutes a two dimensional quantum well (fig. 1c). Since the width of the quantum well is comparable to the de-Broglie wavelengths of electrons, quantization of the energetic states takes place. The former continuum of the states above the band gap, breaks up into a set of discrete quantized states. The spacing between the energetic states is controlled by the physical width (thickness) of the quantum well.

Transitions between the energetic states in such a quantum wells are possible via various mechanism of energetic exchange. If an electron absorbs energy to make a transition from a lower state to a higher state (fig. 1b), we speak from excitation. The opposite process – relaxation - is accompanied by the emission of energy. One of the mechanisms of energy exchange is spontaneous emission of electro-magnetic wave – a photon. These mechanisms are similar to the behavior of electrons in atoms, so with some simplification, one can say, that the quantum well is a semiconductor analogy to an atom. The spontaneous photon emission is a relatively slow process. The carrier lifetime for a photon emission of intra-band transition is typically several pico-seconds (10^{-12} s). Another, much more efficient process, for emission of energy is an exchange of energy from an electron to the crystalline lattice oscillation. We speak from an emission of a longitudinal optical phonon (LO-phonon). The lifetime for this transition is typically in the range of several hundreds of femto-seconds (10^{-15} s) - about ten times shorter than that of the photon emission. Since the energy of optical phonons in a crystal is strictly defined, it is a strongly resonant process. It means that only relaxations between two levels spaced by the corresponding LO-phonon energy can undergo this mechanism.

If two finite - depth quantum wells are separated by a barrier thin enough for overlapping of the wave function tails of electrons in adjacent wells (fig. 1c) a hybrid state is formed. As a result of that, the electron can physically move from one well into another well, although it does not have enough energy to pass over the barrier. This phenomenon is referred to as tunneling².

Modern crystal growth technologies like the molecular beam epitaxy ³ enable for formation of heterostructures with a mono-molecular layer resolution. The systems used for this processes are stable enough to perform the growths of very complex heterostructures, composed of several hundreds of discrete layers. A detailed description of its principles would be out of the scope of this article. Figure two shows a transmission electron micrography of such a heterostructure where the alternating materials grown in one mono crystal appear as brighter and darker layers.

1.2 QCL Design

To obtain a stimulated emission and thus a light amplification or in other words to obtain a gain from a laser, the following conditions need to be fulfilled:

- (1) Population inversion (a state of the gain medium of laser, where higher energetic levels are more populated than the lower ones.
- (2) Feedback – the light emission in the gain medium under condition (1) is stimulated by photons present in it. Therefore there must be some portion of emitted photons re injected into the gain medium.
- (3) Energy supply – a means to maintain the population inversion. In the case of Quantum cascade lasers as well as in majority of the semiconductor lasers it is electrical current.

The mechanisms described in chapter 1.1 are all implemented in the quantum design of the laser gain medium in order to create conditions for population inversion. A first Quantum Cascade Laser (QCL) was demonstrated by Faist et al. in 1994 ⁴. A scheme of such a laser is shown in figure 3. The gain medium of the laser is realized as a cascade of 25 active cell and injector pairs. The active cell itself is constituted by three coupled quantum wells (fig. 3b), providing three discrete energetic levels. The electrons are injected (by means of the electrical current) into the third level. The system is inverted – the higher level (E3) is more populated than the lower level (E2). The electrons undergo a transition (E3-E2). The transition follows the photon generation mechanism in a favorable case. The wavelength of the photon is determined by the energetic spacing between these two levels. The subsequent transition (E2-E1) is tailored to be in resonance with the LO-phonon energy, and thus very fast and efficient. It serves for extraction of the electrons from the level 2 and thus creating conditions for population inversion between level 3 and level 2. Afterward the electrons are evacuated by the injector of the following period. A single electron, successfully passing all the 25 periods can emit 25 photons. However, the photon emission has a lot of competing transition mechanisms in this quantum system, and its quantum yield (electrons passing/photons emitted) for a single period, is in the range of several per mille. A Fabry – Pérot resonator (F-P), based on two parallel mirrors ⁴, or a distributed feedback resonator (DFB) ⁵, based on a grating incorporated into the resonator itself is used as feedback mechanism to assure for stimulated emission.

1.3 Laser fabrication – or why are the lasers not so easy to obtain.

The diversity of analytes and matrices in the various real or potential analytical applications require a big variety of laser wavelengths to be available. This fact denotes a fundamental difference of the QC laser branch to the other laser branches (telecommunication, optical memory media,...). The analytical applications of QC lasers require different, but extremely well defined wavelengths in small quantities, whereas in the telecommunications, a large volume of lasers with identical specifications is needed. Therefore the production of telecommunication lasers may efficiently use a stock and QCLs are mostly made to order. Scheme of the fabrication process flow is presented in figure 4.

The fabrication process starts with a design of the gain medium of the laser. A self consistent calculation of the band structure and the energetic levels, together with the electron wave functions are calculated. Once the design is simulated and optimized, the MBE growth of the active zone is performed. The grown material is subsequently characterized by means of the X-ray diffractography, and an electro-luminescent characterization is performed in order to measure the emission spectral maximum to assess the interval of possible emission wavelengths for the particular material.

Majority of the customers request single mode lasers, necessary detect the fine gas-absorption lines. This implies a necessity of (DFB) technology implementation. The laser-waveguide is simulated, the effective refractive index is determined, and the DFB grating period is proposed. The process continues by fabrication of the calculated grating with the period precision better than one per mille (in the absolute units in the range of 10-9 m). The subsequent overgrowth of the structure by means of the MOCVD, forms the upper laser cladding. The cladding serves together with substrate underneath the gain medium, for a low-loss confinement of the light inside it - it forms a waveguide, with a maximum of the energy in the middle of the gain medium. Lateral structuring and the deposition of the electrical contacts terminate one cycle of the process on the wafer. The wafer is then cleaved into single laser chips, those are bonded to the laser sub mount and the top contact of the laser is wire bonded to the contact pad of the sub mount. The laser is then characterized – spectra and the output characteristics are measured. It is sometimes necessary to re-feed the process - most commonly in order to correct for the wavelength, due to the strict customer's requirements in this parameter.

The material systems actually used for realization of QCLs are GaAs/AlGaAs heterostructures⁶ and heterostructures of InGaAs/InAlAs grown lattice-matched to InP⁴. The latter of the two systems offers a significantly better performance until nowadays.

1.4 Properties of the QCLs

Since the invention, quantum cascade lasers undergone a very dynamical development that made them to a powerful tool for applications in vibrational spectroscopy. Analyzers for atmospheric trace gas, medical

diagnostics or the control of industrial process parameters have to fulfill high demands such as high robustness, room temperature or near room temperature operation, high sensitivity and selectivity as well as compactness. With QCLs these demands can be satisfied. In 1997 the first high power superlattice based Quantum cascade laser was realized ⁷. Operation temperature as high as 425 K in pulsed mode, has been demonstrated in 2001 ⁸ and continuous wave (CW) operation up to -27 °C has been demonstrated in the same year ⁹. Some milestones in the development of QCLs are given in Table-I.

As noted, band structure engineering, together with the modern epitaxial growth technologies allow for full control of the final energetic scheme of the laser. This allows for tailoring the emission wavelength to the particular need, using the very same material system. The only limits are imposed by the possible “depth” of the quantum wells. The so accessible spectral region covered by QCLs ranges with some gaps from 3,2 μm to the far infrared, the so-called terahertz region. But most applications use QCLs in the MID-Infrared, where molecules have their fundamental rotational and vibrational absorption bands, which show a higher absorption coefficient than the overtones in the NIR region. Especially in trace gas detection the two H_2O atmospheric windows at 3-5 μm and 8-13 μm are from great interest. Another great advantage of the QCLs is the possibility of operation at and above room temperature at the demanded wavelength. This was very limited for their lead salt laser – ancestors ¹⁰. The mechanism of light generation from the intersubband transitions subjects a selection rule ², which results in TM polarization of the generated light (electric field vector is always perpendicular to the planes of the grown layers). This may simplify the construction of optical schemes incorporating QCLs in some cases. The laser beam of a typical laser exhibits a divergence in the range of 60° in the vertical axis and about 40° in the horizontal axis. Therefore different optics for collimation and beam shaping has been developed. Some possible optics designs are described in reference ¹¹.

The emission wavelength can be tuned around the nominal center wavelength by means of changing the temperature of the heat sink, or by adding a DC component to the laser driving pulses.

A Fabry-Pérot resonator laser has a typical multimode performance (fig. 5a). The mode spacing depends on the length of the resonator. The center of the emission wavelength is determined by the position of the gain maximum, more specifically by the quantum design and the MBE growth only. On the other hand, a DFB laser (fig. 5b), with an incorporated grating has typically a single mode performance. The emission wavelength is determined by the grating period - as long as the material allows for gain at the corresponding wavelength. Table II summarizes the performance of quantum cascade lasers of both InP and GaAs system.

1.5 Sources of the lasers and the future prospect

New developments in the QC lasers are driven by the interest of the market. The simple fact that these sources offer 10^5 to 10^6 times higher spectral power density of the emitted light, compared to that of the conventional mid-infrared sources makes them very attractive for construction of various target-

spectroscopy applications. The number of the realized wavelengths is constantly growing. New quantum- and optical designs are developed, in order to improve the laser performance at ambient temperature, since their performance at room temperature is an essential feature for the industrial application of the lasers. Since the line width of a laser operated in the continuous wave mode is significantly narrower than that of the pulsed mode, a big effort is also spent on CW laser performance achievement. Concerning tune ability advances may result from development of two segment DFBs where reversible switching between two different DFB modes by current injection control can be achieved¹². Alternatively the use of an external cavity in combination with QCL allows reaching a tuning range of up to 170 wavenumbers¹³. From the point of view of the wavelength, far-infrared or tera-hertz lasers (wavelengths of 60 – 300 microns) are the newest trend in this field¹⁴.

There are several companies commercializing quantum cascade lasers worldwide. The actual price levels are in the range of 10 000 EUR¹⁵ per piece. Recent works demonstrated a QCL grown using Metal-Organic Chemical Vapor Deposition (MOCVD)^{16,17,18}. MOCVD is much more suitable for mass production, compared to the MBE. This indicates a possibility of substantial decrease of the prices, enabling penetration of the QCL technology into many more applications than possible now, since the high price is a strongly limiting factor. So far Europe has taken a leading role in commercialization of QCL technology. A review covering commercially available laser as well as laser systems and their application in Europe has recently been given by Lambrecht¹⁹.

2 Spectroscopic Techniques

2.1 Wavelength tuning

The emission wavelength can either be tuned by variation of the heat sink temperature or variation of the driving conditions. In each case the variation of the refractive index of the active material due to set or induced temperature changes is responsible for wavelength tuning. Both – tuning via temperature as well as driving conditions – are used in practice. In any cases a good thermal management is required to guaranty stable laser emission. The typical range of temperatures for tuning the lasers is from -30°C to +30 °C, allowing for tuning of 0.4% around the central wavelength. Tuneability in terms of wavenumbers decreases with decreasing emission wavenumber. For a DFB QCL emitting at 1000 cm⁻¹ (10 μm) typical tuneability lies in the region of 8 wavenumbers. Using the driving current dependence of the laser wavelengths allows faster tuning than changing the heat sink temperature, but puts more demands on the driving electronic. Modulation of the heat sink temperature is mostly used to record analyte spectra for spectroscopic studies without time pressure^{20,21,22}. A frequently used technique for fast real time applications is based on a sawtooth or pedestal current ramp applied under the threshold level of the QCL at a few Hz^{23,24,25}. This allows for a temperature change in the active region during one single ramp. Pulsing the lasers at different

positions during one ramp allows to change its emission wavelength from pulse to pulse. The pulse frequency itself has also an influence on the laser temperature as higher repetition rates lead to an increased temperature of the active region and hence longer emission wavelengths²⁶. In case a fast detector is available also the temperature rise in the active region during one prolonged pulse (>100ns) can be utilized. The resulting wavelength shift during a pulse is called frequency downchirp and offers the possibility to scan over one or more absorption lines during a single pulse^{27,28,29}. Furthermore this technique also provides access to background (I_0) and sample (I) intensities required to calculate the analyte absorption. Expanded tuning ranges can be achieved when coupling QCLs to an external cavity. For achieving a maximum tuning range heterostructures with a broader gain bandwidth are preferred. Appropriate gain bandwidths may be achieved by putting together dissimilar optical transitions or by using bound-to-continuum QCLs. With a latter QCL operated in the pulsed mode and using a Littrow external cavity design a tuning range up to 150 cm^{-1} has been reported already³⁰. Improved external cavity QCL systems may be expected once room temperature CW QCLs become standard. A plentiful of different spectroscopic applications would benefit from such a development.

2.2 *Determination of laser emission wavelengths*

Wavelength accuracy of QCLs is of importance for spectroscopic applications. This is especially true for applications in gas phase where sharp vibrational-rotational absorption lines are present. For rapid off-line wavelength calibration the QCL under study can be mounted instead of a thermal light source of an FTIR spectrometer. When operating the laser at pulse frequencies of 50-100 kHz and when sampling the interferogram slowly (20 kHz) the laser appears as a quasi continuous light source³¹. In that manner for each setting of the operating parameters the corresponding pulse averaged emission spectra can be recorded^{32,33}. Apart from QCL characterization purposes combination of QCLs and FTIR spectrometers have also been used for qualitative studies in gas phase spectroscopy^{20,28}.

In addition to the use of a spectrometer for emission wavelength testing and calibration, wavelength calibration standards such as CF_2CH_2 ²⁸ or the rovibrational transitions of the 9P branch of gaseous carbon dioxide³⁶ have been used too. Based on the comparison of recorded and known spectra as well as calculated spectra using HITRAN database an instrumental set-up can be characterized. A further possibility for wavelength calibration is based on the interference fringes from etalons^{21,23,24}. Both, wavelength calibration standards and etalons can be used for following the frequency downchirp during a laser pulse. Detailed characterization of the emission characteristics of a pulsed laser can be obtained using time resolved step-scan FTIR spectroscopy³⁰.

2.3 Absorption measurements

2.3.1 Direct absorption measurements

2.3.1.1 Gas Phase

Properties of QCL like room temperature operation or tuning range over few wave numbers, a compact design and high efficiency make them to attractive tools for absorption measurements of gases³⁴. Because of the possibility of wavelength tuning QCL based absorption techniques are sometimes referred as tunable infrared laser differential absorption spectroscopy (TILDAS)⁴⁰. A tunable light source offers also the possibility to carry out wavelength modulation spectroscopy. This technique is based on a periodical wavelength scan across an absorption line of the analyte. The resulting absorbance is changing with double the frequency of the wavelength modulation. Signal changes with different frequencies can be addressed as noise and can be suppressed using a lock in amplifier.

CW operation of the QCL is – if possible – preferred for measurements at fixed wavelengths because the line width is approximately 5 times smaller⁷⁷ than in pulsed operation. Furthermore, laser operation in general is more stable both in laser wavelength and emission power. Requirements for driving and evaluation electronics are normally also lower. So far most applications requiring room temperature and/or with the need for high power are QCLs in pulsed mode. But this should change in the future with the further development of CW QCLs.

For measurements of gases, different designs of the sample cell have been developed. In first applications a 10 cm single pass gas cell were used³⁵. To suppress optical interference fringes from cell windows as well as from the output window of the laser housing, the windows can be tilted³². A further reduction in optical interferences can be achieved using cells equipped with Brewster windows that allow p-polarized light to pass completely²⁶. The optical path in single path cells is limited by the size of the experimental set up. However, increased absorption paths result in higher absorptions values and therefore lower detection limits. For open path measurements no cell is required, hence optical path lengths up to 34 meters have been reported²⁷. To increase the optical path while maintaining the geometrical dimensions small single^{36,37} as well as multi-reflection gas cells have been used. Using White²⁹ or Herriott cells^{24,28} path lengths of up to 210 meters can be realized^{38,40}. Another possibility to increase the optical path is the use of a hollow-waveguide instead of a gas cell. The waveguide acts as a lightpipe and if the sample is injected into the core it acts simultaneously as a miniaturized gas cell³⁹. An overview of different cell designs is given in figure 6. To compensate fluctuations in the laser output power a two-beam set up can be used. A beam splitter divides the laser light into a reference and a sample beam. The intensity of the signal is normalized to the reference signal and therefore independent of pulse-to-pulse fluctuations. An elegant approach to avoid the beamsplitter in such a system is described in ref. ³⁸ where the tilted window of the gas cell is used instead. In this case the beam reflected from the cell window is used as reference. In these applications conditions

are set such that only a small fraction of the light pulse is used for reference measurement whereas the majority of the available intensity is used for sample measurement.

Such a system can work with one^{24,40} or two independent detectors and amplifier systems^{38,41,42}. The advantage of the two-detector option is that it can also be used for CW-Lasers. However, if two detectors are used the characteristics of both are probably not completely the same, even if the same model is used. Small drifts or non-linearity of one system can theoretically cause lower performance compared to one-detector systems. Focusing the sample as well as the reference beam on one detector puts higher demands on the optical alignment and requires faster signal processing. A time delay typically ranging from 120⁹⁶ to several hundred nanoseconds⁴⁰ between the reference and the signal pulses from 5 – 25 nanoseconds is essential and the signal processing has to be fast enough to discriminate both pulses. Mostly this option can be found in combination with multi pass cells. The distance, which the light has to travel inside the cell, is long enough to have an adequate time delay between reference and sample signal.

Another method to compensate fluctuations in the output power is described in reference 36. In this work the spectra are recorded by tuning the emission wavelength of the QCL by temperature scanning. The recorded spectra consist of broad (low frequency) and narrow (high frequency) spectral variations. Drifts in the base line appear as low frequency changes in the spectra. Spectral variations caused by the analyte show higher frequencies. A mathematical smoothing function “low-pass filter” is used to subtract the low modulated baseline drift from the spectra. Quantitation is based on the obtained difference absorption spectra with the advantage that no assumption on the actual baseline is required. In a recent review Duxbury and co-workers summarized experimental strategies and results for gas phase spectroscopy using absorption techniques. Focus was put on the long pulse technique where a micro-spectral region can be probed due to the frequency downchirp during one laser pulse. Applications in gas sensing as well as non-linear optics are discussed in detail⁴³. In the long-pulse technique scanning across a full ro-vibrational line is achieved. As has been pointed out recently, measurement of the full band provides experimental access to the integral absorption coefficient which is a natural constant for a particular molecule. Thus in case this coefficient is known for the target analyte vibration a calibration free method can be devised⁴⁴. Zahniser gave an overview on the current state of the art in gas sensing using the dual QCL instrument incorporating a multipass absorption cells for applications in atmospheric trace gas measurements as well as characterization of aircraft exhausts for a number of different analytes⁴⁵.

2.3.1.2 Measurements in liquid phase

In condensed phase absorption bands are much broader than in gas phase, furthermore spectral overlap of different analytes is frequent. At first glance this situation seems to discourage the use of QCLs for measurements of liquids. However, because of the high spectral power density compared to thermal light sources, QCLs may bring about substantial advantages also for measurement in liquid phase. In general the solvents used in liquid phase measurements show absorptions in the mid infrared spectral region. As a

consequence achievable sensitivities in absorbance measurements are generally determined by the extent of solvent absorption in the spectral region of interest. For instance measurements of the amide I band of protein in aqueous solution requires path length below 9 μm using state-of-the-art FTIR spectrometers. In addition to limited sensitivity, short pathlengths may also cause practical problems when particle containing solutions need to be monitored. In light of this situation the use of QCLs is highly interesting also for measurements in liquid phase. Apart from OCL absorption measurements in a transmission cell also measurements based on internal reflections are possible. So far absorption measurements have been shown in dedicated small volume fiber optic flow cells employing either silver halide fibers or hollow fibers which have been capped with diamond windows towards the liquid phase side. Alternatively conventional flow cells made of BaF_2 ⁴⁶ or CaF_2 ^{33,105,104} windows have been used too. For internal reflection measurements planer waveguides⁴⁷ made of silver halide as well as micro-machined thin film GaAs waveguides⁴⁸.

For achieving selectivity in liquid phase measurements additional efforts needs to be made as compared to gas phase spectroscopy due to the present broad and overlapping absorption bands. Additional selectivity can be added by employing multiple QCLs^{46,49,50} or by controlled shifting of the emission wavelength of one QCL⁵¹. Alternatively, or in combination with multiple wavelength recording, additional selectivity may be achieved by performing QCL detection in combination with liquid chromatography¹⁰⁴, capillary electrophoresis¹⁰⁵ or flow injection analysis¹⁰⁶.

2.3.1.3 Imaging using QCL

A new field of possible applications of quantum cascade lasers concerns imaging. In this respect different research areas seem to develop. On the one hand the combination of tip scattering near field microscopy with IR laser technology allows to obtain information rich spectral contrasts of the mid-IR spectral region at the high spatial resolution of tip probe techniques. Successful combinations of AFM tips with CO and CO_2 lasers have been shown already which benefited from the high power of these lasers. The use of QCL in these experiments is appealing due to flexibility in possible wavelengths, however, a further increase in QCL emitting power is needed for truly successful combination with tip scattering near field techniques⁵². Imaging in transmission using 4 different DFB QCLs (4.6, 5.1, 6, and 9.3 μm) and focal plane array detectors has been shown in a technical feasibility study. Despite of not fully optimized conditions for data read-out convincing images on animal tissue, celery, as well as polymer laminates have been obtained⁵³. Imaging using QCL technology is also interesting considering the THz spectral region. Interest in QCL based imaging system stem from their possible applications in security technology as well as from the biomedical field. So far experimental set-ups for imaging in transmission as well as reflection mode have been demonstrated. Spatial resolution in the order of the diffraction limit has been achieved using a pulsed 3.4 THz QCL operating at 5 K and with a repetition frequency of 400 Hz.⁵⁴ The spatial resolution has been investigated using on a object phantom which carries series of gold stripes of different width and

determined to be about 170 and 240 μm when scanning in the sample plane. The imaging system was applied to sections of animal brain which had been perfused transcardially with paraformaldehyde (4%) cyrotomed at a thickness of 32 μm . The sections were stored in ethylene and for THz imaging were mounted on a gold-coated flat glass substrate. The obtained images based largely on contrast derived from differential absorption of THz frequencies by lipid-rich and water-rich tissues. Slices of rat brain and liver fixed in formalin and with a thickness of 2 mm have been successfully imaged using a 3.7 THz QCL⁵⁵. In this application the laser was operated at 28 K producing 300 ns pulses at a frequency of 1kHz. Achieved spatial resolution of 280 μm (x) and 340 μm (y) have been reported. In addition to healthy rat liver also metastasis liver has been imaged revealing distinct spectral contrast. Also in this application differences in spectral contrasts are mainly related to differences in fat /water content of the imaged tissues. A dual wavelength system has been reported for imaging in transmission as well as reflection mode⁵⁶. THz QCLs at 87 and 130 μm have been used reporting in both cases spatial resolutions of approximately 320 μm for transmission as well as 400 μm for reflection measurements. The authors show results on imaging of a box cutter blade inside paper envelopes spray-on foam insulation used on the space shuttle tanks as well as dried drops of milk products. Whereas the measurements on both laser wavelengths were carried out differences between the two lasers in terms of spectral contrasts as well penetration through material were experimentally obtained which have been considered important for the development of more viable THz imaging system.

2.3.2 Absorption measurements using high-finesse optical cavity

The use of high finesse cavities for quantitative gas phase spectroscopy is an interesting alternative to conventional absorption spectroscopy in single or multiple path cells. Using optical cavities more sensitive types of gas phase spectroscopy have been developed. The constructive differences between cavity based measurements and conventional multiple path absorption cells lies in the mirrors used in high finesse cavities. These mirrors, mostly based on dielectric materials, show a reflectivity up to 99,995 %. Furthermore the remaining portion of the light passes the mirrors and can be detected. The development of such mirrors in the infrared region was a pre-requisite for the development of cavity based measurement technologies. The effective path length (L) in cavity based measurements depends on the reflection coefficient (R) of the mirrors as well as on the spacing between them (l) according to the equation $L = l / (1 - R)^{34}$. Using a cavity length of a few centimeters hence allows generation of effective path up to hundreds of meters. As the analytical information is retrieved from measurement of the light, leaking out of the cavity new ways of data analysis have become feasible too. Using high finesse cavities a broad range of different set-ups and techniques have been developed so far. Here those where QCL have been employed are outlined in detail below.

2.3.2.1 Cavity ring down Spectroscopy (CRDS)

In CRDS a light pulse is generally injected into the cavity. The light pulse which is bouncing inside the cavity is gradually leaking out of one mirror where the decay in intensity is recorded. In such an experiment the rate of intensity decay is independent from the original pulse intensity. As a consequence the method is independent of pulse to pulse fluctuations in emission power of the used light source. If an absorber (analyte) is present inside the cell, the decay time is increasing. In CRDS this information is used to determine the concentration of the analyte⁵⁷. Pulses can be either generated using pulsed lasers or by other means in case of cw laser sources, e.g. using a chopper.

The throughput of a ring down cell can be optimized if the emitted laser light fits to a cavity mode. Highest throughput is achieved in case of narrow laser lines being equal to a cavity mode.

When currently available QCLs would be used in pulsed mode the signal leaking out of the high reflecting mirror would be too weak to be detected during a ring down. Therefore in CRDS, cw QCL are used to fill the cavity with radiation prior to interrupting the light by setting the laser off resonance.

The first paper on QCL - CRDS reported measurement of ammonia in the low ppbv range was published in 2000⁵⁸. In this application a cryostatic cw DFB-QCL at 8,5 μm was used. In a further development a reference cell filled with the analyte was used for wavelength calibration⁵⁷. In both cases the laser line was scanned across the absorption line of interest. To ensure a constant match of the laser frequency with a cavity mode upon performing a temperature scan, one of the mirrors was piezoactuated to precisely control its position. The detectors employed for these studies had a bandwidth of 20 MHz (time resolution up to 50 ns) in order to follow typical ring down times of a few tens of microseconds.

2.3.2.2 Integrated Cavity Output Spectroscopy / Cavity Enhanced Spectroscopy

The technique described in the following was first published in 1998 under 2 different names: integrated cavity output spectroscopy (ICOS)⁵⁹ and cavity enhanced spectroscopy (CES)⁶⁰. In the following only the expression ICOS will be used. The experimental realization of ICOS is ought to be less demanding compared to CRDS as the laser does not need to hit a single cavity mode.³⁴ Thus, the laser line width may thus be much broader than the cavity mode spacing. As a consequence many cavity modes are excited rendering a higher throughput of a ICOS cell compared to CRD cells. If several cavity modes can not be covered by the laser light dithering of one mirror can be used to generate random jittering of the cavity modes³⁴. The light throughput is an average signal over all excited cavity modes. The more cavity modes are excited the better cavity throughput fluctuations can be suppressed. In difference to CRDS no intensity decay is measured in ICOS. Quantitation is based on Beers law using a reference intensity measured e.g. in a reference cell.

A direct comparison between ICOS and absorption measurements in a 100 m multi path cell using a CW QCL at 5,2 μm for NO measurement has been reported.⁶¹ Despite of achieving an effective path length of 670 m in the ICOS set-up higher sensitivities were obtained with a standard multi path cell due to a reduced noise level. The authors however mentioned reduced size of the set-up, the significantly smaller probe volume, a higher dynamic range as well as lower cost as the advantages of the ICOS set-up.

For improvement of the S/N ratio a further development of ICOS can be used. In off axis ICOS (OAICOS) the laser beam is directed at an angle to the cell so that the reflection spots are lying on a ellipse or a circle around the axis²³. The advantage of the off-axis setup is an increased density of cavity modes, a higher light throughput and as a result a reduction of noise.

2.4 Photoacoustic spectroscopy

In photoacoustic spectroscopy (PAS) intensity modulated light is used to excite the analytes in a sample. Upon relaxation the absorbed energy is partly transformed into heat, which in turn causes a local pressure rise. The modulation of the light source induces a modulated pressure wave, which can be detected as an acoustic wave using a microphone. In case of gas phase PAS the signal may be amplified substantially if the frequency of the resulting acoustic wave matches the resonance frequency of the used photoacoustic cell (PAC). The magnitude of amplification is referred to as the Q-factor of a given photoacoustic cell.

PAS is an indirect spectroscopic method. Whereas in conventional absorption spectroscopy the light not being absorbed by the sample is measured, in PAS the effect caused by light absorption, e.g. generation of pressure waves is measured³⁴. This principle brings about interesting advantages of PAS with respect to direct absorption spectroscopy. In principle PAS, is a background free method because a signal is only obtained if an analyte is present. However, heating of the cell windows as well as changing gas flow rates may cause acoustic noise. Therefore in PAS experiments buffer gas volumes are often used before and after the photoacoustic cell. In contrast to absorption measurement the obtained signal is direct proportional to the concentration of the analyte. Furthermore the magnitude of the PAS signal is direct proportional to the light intensity of the source. Therefore, in contrast to absorption measurements an increase in laser power will directly translate to higher signals. Another often mentioned attractive feature of PAS is its wide dynamic range, which usually covers 4 to 5 order of magnitudes of analyte concentration. Furthermore, replacement of expensive infrared detectors by more economic microphones as a detection element constitutes an additional advantage.

The first application using a QCL for PAS was reported in 1999⁶². The laser was a cw-QCL-DFB, which was mechanically chopped at 1660 Hz with a duty cycle of 50%. In this first application a MCT detector was used in addition to the photoacoustic detection to be able to detect and correct for intensity variations of the QCL. By temperature tuning of the laser emission wavelength over 35 nm, NH_3 and H_2O could be detected using one PAS system.

Similar to cells used in absorption spectroscopy, also photoacoustic cells can be equipped with mirrors so that the light is passing the cell several times to give rise to increased photoacoustic signals. Using a dedicated PAC allowing 36 reflections a path of 15 to 24 m could be realized^{63,64}. In contrast to the previous discussed publication the laser was operated in pulsed mode. As a consequence the operation parameters were optimized to minimize line width during one laser pulse for optimum sensitivity. Another development presented in these publications is the use of a radial microphone array composed of 16 microphones which allowed improvement of the S/N by a factor of four as compared to the use of a single microphone⁶³. Furthermore the authors are highlighting the advantages of QCLs compared with CO₂ lasers, normally used in PAS⁶⁴. Even if CO₂-lasers are more powerful and hence allow for lower limit of detection, QCLs can reach wavelengths regions not accessible with CO₂-lasers. They are tunable to individual molecular absorption lines and the dimensions and costs of a PAS system can be reduced.

In all applications described above a cylindrically photoacoustic cell was used by fundamental longitudinal acoustic mode operation. An improved version of a resonant cell for QCL PAS was introduced subsequently⁶⁵. The so called Helmholtz resonator consists of two chambers connected by two channels, where the signal is generated in the first chamber and detected in the second one⁶⁶. Contrary to a conventional cylindrically photoacoustic cell, a Helmholtz resonator does not rely on the generation of standing waves. Instead sound amplification is obtained via left to right oscillations of the gas volume inside the channels. The Helmholtz resonator design matches particularly well with the strongly divergent shape of a QCL beam. Therefore it is not necessary to produce a parallel beam like for controlled multi reflections between two mirrors to achieve enhancement due to resonance. By focusing the QCL light through a pinhole drilled in the middle of the outer side of the PAC the major part of the first chamber is illuminated by the QCL (see fig. 7).

In a further refined QCL PAS experimental design the QCL was placed directly inside the photoacoustic cell. In doing so noise resulting from absorption at the cell windows would be avoided. In addition more efficient use of the available light is made, as no collimating optics are needed. A PAC fabricated out of a copper block and containing the QCL inside has recently been reported⁶⁷. As the employed QCL emitted on both sides of its cavity and because of the large beam divergence and the multiple reflections on the polished surface efficient use of the available QCL light was made.

The latest development in photoacoustic cell design in combination with QCL excitation is called quartz enhanced PAS (QEPAS)^{68,69}. Instead of a microphone placed inside a resonant cell, a quartz tuning fork is used for detection. A cell is optional but not required. The light emitted by the QCL is focused between the prongs of the tuning fork. The excitation of the quartz tuning fork as a consequence of the photoacoustic effect generates a piezoelectric current. The modulation of the radiation takes place in the range of the frequency of the tuning fork which is in the range of 30-40 kHz, so much higher than a typically PAC shows (1 kHz)⁶⁸. QEPAS shows some advantages compared to conventional PAS. First of all a higher acoustic amplification given by a Q-factor up to 10000 instead of 20-200 as in conventional PAS can be achieved. Secondly the size of a QEPAS cell is about 1 cm³ and thus up to 20 times smaller than resonant

PACs, resulting in faster response time. Furthermore, the QEPAS cell is insensitive to ambient acoustic and flow noise, contrary to the traditional PAS cell.

In an optimum case the QCL wavelength matches an isolated absorption line of one analyte. If the absorption bands of several analytes are overlapping strategies to distinguish them need to be developed. One possibility is to make use of molecular specific differences in the decay time of the excited states, e.g. the time required to transfer ro-vibrational excitations into translational molecular degrees of freedom (V-T relaxation time)⁶⁸. As a consequence of the decay time, a phase shift between the light modulation and the PA signal occurs. In addition to the influence of the V-T relaxation time on the phase shift it is also influenced by the modulation frequency. A rise in modulation frequency increases the phase shift as the portion of the V-T relaxation time with respect to the excitation length is increased. As the V-T relaxation time is different for all chemical species it is possible to obtain information about a desired analyte even if the investigated absorption line is overlapped by absorption of the matrix. For a high selectivity operation parameters have to be chosen to maximize the differences in the photoacoustic phase shift of the analytes. This can be realized either by low pressure, which increases the V-T relaxation time, or by working at higher modulation frequencies. As both conditions can be realized with QEPAS this technique results especially useful to exploit differences in phase shift for analytical applications.

2.5 Faraday modulation spectroscopy

So far Faraday modulation spectroscopy (FMS) is the only known technique which takes advantage of the polarization of the QCL beam. The technique is based on the Faraday effect that is observed only for paramagnetic molecules such as free radicals. If the QCL frequency is resonant with a transition of the target molecule and a magnetic field is applied, the polarization axis of the laser beam is rotated⁷⁰. The degree the polarization axis is rotated depends on the concentration of the analyte and the quality of the match between the laser frequency and the absorption frequency. Using a QCL the emission wavelength can be matched with the absorption frequency of the target molecule. The external magnetic field is then modulated and the resulting modulation of the polarization axis is detected using an analyzer in front of the IR-detector. Other molecules present in the sample besides the analyte are not contributing to the signal as long as they are diamagnetic even if they show absorption at the same wavelength. For effective use of the FMS an additional polarizer has to be added as the polarization degree of the QCL beam itself is not sufficient. Whereas FMS is an interesting and sensitive technique it is limited to paramagnetic analytes and has only been shown for NO detection when using a QCL light source.^{71,70}

3 Applications

3.1 Atmospheric trace gas

Traces of different gases present in the atmosphere play an important role in atmospheric chemistry which governs issues like aerosol or ozone formation, global warming, acid rain among others. For a better understanding of the underlying mechanism in atmospheric chemistry, accurate, sensitive and selective measurements of the relevant species are required. In an ideal case information on the concentration of selected molecules is made available in real-time by deployable and remotely working sensors. This information may also contribute to determine sources and sinks of chemical species or to distinguish between anthropogenic and natural origin. Therefore different research efforts on atmospheric trace gas detection have been published.

A QCL based tunable ($1880\text{--}1900\text{ cm}^{-1}$) infrared laser differential absorption spectroscopy (TILDAS) instrument was used to detect NO in the sub-ppb range⁴⁰. The system was equipped with a 210 m multipass cell and a beam splitter for measurement of a reference signal to account for fluctuations in emission power. Because of the time delay between sample and reference signal one detector could be used. The performance of the QCL sensor system was compared with a similar optical set-up employing a tunable lead salt diode laser (measuring the NO transition at 1896.98) showing good agreement in sensitivity.

A system for QCL based absorption spectroscopy employing two detectors, one for sample the other for reference measurement, was developed for quasi continuous CO⁴¹ monitoring. Air was sampled periodically via a computer controlled valve and pressure controller to avoid pressure induced signal fluctuations. First long time tests were performed using ultra-high priority grade N₂ and Niwot Ridge, Colorado mountain air revealing a noise level corresponding to 12 ppb of CO. The system was also used to monitor the CO concentration in the ambient laboratory air over 24 hours. Interestingly, an increase in CO concentration in the laboratory was determined during morning and evening traffic with short time fluctuations due to changing meteorological conditions, such as wind.

Another method for atmospheric CO monitoring was carried out using QEPAS⁶⁹. To assure a match between the laser emission line and the analyte absorption part of the QCL radiation was deflected at a beam splitter and guided to a reference cell containing the analyte. Most of the radiation passed the beam splitter and was recorded on a power meter for normalization. The detection limit of the method was expressed as noise equivalent sensitivity and corresponded to 280 ppbv in nitrogen, which however was not sufficient to monitor atmospheric CO. The reason for this is seen in the vibrational relaxation of CO, which is too slow to produce a measurable QEPAS signal. When applied for sensing of N₂O the same set-up showed a much better performance reaching noise equivalent sensitivities of 4 ppbv.

Off-axis integrated cavity output spectroscopy has been used to set-up a autonomous instrument for CO detection at trace levels⁷². For measurement a cw-QCL at 2172.8 cm^{-1} being injection-current tuned at an 800Hz rate about 0.5 cm^{-1} was used for high resolution measurements of the CO R(7) line. The line shape of the measured cavity enhanced absorbance spectrum was fitted to a Voigt profile and combined with

measured values of gas temperature and pressure in the cell for determination of the CO mixing ratio. Successful measurements onboard a NASA DC-8 aircraft up to altitudes of 12.5 km allowed to precisely measure the CO mixing ratio in the troposphere and tropopause. Accuracy of the results was assured by periodic measurement of a reference gas with a CO mixing ratio of 550 ppbv. Lowest measured CO concentration was 32.1 ppbv with typical precision of 0.2 ppbv achieved at a 1 second averaging time.

N₂O together with CO₂ and methane have also been measured in a set-up based on multi-path absorption measurements employing thermoelectrically cooled QCLs and detectors. The authors expressed the analytical performance of the set-up as precision (rms), stating values of 0.3 ppb for N₂O and 4 ppb for methane⁷³. The reported set-up allowed long-term, unattended continuous operation, which are important characteristics for remote measurement stations. The system was based on a multipass absorption cell and a two beam principle using one detector for reference measurements. The long time stability of the system was tested successfully by measuring N₂O and CO₂ in ambient air over a 2 month period. In order to be able to detect simultaneously N₂O and methane, the originally chosen wavelength of around 4.5 μ m was changed to the region of 7.8 μ m where methane also shows absorption lines. A comparison of the precision achieved using a thermoelectrically cooled detector versus a LN₂ cooled detector showed approximate equal performance at short wavelengths whereas TE cooled detectors showed a significant poorer performance for longer wavelengths.

Methane and N₂O measurements have also been carried out successfully directly in the stratosphere⁷⁴. A QCL operating near 8 μ m as well as three lead salt lasers were placed in the same Dewar of an aircraft laser infrared absorption spectrometer (ALIAS⁷⁵). The ALIAS has been flown on an ER-2 aircraft up to the stratosphere for a series of 20 flights. The performance of the QCL was compared with that of the lead salt lasers. The QCL showed superior performance due to a significant smaller line width, a 10 times higher output power as well as better mode purities. A minimum detectable absorbance of 5E-5 corresponding to 2 ppbv of methane has been reported when using the QCL. This is a significant improvement by a factor of approximately 3 compared to lead salt lasers.

A flexible and compact mid-IR laser spectrometer termed QUALITAS incorporating a multipass absorption cell for measurements of trace gases such as CO, NO and methane in the clean atmosphere has been reported. In this spectrometer either lead salt or quantum cascade lasers requiring cryogenic temperatures can be used. Qualitas has been used for airborne CO measurements. For this purpose the R3 line at 2158.3 cm⁻¹ has been selected for measurements using cw-QCL at 102 K. A standard 2f – wavelength modulation scheme at 18 kHz has been applied to record the optical density used for data analysis. The varying CO concentration in the tropopause could be measured with a estimated detection limit of 0.59 ppbv. Calibration of the instrument was performed periodically using pressurized air with a CO mixing ratio of 106.4 ppbv⁷⁶.

NH₃ and SO₂ are further important trace gases, which have been measured using absorption spectroscopy⁷⁷. In addition to spectroscopic studies on SO₂, quantitative results have been reported for NH₃. Direct absorption spectroscopy and wavelength modulation spectroscopy were performed for the NH₃

measurements. The authors state a 18 ppm noise equivalent sensitivity achieved for 1 meter of absorption path length. An increase in sensitivity by a factor of 3 could be achieved using wavelength modulation spectroscopy. The so far most sensitive NH_3 measurements were achieved already 2000 using CRDS⁵⁸. The system was used to analyze NH_3 in nitrogen. The authors report an estimated limit of detection of 0,25 ppbv with the lowest available concentration for measurements being 10 ppbv.

Information about the source and the history of atmospheric compounds can be obtained from their isotope ratio. Recently the development of a spectrometer for measurements of CO_2 isotopes has been reported⁷⁸. The instrument was designed to measure the $^{13}\text{C}/^{12}\text{C}$ isotope ratio in CO_2 released from volcanic vents. It comprises a dual multipass cell design, where a short 0.024 m path and a long 36m path were used for $^{12}\text{CO}_2$ and for $^{13}\text{CO}_2$ measurements respectively. The design was outlined for the estimated CO_2 concentration above 1% in real samples. First laboratory tests measuring the $^{16}\text{O}^{12}\text{C}^{18}\text{O}$ concentration in a N_2 matrix with a total amount of CO_2 of 1% were performed to demonstrate the basic concept of the sensor. In a further contribution this group discusses criteria for optimum wavelength selection for a planned spectrometer for accurate measuring the isotopic ratio of $^{13}/^{12}\text{CO}_2$ requiring only a single gas cell⁷⁹.

The principle of differential absorption spectroscopy was tested on the example of ozone³⁶. A gas cell was filled with high purity oxygen and a background spectrum recorded. Ozone was subsequently generated in the absorption cell by use of a homemade oxygen photolyzer equipped with three low-pressure Hg lamps. Ozone was formed and an absorption spectrum calculated. The studied concentration ranged from 1 to 700 ppm. Real time reference measurements were carried out simultaneously using standard technology. The obtained spectra were either evaluated directly achieving an obtained sensitivity stated as 14 ppm m for absolute absorption or evaluated on the principles of differential absorption spectroscopy where a sensitivity corresponding to 25 ppm m has been achieved. The advantage of the differential absorption technique was mainly seen in its higher reliability and precision at concentrations below 80 ppm m. A sensitivity of 100 ppbv for ozone could be reached with PAS²². The transmitted light power was measured with a power meter to correct for fluctuations in laser intensity. Ozone standards containing 100 to 4300 ppbv were prepared by feeding mixtures of synthetic air and pure nitrogen through an ozone generator, based on an electrical discharge. Reference analysis was again performed using an UV photometric ozone analyzer. In addition to the improved sensitivity obtained with PAS as with respect to absorption measurement³⁶ the inherent simplicity of the QCL-PAS instrument has been highlighted by the authors. Recently open path measurements of ozone have been reported⁸⁰. The open path experiments covering a 5800 m pathlength were carried out with a monostatic (transmitter-retroreflector-receiver) configuration. To avoid line-distortion from atmospheric turbulence fast wavelength scanning was essential. For this reason 140 ns laser pulses have been used exploiting the fast frequency downchirp of the QCL centered at 1031.2 cm^{-1} . The lowest detection limit of 0.3 ppmm was estimated from the minimum detectable differential absorption. Due to the long optical path ozone concentrations ranging from 10 to 70 ppb in ambient air could be detected.

An interesting concept for achieving sensitive gas measurements in a compact and fast responding set-up is based on using hollow waveguides which as miniature gas cells⁸¹. First application of this sensing concept using QCL was demonstrated on the example of ethylene measurement using a cryogenically cooled pulsed QCL emitting at 10 μm . In these early measurement a detection threshold of 250 ppm has been reported⁸². In a further feasibility study where ethylchloride was used as test analyte, a room temperature DFB-QCL at 971 cm^{-1} allowed to achieve a limit of detection of 0.5 ppm when using a 4 m waveguide⁸³. Recently the authors reported an improved set-up based on a 1 m photonic band-gap hollow waveguides developed for medical laser delivery. Using a beam splitter and a reference detector to compensate for pulse to pulse intensity fluctuations detection limits of 30-40 ppb have been reported based on results achieved in a gas dilution experiment⁸⁴.

3.2 Traffic and combustion

An important part of the atmospheric pollution is of anthropogenic origin. For this reason it is not only necessary to monitor the atmospheric concentration, but also to monitor sources such as traffic and other combustion processes. Information on the time course of pollutant emission can help to improve technology with the aim to reduce or even avoid emission of environmental hazardous substances. Typical analytes of interest in this context are CO, CO₂, NO, NO₂, SO₂, SO₃, hydrocarbons, as well as NH₃ and ozone. These analytes are either produced directly in combustion engines or formed via secondary reaction pathways in the atmosphere. So far a variety of experimental set-up based on QCL detection have been reported with some of them already used in real world applications.

The problem of troposphere ozone especially in urban areas is a consequence of emissions of multiple chemical species. Ethylene promotes the formation of ozone in the presence of OH radicals and nitrogen oxides. Possible sources for ethylene are motor vehicle exhaust and industrial fugitive emissions. For that reason, a QCL based gas sensor for ethylene detection was developed²⁴. A Herriott multipass cell was used for absorption measurements. Compensation of the pulse to pulse fluctuations were performed using a beam splitter and a time delay between the reference and the sample signal, recorded with the same detector. The system had a noise equivalent sensitivity of 30 ppb. The feasibility of ethylene detection in real samples has been shown as well. Samples taken from the exhaust pipe of a car as well as from a high-traffic urban tunnel were investigated with this instrument. In both cases the ethylene concentrations could be monitored.

QCL based monitoring of emissions from traffic focusing on the CO₂, NH₃ and NO has also been reported²⁷. The used QCLs were driven with 35-100 ns long pulses and the frequency downchirp used to scan over the absorption line. The QCL and the detector were TE cooled. First measurements were established using a 10 cm long absorption cell reaching limits of detection below 1 ppm m for all analytes. The system was further adapted for roadside measurements. The QCL beam passed 17 m free optical space before it was reflected back to the instrument with a cube corner reflector. The total optical path could be

determined by evaluating the time delay of the QCL pulse and the detector response. The obtained concentration was integrated above the whole distance. First results for NO measurements showed the capability of the system to trace NO emission from passing cars.

A system based on wavelength modulation absorption measurements was developed to detect NO in automobile exhaust gas⁸⁵. The system was calibrated with mixtures of NO and/or NO₂ in N₂. A heated catalyst for conversion of NO₂ to NO with an included bypass system was preceding the used multi-pass (100 m) cell. As NO tends to adsorb on the cell walls a continuous flowing gas system was used for all measurements. Samples from automobile exhaust gases used for vehicle emissions certification were analyzed. The samples were measured with and without the catalyst to distinguish between the two NO_x species. The system showed a capability of detecting NO in the low ppb range.

Nitric oxide has also been determined using photoacoustic spectroscopy achieving detection limits of 500 ppb. A resonant cell and a pulsed DFB QCL have been employed for detection of the NO line at 1871,06 cm⁻¹. The FWHM of the laser pulse extended over about 0,6 cm⁻¹. Despite of the presence of closely spaces CO₂ lines (1870,817 and 1870,904 cm⁻¹) NO determination was not affected by CO₂ concentrations up to 1000 ppmv. However, the water line at 1870,805 cm⁻¹ caused significant interferences suggesting the use of water vapor filters or differential PA technique for measurements of NO in ambient or open air. The authors stressed the advantages of the PA technique as being simpler and cheaper than detection schemes requiring multipass cells for achieving similar sensitivities⁸⁶. The advent of single mode thermoelectrically cooled cw QCL at 1850,18 cm⁻¹ has allowed to use wavelength modulation spectroscopy (250 kHz) for the determination of NO in an astigmatic 76m multipass cell. A detection limit of 0.2 ppbv over 30 s has been reported. Samples aspirated from a nearby road were collected via 40 m Teflon tube and dried with CaCl₂ to remove water vapour to avoid spectral interferences. The fast response time of the system allowed to trace passage of single vehicles on the road due to their NO emission⁸⁷.

Concern over the global atmospheric and climatic effects of sulfur oxides exhausted into the upper atmosphere by jet engines has prompted the need for direct determinations of SO₂ and SO₃ in test combustor exhausts at simulated high-altitude conditions. A dual QCL laser sensor employing room temperature DFB QCLs emitting at 7,50 and 7,16 μm for SO₂ and SO₃ respectively and a single pass 1.4 m gas cell. Laser pulses of 10 ns and below have been used resulting in laser bandwidths of less than 0.03 cm⁻¹. Using a sub-threshold sawtooth current ramp the laser emission was tuned across the absorption feature of interest. Using this set-up detection limits for both SO₂ and SO₃ of 1-2 ppmv m/Hz^{1/2} have been achieved.⁸⁸

Using a room temperature pulsed DFB QCL emitting at 10.26μm and an astigmatic Herriott cell for direct absorption measurement allowed both detection and real time observation of the evolution of carbon dioxide and ethylene in the exhaust of several cars⁸⁹. For data acquisition a 140 ns pulse has been used. In this application a spectral micro-window extending from 973 to 974.4 cm⁻¹ could be covered allowing the simultaneous measurement of CO₂ and ethylene absorption bands. The pressure for measurement was set to 35 Torr in order to avoid rapid passage effects. Rapid passage effects occur when the sweep rate is much

faster than the relaxation rate of the medium which here corresponds to the time required for collision of the gas molecules. In such a case asymmetric instrument functions are obtained due to nonequilibrium transfer of population between the lower and upper states of the transition. The authors stress the capability of their instrument to fully resolve almost completely the rotational structure within the recorded micro-window and the resulting advantages in terms of sensitivity and selectivity. Experimental data showed achieved sensitivities of ~ 1.5 ppm which could be improved by optimized to 250 ppb by adapting experimental conditions successfully employed for measurement of nitrous oxide in cigarette smoke⁴³.

Combustion products in cigarette smoke were investigated in Ref. 38 and 90. The instrument was developed for real-time monitoring of selected analytes to gain a better understanding in formation processes of gas components in the smoke. While the first spectrometer³⁸ was able to detect NH_3 , ethylene and NO, the further development⁹⁰ was able to detect also CO_2 and N_2O . Analytes were measured in the gas stream passing the cigarette and in the smoke emitted by the cigarette using separate multi-path gas cells. By means of an elaborate four laser module containing a pyramidal mirror four QCL beams could be combined into one path. A set of beam splitters allowed to perform measurement in both gas cells simultaneously including reference measurement to account for fluctuations in laser power. Operation of each laser was individually optimized to match laser frequency and line width with analyte absorption. The first QCL (967 cm^{-1}) was used for NH_3 and ethylene, the second QCL (1900 cm^{-1}) was used for NO, the third QCL (2240 cm^{-1}) was used for CO_2 and N_2O and the forth QCL (963 cm^{-1}) again for NH_3 and ethylene. With the analyzer data could be collected at 20 Hz, which resulted fast enough to obtain concentration profiles of all five analytes during and after each 2s puffs.

3.3 Medical and biological applications

Some simple molecules such as NO, CO or COS play an important role in physiological processes. These molecules can be seen as physiological messengers. Some trace gases in exhaled breath are biomarkers for special diseases, e.g. NO is a tracer for several lung diseases such as asthma or other inflammatory processes in the respiratory tract^{91,92}. Liver diseases can cause increased levels of COS in exhaled breath⁹³. Elevated COS concentrations are also reported in lung transplant recipients suffering from acute rejection. Since typical concentrations of these biomarkers are quite low analysis is required in the low ppb range. QCL based analyzers are of interest also for these applications because of their fast response and the non-invasive character of diagnosis as opposed to current techniques based on biopsies.

As CRDS is a high sensitive technique it is well suitable for the demands on medical diagnostics. The development of a spectroscopic gas sensor for NO based on CRDS has been reported⁵⁷. First the technique was developed and tested using mixtures of NO in pure N_2 . The lowest inserted concentration in the system was 48,4 ppb and the standard error for this measurement was found to be 0,7 ppb. The tuning range of the used QCL covered also a weak absorption line of CO_2 . This line was used to determine the CO_2 concentration in the laboratory air. Finally the system was tested for measurements of NO in air exhaled through the mouth. Samples were collected in plastic bags prior to analysis. The high concentrations of

H₂O and CO₂ in the samples made it impossible to detect NO because of strong background absorption. The authors suggested using a different absorption line of NO (instead of the used one at 1921,6 cm⁻¹) for these measurements, but a corresponding QCL was not available.

A publication aiming at the same problematic of NO detection was using absorption spectroscopy with a multi pass cell and in a second approach integrated cavity output spectroscopy (ICOS)⁶¹. For the measurements the region around 1918,7 cm⁻¹ were used for the multi pass cell and the region around 1920,5 cm⁻¹ for the ICOS. The applied frequency scan was in the order of 0,5 cm⁻¹. In both cases the absorption lines from NO, H₂O and CO₂ were clearly separated. The reported limits of detection are 3 ppb for absorption spectroscopy in the multi pass cell and 16 ppb for ICOS. Both techniques were tested using real samples from humans. The air was exhaled via mouth or nose and collected in plastic bags prior to transfer into the cell. A typical concentration of NO in air exhaled through the nose is in the order of 100 ppb which is 10 times higher than the concentrations found in air exhaled through the mouth. Therefore it was found that ICOS is only applicable for the samples taken from the nose.

A further development of ICOS is the off-axis ICOS. This technique was used to detect NO in nitrogen as well as in nasal air²³. The system was calibrated using two mixtures of NO in N₂ (490 and 94,9 ppbv). The off-axis ICOS sensor showed a noise equivalent sensitivity of 10 ppbv. A further improvement was achieved by performing wavelength modulation spectroscopy in combination with off-axis ICOS. A triangular current ramp with a superimposed sinusoidal dither was used to scan the laser across the absorption line. The second harmonic signal was sampled with a lock-in amplifier and averaged. Using wavelength modulation a noise equivalent sensitivity of 2 ppb was obtained. With this set-up real samples taken from nasal exhaled breath were measured successfully. The authors also suggested to take advantage of the CO₂ and H₂O lines which have been measured also during one scan to provide information on lung function which is required for referencing the result of NO analysis.

A sensor based on Faraday modulation spectroscopy was used for continuous monitoring of the NO release rates from nitrite solutions and human sweat. This QCL based technique for NO measurements is free from interferences from CO₂ and H₂O^{70,71}. The noise equivalent sensitivity was reported to be 4 ppb⁷⁰. The samples were placed in a temperature controlled glass cuvette containing a frit through which a gas flow was directed. The gas containing released NO and water vapor was fed through the measurement cell. Aqueous nitrite solution and nitrite spiked human sweat were investigated for their NO release under exposition to UVA light. Interestingly, it was found that biogenic NO release from human sweat is around 20 times lower than from an aqueous solution containing the same amount of nitrite. Sensitive NO detection requiring has been demonstrated using a coiled 9 m hollow waveguide (i.d.: 1 mm). In nitrogen the reported limit of detection was 58,8 ppb with a response time (0-90%) of only 0,48 s. For NO the QC laser was operated at room temp. in pulsed current mode near 5,4 μm. This sensor targets rapid analysis of exhaled breath⁹⁴.

For carbonyl sulfide (COS) detection an absorption spectrometer was developed⁹⁵. In the presence of water a detection limit of 30 ppb was estimated. Furthermore the developed system was capable to differentiate

between two stable isotopes, $^{12}\text{C}^{16}\text{O}^{32}\text{S}$ and $^{12}\text{C}^{16}\text{O}^{34}\text{S}$. The feasibility of COS detection in human breath was proved by measurement of human breath samples spiked with COS. While strong interferences with CO_2 has been found for some COS absorption lines, comparable results could be achieved in nitrogen and human breath when evaluation was based on the interference free line at 2054,078 wavenumbers. An improvement in the limit of detection of more than one order of magnitude was achieved in another paper by fast wavelength scanning and improved data acquisition and processing techniques⁹⁶. This system was used for concentration measurement of low ppb COS levels in human breath samples from lung transplant recipients.

Beside investigations of trace gas levels released from the human body, investigations of biomarkers released from cell cultures were also carried out using QCL technology⁴². For this application the target molecule was CO, which is produced from heme catabolism by the enzyme heme oxygenase. This work was motivated by the need for a fast and sensitive detection method to be able to characterize the formation kinetics at the normally low levels of CO (ppb) encountered in this application. The investigated vascular cell cultures were placed in a sealed vessel stabilized at 37°C and ventilated prior measurement with a gas mixture containing 5% of CO_2 . The QCL output was again split into a signal and a reference beam. The signal beam was guided by multiple reflections directly above the cell culture. During measurement the purge valves had been closed to be able to follow CO formation. The minimum detectable CO concentration was reported as 20 ppb for a one meter optical path. The system was able to monitor the CO production rate above the cell cultures with rates that agreed well with those previously reported.

3.4 Spectroscopic studies

For investigations of absorption band structures it is necessary to use techniques with a high spectral resolution in order to be able to separate narrow and almost overlapping absorption lines. For measurements of weak absorption lines it is also necessary to use light sources with sufficient power. DFB QCL are able to provide both narrow line width and high power. Therefore, they are well suited for spectroscopic studies. In this section applications are presented which focused on the investigation of absorption lines of molecules, isotopomers and the finger print region of organic substances.

In the first example wavelength modulation spectroscopy was performed on CH_4 and N_2O stable isotopes using a continuous wave QCL at $1240,7\text{ cm}^{-1}$ ⁹⁷. For the measurements a gas cell was filled with the pure analyte (CH_4 or N_2O) under reduced pressure and spectra measured several times. The significant advantage of QCL over NIR lasers in the determination of isotope ratio is seen in the access to fundamental ro-vibrational lines, their wide tunability and high spectral purity. Currently achieved reproducibility of isotopic ratio measurements was given as a few ‰ by the authors. The natural isotopic abundances of $^{12}\text{CH}_4$, $^{13}\text{CH}_4$ and $^{14}\text{N}_2^{16}\text{O}$, $^{15}\text{N}^{14}\text{N}^{16}\text{O}$, $^{14}\text{N}_2^{18}\text{O}$, $^{14}\text{N}_2^{17}\text{O}$ have been investigated in this study. A cryogenically cooled QCL emitting around $8,06\text{ }\mu\text{m}$ was used for absorption spectroscopy of CH_4 and N_2O stable isotopomers. Ro-vibrational transitions belonging to $^{12}\text{CH}_4$, $^{13}\text{CH}_4$, $^{14}\text{N}_2^{16}\text{O}$, $^{15}\text{N}^{14}\text{N}^{16}\text{O}$, $^{14}\text{N}_2^{18}\text{O}$,

$^{14}\text{N}_2^{17}\text{O}$ fundamental bands, around 1240 cm^{-1} were detected in pure methane and nitrous oxide samples using wavelength modulation spectroscopy at 1-10kHz and first harmonic phase sensitive detection. For wavelength calibration and a test of frequency scan linearity were performed using pairs of well-known CH_3J absorption lines as frequency references.⁹⁸

Spectroscopic studies of ethylene and NH_3 with a pulsed QCL⁹⁹ and SO_2 with a cw QCL²¹ were performed using absorption spectroscopy. Gas cells filled either with pure analyte or with analyte gas diluted in ambient air were used for measurement. Transmission spectra were recorded and compared with calculated spectra from the HITRAN database. The spectrum of ethylene and NH_3 showed good agreement in the position of the lines with the database but showed deviations with respect to line intensities. The authors investigated band broadening as a function of laser pulse duration due to frequency down-chirp during the laser pulse. Using the cw-QCL for the study of SO_2 discrepancies in line intensities and line width between measured and calculated spectra were found. Additionally, few lines found in the measured spectra were missing in the simulations. The self-broadening coefficient of nine transition were calculated and found to be in good agreement with previous measurements carried out with a lead salt laser.

For sensitive high-resolution spectroscopy a spectrometer based on the downchirp of a QCL pulse was developed^{28,29}. The spectrometer allows tuning over $2,5\text{ cm}^{-1}$ wavenumbers in the region of 974 cm^{-1} . By using the down-chirp of the pulse it is not necessary to step tune the QCL through the absorption band. That way the spectrometer provides a real time display of a section of the spectral finger print of molecular gases. The spectral resolution (approx. $0,015\text{ cm}^{-1}$) was limited by the time resolution of the detection system and a function of the pulse current. With higher pulse currents the accessible wave number range increased whereas spectral resolution decreased. The spectrometer was successfully used for measurements of CF_2CH_2 and COF_2 . The authors stress the capability to rapidly record a spectral fingerprint as well as the capability of the system to perform sensitive quantitative analysis being able to measure fractional absorbance of $4 \cdot 10^{-4}$.

3.5 *Process monitoring*

The usefulness of QCL based analyzers to measure key components in production processes has also been recognized. An example is the measurement of C_2H_4 and NH_3 during biogas production or biomass steam gasification. Knowledge of these and other key components would allow to optimize the production process. Using a pulsed QCL placed in a liquid nitrogen cooled thermostat and a 44 cm gas cell absorption measurements were performed to monitor the concentration of C_2H_4 and NH_3 in both process gases³². Using temperature tuning the spectra of the target analytes were recorded. Estimated limit of detection were given as 0,5 % for C_2H_4 and 500 ppm for NH_3 . Further, biogas and product gas from a biomass steam gasification pilot plant were measured. NH_3 could not be detected and C_2H_4 was only found in the product gas.

Propylene is an important raw material for the production of polymers. Impurities of CO in the monomer can poison the catalyst. As absorption from the propylene matrix interferes strongly with the CO bands, a selective technique is required that is able to distinguish the two molecules. A QEPAS system with phase shift discrimination was found to be an appropriate method⁶⁸. CO concentrations of few ppm could be quantified with an accuracy of 0,5 ppm. Beside quantitative measurements the system was also used to evaluate V-T relaxation rates of CO and N₂O in propylene. Determination of hexamethyldisilazane traces in semiconductor manufacturing process applications down to 200 pbbv has been shown using QCL based photoacoustic detection. A resonant PA cell consisting of a cylindrical stainless steel resonator of 12 cm length and 4 mm radius to which 4 electric microphones had been attached was used. The FP QCL (emission around 1183 cm⁻¹) was mounted on a Helium cryostat and operated at 20 K achieving peak power of approximately 2 W and 100 ns pulse lengths. The acoustic signal at a frequency of 1380 Hz was detected using a lock-in amplifier.¹⁰⁰ On-line process monitoring in the gas phase has been successfully applied to study the gas phase chemistry in a 2 kW MW plasma enhanced reactor during diamond chemical vapor deposition. Specifically both CH₄ and C₂H₂ molecules and their interconversions have been monitored as a function of the process conditions. Providing valuable insight in the occurring reactions. For measurement the long pulse spectrometer from Cascade Technologies has been used based on a 2 μs laser pulses of a 8 μm QCL. These long pulses allowed to record the microspectral window extending from 1273.0 to 1277.6 wavenumbers¹⁰¹.

3.6 Applications in the liquid phase

Functional group specific detection using QCLs was shown in separate experiments using a simple flow injection system for automated sample delivery¹⁰². Two lasers at different wavelength were used, one within an absorption band of the C=N-C vibration and another one within an absorption band of the carbohydrate C-O stretching vibration. Xanthosine showing both functional groups could be detected at both wavelength, where adenine has no carbohydrate group and showed negligible absorbance at the corresponding wavelength.

Measurement of glucose in serum has been demonstrated using a QCL at 1036 cm⁻¹ and performing absorbance measurement in a 26,4 μm BaF₂ flow cell and using an MCT detector⁴⁶. To improve correction for underlying water absorption measurement at a second wavenumber (1194 cm⁻¹) was proposed for situations where no background value at 1036 cm⁻¹ would be available. In this report a laser exchange was required for dual wavenumber recording. The average predictive standard deviation of the mean was 24.7 mg/dl when using recordings at both wavenumbers. The authors pointed out that the limiting source of error in their determination was the tolerance of the used power supply.

Two pulsed Fabry-Perot quantum cascade lasers (QCL) have been employed for the simultaneous measurement of glucose and acetate in aqueous solutions. For sample delivery a single line flow injection system was used. Two laser beams (1393 and 1080 cm⁻¹) were combined by an optical system of parabolic

mirrors and a ZnSe-beam splitter. Measurements were made in transmission using a 41 μm CaF₂-flow cell and a MCT detector. The laser pulses were spaced by 55 ns and evaluated using a 10 ns gate of the boxcar integrator. The use of the two lasers gives quantitative information about the analytes, even when they show overlapping absorption bands typically found in condensed phase⁴⁹. A similar dual beam set-up using the same lasers has also been successfully used for on-line monitoring of the oxidation of sulfite to sulfate using hydrogen peroxide⁵⁰.

The potential of internal reflection spectroscopy using QCL has been demonstrated using free standing thin film planar silver halide waveguide and a DFB QCLs at 1650 and 974 wavenumbers. At 1650 cm^{-1} urea crystals have been measured which were formed by evaporation of a urea containing solution placed on the waveguide with a minimum amount of 80,7 μg being detected. At 974 cm^{-1} volumes as low as 10 nL of a 1% acetic anhydride solution in acetonitril were measured. In order to compensate for pulse to pulse fluctuations of the laser power the authors used a beam splitter prior to the waveguide to produce a reference beam. Complementary they show first results of a pigtailed coupling of the QCL to the waveguide yielding improved radiation throughput, however losing the possibility to split the IR radiation into two separate channels for referencing. In a continued development towards dedicated miniaturized QCL based sensors a GaAs waveguides have been fabricated using molecular beam epitaxy⁴⁸. The aim was to produce mono mode waveguides which carry a large fraction of power outside the waveguide core. For QCL measurements again a pigtailed set-up was used and a five-fold increase in sensitivity compared to multimode silver halide waveguides obtained. As a sample drops of acetic anhydride of 0.5 μl were placed on the waveguide and detected.

Droplets of α -tocopherol in squalane and acetone in aqueous solutions placed on multi-mode silver halogenide waveguides have been measured using FP-QCLs at 1208 and 1363 cm^{-1} respectively. Experiments were carried out in open space with a 25 mm droplet immersion lengths being able to detect 1 % of α -tocopherol in squalane and 2% of acetone in water respectively¹⁰³.

Direct, selective measurement of analytes in liquid phase is of practical relevance as the direct determination of carbon dioxide in beverages³³ shows. Standards containing dissolved CO₂ in distilled water were pumped through a flow through cell and the absorption at 2330 cm^{-1} recorded. At this wavenumber the edge of CO₂*aq band, centered at 2342 cm^{-1} , could be monitored. Typical limits of detection lay in the low mg/L range and were limited by the performance of the QCL driving electronics. Despite that the CO₂*aq band is free from direct interferences from sugars, organic acids or ethanol the underlying water background is affected by the presence of these molecules. As a result sloping baselines are obtained hinder robust CO₂ determination in soft-drinks or beer. A solution to this problem is seen in shifting the emission wavelength of a standard DFB-QCL by working with two distinct driving currents. Wavelength modulation by 0.2 cm^{-1} and evaluation of the obtained absorbance differences proved to be appropriate to eliminate interferences of sugars in the determination of carbon dioxide in aqueous solution⁵¹.

In case direct measurements do not offer sufficient selectivity a flow system may be added prior to detection. In case of using a separation technique being high performance liquid chromatography (HPLC) or capillary electrophoresis (CE) the analytes of interest are separated and detected sequentially. In case of flow injection analysis (FIA) chemical reactions are used to gain selectivity in analysis.

The hyphenation between HPLC and QCL detection was achieved again using a fiber optic flow through cell to assure a minimum internal volume of the flow cell¹⁰⁴. To withstand the acidic carrier employed in the chromatographic separation hollow fibers sealed with diamond windows have been used. On the example of the separation of sugars and organic acids the possibility to record functional group specific chromatograms using QCL based detection has been shown.

In capillary electrophoresis the sample is injected into a fused capillary and high potential is applied. Due to the resulting electrosmotic flow inside the capillary and due to different electrophoretic mobilities of the analytes inside the capillary they are separated on their way to the detector. In case of UV detection absorption measurements are performed through the capillary. As these capillaries are not transparent in the mid-IR spectral region dedicated micromachined flow-cells made of CaF_2 had to be developed for QCL detection in capillary electrophoresis¹⁰⁵. In the given application the authors show separation of adenosine, guanosine, xanthosine and adenosine-5-monophosphate using a 60 μm flow cell and a FP-QCL at 1080 cm^{-1} .

Phosphate was determined in soft drinks using a flow injection system and a 106 μm fiber optic flow cell¹⁰⁶. The optical path of the cell could be adjusted by changing the positions of the fibers made of silver halide. After passing the detection volume the beam was collected again by a fiber connected directly with the detector housing of a MCT-detector. The analytical readout in this study was the different absorption values of phosphate at different pH-values according to acid-base reaction. That way the method was selective despite strong background absorption of water and the sample matrix.

4 References

- ¹ C. Kittel, Introduction to Solid State Physics, 8th Edition, ISBN: 0-471-41526-X, 2005;
- ² J. Singh, Quantum Mechanics: fundamentals and applications to technology, ISBN 0-471-15758-9, 1996
- ³ M. A. Herman, H. Sitter, Molecular Beam Epitaxy (Springer, Berlin, 1996); ISBN 0387605940
- ⁴ J. Faist, F. Capasso, C. Sirtori, D.L. Sivco, A.L. Hutchinson, and A.Y. Cho, Quantum cascade laser, Science **264**, 553 (1994)
- ⁵ H. Kogelnik and C. V. Shank, J. Appl. Phys. **43**, 2327 (1972)
- ⁶ C. Sirtori, P. Kruck, S. Barbieri, P. Collot, J. Nagle, M. Beck, J. Faist, and U. Oesterle, Appl. Phys. Lett., **73**, 3486 (1998)
- ⁷ G. Scamarcio, F. Capasso, J. Faist, C. Sirtori, D. L. Sivco, A. L. Hutchinson, and A. Y. Cho, Science **276**, 773 (1997)
- ⁸ A. Tahouri, A. Matlis, S. Slivken, J. Diaz, and M. Razeghi, Appl. Phys. Lett., **78**, 416 (2001)
- ⁹ D. Hofstetter, M. Beck, T. Allen, J. Faist, U. Oesterle, M. Ilgems, E. Gini, and H. Melchior, Appl. Phys. Lett., **78**, 1964 (2001)
- ¹⁰ M. Tacke, Infrared Phys. **36**, 447 (1995)
- ¹¹ F.K. Tittel, D. Richter, and A. Fried, Mid-Infrared Laser Applications in Spectroscopy, Topics in Applied Physics **89**, 445 (2003)
- ¹² S. Hoefling, J. Seufert, M. Fischer, B. Roesener, J. Koeth, J.P. Reithmaier, and A. Forchel, Mode switching and singlemode tuning in two-segment distributed feedback quantum cascade lasers Electronics Letters **42**, 220 (2006)
- ¹³ R. Maulini, D.A. Yarekha, J. Bulliard, M. Beck, M. Giovannini, J. Faist, and E. Gini, Broadly tunable external cavity quantum - cascade lasers, Proceedings of SPIE-The International Society for Optical Engineering **6010** (Infrared to Terahertz Technologies for Health and the Environment), 601001/1-601001/11 (2005)
- ¹⁴ A. Tredicucci, L. Mahler, T. Losco, J. Xu, C. Mauro, R. Koehler, H.E. Beere, D.A. Ritchie, and E.H. Linfield, Advances in THz quantum cascade lasers : fulfilling the application potential, Proceedings of SPIE-The International Society for Optical Engineering **5738** (Novel In-Plane Semiconductor Lasers IV), 146 (2005)
- ¹⁵ www.alpeslasers.com
- ¹⁶ D. Bour, M. Troccoli, F. Capasso, S. Corzine, A. Tandon, D. Mars, and G. Hoefler, Journal of Crystal Growth, **272**, 526 (2004)
- ¹⁷ D. Bour, S. Corzine, G. Hoefler, A. Tandon, D. Mars, D. Smit, L. Diehl, and F. Capasso, Appl. Phys. Lett. **85**, 5842 (2004)
- ¹⁸ R.P. Green, L.R. Willson, E.A. Zibik, D.G. Revin, J.W. Cockburn, C. Pfluegl, W. Schrenk, G. Strasser, A.B. Krysa, J.S. Roberts, C.M. Tey, and A.G. Cullis, Appl. Phys. Lett. **85**, 5529 (2004)
- ¹⁹ A. Lambrecht, Quantum cascade lasers, systems, and applications in Europe, Proceedings of SPIE-The International Society for Optical Engineering **5732** (Quantum Sensing and Nanophotonic Devices II), 122, (2005)
- ²⁰ M. Garcia, E. Normand, C.R. Stanley, C.N Ironside, C.D. Farmer, G. Duxbury, and N. Langford, An AlGaAs-GaAs quantum cascade laser operating with a thermoelectric cooler for spectroscopy of NH₃, Optics Communications **226**, 39 (2003)
- ²¹ L. Joly, V. Zéninari, B. Parvitte, D. Weidmann, D. Courtois, Y. Bonetti, T. Aellen, M. Beck, J. Faist, and D. Hofstetter, Spectroscopic study of the ν_1 band of SO₂ using a continuous-wave DFB QCL at 9.1 μm , Appl. Phys. B **77**, 703 (2003)
- ²² M.G. da Silva, H. Vargas, A. Miklos, and P. Hess, Photoacoustic detection of ozone using a quantum cascade laser, Appl. Phys. B **78**, 677 (2004)
- ²³ Y.A. Bakhirkin, A.A. Kosterev, C. Roller, R.F. Curl, and F.K. Tittel, Mid-infrared quantum cascade laser based off-axis integrated cavity output spectroscopy for biogenic nitric oxide detection, Applied Optics **43**, 2257 (2004)
- ²⁴ D. Weidmann, A.A Kosterev, C. Roller, R.F. Curl, M.P Fraser, and F.K. Tittel, Monitoring of ethylene by a pulsed quantum cascade laser, Applied Optics **43**, 3329 (2004)

- ²⁵ G. Wysocki, A.A. Kosterev and F.K. Tittel *Appl. Phys. B* **80**, 617-625 (2005)
- ²⁶ A.A. Kosterev, R.F. Curl, F.K. Tittel, M. Rochat, M. Beck, D. Hofstetter, and J. Faist, Chemical sensing with pulsed QC-DFB lasers operating at 15.6 μm , *Appl. Phys. B* **75**, 351 (2002)
- ²⁷ A. Lambrecht, T. Beyer, M. Braun, A. Peter, and S. Hartwig, Fast gas spectroscopy using pulsed quantum cascade lasers, *Technisches Messen* **71**, 311 (2004)
- ²⁸ M.T. McCulloch, E.L. Normand, N. Langford, and G. Duxbury, Highly sensitive detection of trace gases using the time-resolved frequency downchirp from pulsed quantum-cascade lasers, *J. Opt.Soc. Am. B* **20**, 1761 (2003)
- ²⁹ E. Normand, M. McCulloch, G. Duxbury, and N. Langford, Fast. Real-time spectrometer based on a pulsed quantum-cascade laser, *Optics Letters* **28**, 16 (2003)
- ³⁰ R. Maulini, M. Beck, J. Faist, and E. Gini, Broadband tuning of external cavity bound-to-continuum quantum-cascade lasers, *Appl. Phys. Lett.* **84**, 1659 (2004)
- ³¹ E. Normand, G. Duxbury, and N. Langford, Characterisation of the spectral behaviour of pulsed quantum cascade lasers using a high resolution Fourier transform infrared spectrometer *Opt. Commun* **197**, 115 (2001)
- ³² M. Lackner, C. Forsich, F. Winter, S. Anders, and G. Strasser, Investigation of biomass steam gasification gas using a GaAs based quantum cascade laser emitting at 11 μm , *Optics Communications* **216**, 357 (2003)
- ³³ S. Schaden, M. Haberkorn, J. Frank, J.R. Baena, and B. Lendl, Direct Determination of Carbon Dioxide in Aqueous Solution Using Mid-Infrared Quantum Cascade Lasers, *Appl. Spectrosc.* **58**, 667 (2004)
- ³⁴ A.A. Kosterev, and F.K. Tittel, Chemical Sensors based on Quantum Cascade Lasers, *IEEE Journal of Quantum Electronics* **38**, 582 (2002)
- ³⁵ K. Namjou, S. Cai, and E-A- Whittaker, Sensitive absorption spectroscopy with a room-temperature distributed-feedback quantum-cascade laser, *Optics Letters* **23**, 219 (1998)
- ³⁶ R. Jimenez, M. Taslakov, V. Simeonov, B. Calpini, F. Jeanneret, D. Hofstetter, M. Beck, J. Faist, and H. van den Bergh, Ozone detection by differential absorption spectroscopy at ambient pressure with a 9.6 μm pulsed quantum-cascade laser, *Appl. Phys B* **78**, 249 (2004)
- ³⁷ A.A. Kosterev, R.F. Curl, F.K. Tittel, R. Köhler, C. Gmachl, F. Capasso, D.L. Sivco, and A.Y. Cho, Transportable automated ammonia sensor based on a pulsed thermoelectrically cooled quantum -cascade distributed feedback laser, *Applied Optics* **41**, 573 (2002)
- ³⁸ Q. Shi, D.D. Nelson, J.B. McManus, M.S. Zahniser, M.E. Parrish, R.E. Baren, K.H. Shafer, and C.N. Harward, Quantum Cascade Infrared Laser Spectroscopy for Real-Time Cigarette Smoke Analysis, *Anal. Chem.* **75**, 5180 (2003)
- ³⁹ C. Charlton, F. de Melas, A. Inberg, N. Croitoru, and B. Mizaikoff, Hollow-waveguide gas sensing with room-temperature quantum cascade lasers, *IEEE Proceedings-Optoelectronics* **150**, 306 (2003)
- ⁴⁰ D.D. Nelson, J.H. Shorter, J.B. McManus, and M.S. Zahniser, Sub-part-per-billion detection of nitric oxide in air using a thermoelectrically cooled mid-infrared quantum cascade laser spectrometer, *Appl. Phys. B* **75**, 343 (2002)
- ⁴¹ A.A. Kosterev, F.K. Tittel, R. Köhler, C. Gmachl, F. Capasso, D.L. Sivco, A.Y. Cho, S. Wehe, and M.G. Allen, Thermoelectrically cooled quantum-cascade-laser-based sensor for the continuous monitoring of ambient atmospheric carbon monoxide, *Applied Optics* **41**, 1169 (2002)
- ⁴² A.A. Kosterev, F.K. Tittel, W. Durante, M. Allen, R. Köhler, C. Gmachl, F. Capasso, D.L. Sivco, and A.Y. Cho, Detection of biogenic CO production above vascular cell cultures using a near-room-temperature QC-DFB laser, *Appl. Phys. B* **74**, 95 (2002)
- ⁴³ G. Duxbury, N. Langford, M.T. McCulloch, and S. Wright, Quantum cascade semiconductor infrared and far-infrared lasers: from trace gas sensing to non-linear optics, *Chemical Society Reviews* **34**, 921, (2005)
- ⁴⁴ O. Werhan, J. Koelliker Delgado, and D. Schiel, *Technisches Messen*, **72**, 396, (2005)
- ⁴⁵ R. Jimenez, S. Herndon, J.H. Shorter, D.D. Nelson, J.B. McManus, and M.S. Zahniser, Atmospheric trace gas measurements using a dual quantum - cascade laser mid-infrared absorption spectrometer, *Proceedings of SPIE-The International Society for Optical Engineering* **5738** (Novel In-Plane Semiconductor Lasers IV), 318 (2005)
- ⁴⁶ W. Blake Martin, S. Mirov, and R. Venugopalan, Middle Infrared, Quantum Cascade Laser Optoelectronic Absorption System for Monitoring Glucose in Serum, *Applied Spectroscopy* **59**, 881 (2005)

- ⁴⁷ C. Charlton, A. Katzir, and B. Mizaikoff, Infrared evanescent field sensing with quantum cascade lasers and planar silver halide waveguides, *Analytical Chemistry* **77**, 4398, (2005)
- ⁴⁸ C. Charlton, M. Giovannini, J. Faist, and B. Mizaikoff, Fabrication and Characterization of Molecular Beam Epitaxy Grown Thin-Film GaAs Waveguides for Mid-Infrared Evanescent Field Chemical Sensing, *Analytical Chemistry* **78**, 4224, (2006)
- ⁴⁹ S. Schaden, A. Dominguez-Vidal, and B. Lendl, Simultaneous measurement of two compounds in aqueous solution with dual quantum cascade laser absorption spectroscopy, *Applied Physics B* **83**, 135 (2006)
- ⁵⁰ S. Schaden, A. Dominguez-Vidal, and B. Lendl, Online reaction monitoring in liquid phase using two mid-IR quantum cascade lasers simultaneously, *Applied Spectroscopy* **60**, in press (2006)
- ⁵¹ S. Schaden, A. Dominguez-Vidal, and B. Lendl, Quantum cascade laser modulation for correction of matrix induced background changes in aqueous samples, submitted
- ⁵² F. Keilmann, Tip-scattering near-field microscopy in the infrared Abstracts of Papers, 227th ACS National Meeting, Anaheim, CA, United States, March 28-April 1, 2004 (2004)
- ⁵³ B. Guo, Y. Wang, C. Peng, G.P. Luo, and H.Q. Le, Multi-wavelength mid-infrared micro-spectral imaging using semiconductor lasers, *Applied Spectroscopy* **57**, 811, (2003)
- ⁵⁴ J. Darmo, V. Tamosiunas, G. Fasching, J. Kröll, K. Unterrainer, M. Beck, M. Giovannini, J. Faist, C. Kremser, and P. Debbage, Imaging with a Terahertz quantum cascade laser, *Optics Express* **12**, 1879, (2004)
- ⁵⁵ K.M. Seongsin, F. Hatami, J.S. Harris, A.W. Kurian, J. Ford, D. King, G. Scalari, M. Giovannini, N. Hoyler, J. Faist, and G. Harris, Biomedical terahertz imaging with a quantum cascade laser, *Applied Physics Letters* **88**, 153903 (2006)
- ⁵⁶ D.R. Chamberlin, P.R. Robrish, W.R. Jr. Trutna, G. Scalari, M. Giovannini, L. Ajili, J. Faist, H.E. Beere, and D.A. Ritchie, Dual-wavelength THz imaging with quantum cascade lasers, *Proceedings of SPIE-The International Society for Optical Engineering*, **5727** (Terahertz and Gigahertz Electronics and Photonics IV), 107 (2005)
- ⁵⁷ A.A. Kosterev, A.L. Malinovsky, F.K. Tittel, C. Gmachl, F. Capasso, D.L. Sivco, J.N. Baillargeon, A.L. Hutchinson, and A.Y. Cho, Cavity ringdown spectroscopic detection of nitric oxide with a continuous-wave quantum-cascade laser, *Applied Optics* **4**, 5522 (2001)
- ⁵⁸ B.A. Paldus, C.C. Harb, T.G. Spence, R.N. Zare, C. Gmachl, F. Capasso, D.L. Sivco, J.N. Baillargeon, A.L. Hutchinson, and A.Y. Cho, Cavity ringdown spectroscopy using mid-infrared quantum-cascade lasers, *Optics Letters* **25**, 666 (2000)
- ⁵⁹ A. O'Keefe, Integrated cavity output analysis of ultra-weak absorption, *Chem. Phys. Lett.* **293**, 331 (1998)
- ⁶⁰ R. Engeln, G. Berden, R. Peeters, and G. Meijer, Cavity enhanced absorption and cavity enhanced magnetic rotation spectroscopy, *rev. Sci. Instrum.* **69**, 3763 (1998)
- ⁶¹ L. Menzel, A.A. Kosterev, R.F. Curl, F.K. Tittel, C. Gmachl, F. Capasso, D.L. Sivco, J.N. Baillargeon, A.L. Hutchinson, A.Y. Cho, and W. Urban, Spectroscopic detection of biological NO with a quantum cascade laser, *Appl. Phys. B* **72**, 859 (2001)
- ⁶² B.A. Paldus, T.G. Spence, R.N. Zare, J. Oomens, F.J.M. Harren, D.H. Parker, C. Gmachl, F. Capasso, D.L. Sivco, J.N. Baillargeon, A.L. Hutchinson, and A.Y. Cho, Photoacoustic spectroscopy using quantum-cascade lasers, *Optics Letters* **24**, 178 (1999)
- ⁶³ D. Hofstetter, M. Beck, J. Faist, M. Nägele, and M.W. Sigrüst, Photoacoustic spectroscopy with quantum cascade distributed-feedback laser, *Optics Letters* **26**, 887 (2001)
- ⁶⁴ M. Nägele, D. Hofstetter, J. Faist, and M.W. Sigrüst, Low power quantum-cascade laser photoacoustic spectrometer for trace-gas monitoring, *Analytical Sciences* **17**, 497 (2001)
- ⁶⁵ S. Barbieri, J.P. Pellaux, E. Studemann, and D. Rosset, Gas detection with quantum cascade lasers: An adapted photoacoustic sensor based on Helmholtz resonance, *Review of Scientific Instruments* **73**, 2458 (2004)
- ⁶⁶ V.P. Zharov and V.S. Letokhov, *Laser Photoacoustic spectroscopy*, T. Tamir, Ed. (Springer-Verlag, Berlin, 1986) Volume 37, Chap. 5, p 102
- ⁶⁷ S. Danworaphong, I.G. Calasso, A. Beveridge, G.J. Diebold, C. Gmachl, F. Capasso, D.L. Sivco, and A.Y. Cho, Internal excited acoustic resonator for photoacoustic trace detection, *Applied Optics* **27**, 5561 (2003)

- ⁶⁸ A.A. Kosterev, Y.A. Bakhrkin, F.K. Tittel, S. Blaser, Y. Bonetti, and L. Hvozdar, Photoacoustic phase shift as a chemically selective spectroscopic parameter, *Appl. Phys. B* **78**, 673 (2004)
- ⁶⁹ A.A. Kosterev, Y.A. Bakhrkin, and F.K. Tittel, Ultrasensitive gas detection by quartz-enhanced photoacoustic spectroscopy in the fundamental molecular absorption bands region, *Appl. Phys. B* **80**, 133 (2005)
- ⁷⁰ H. Ganser, M. Horstjann, C.V. Suschek, P. Hering, and M. Mürzt, Online monitoring of biogenic nitric oxide with a QC laser-based Faraday modulation technique, *Appl. Phys. B* **78**, 513 (2004)
- ⁷¹ H. Ganser, W. Urban, and J.M. Brown, The sensitive detection of NO by Faraday modulation spectroscopy with a quantum cascade laser, *Molecular Physics* **101**, 545 (2003)
- ⁷² R. Provencal, M. Gupta, T.G. Owano, D.S. Baer, K.N. Ricci, A. O'Keefe J. R. Podolske, Cavity-enhanced quantum-cascade laser-based instrument for carbon monoxide measurements, *Applied Optics* **44**, 6712, (2005)
- ⁷³ D.D. Nelson, B. McManus, S. Urbanski, S. Herndon, and M.S. Zahniser, High precision measurements of atmospheric nitrous oxide and methane using thermoelectrically cooled mid-infrared quantum cascade lasers and detectors, *Spectrochimica Acta Part A* **60**, 3325 (2004)
- ⁷⁴ C.R. Webster, G.J. Flesch, D.C. Scott, J.E. Swanson, R.D. May, W.S. Woodward, C. Gmachl, F. Capasso, D.L. Sivco, J.N. Baillargeon, A.L. Hutchinson, and A.Y. Cho, Quantum-cascade laser measurements of stratospheric methane and nitrous oxide, *Applied Optics* **40**, 321 (2001)
- ⁷⁵ C.R. Webster, R.D. May, C.A. Trimble, R.G. Chave, and J. Kendall, Aircraft (ER-2) laser infrared absorption spectrometer (ALIAS) for in-situ stratospheric measurements of HCl, N₂O, CH₄, NO₂ and HNO₃, *Applied Optics* **33**, 454 (1994)
- ⁷⁶ R. Kormann, R. Königstedt, U. Parchatka, J. Lelieveld, and H. Fischer, QUALITAS : a mid-infrared spectrometer for sensitive trace gas measurements based on quantum cascade lasers in CW operation, *Review of Scientific Instruments* **76**, 075102/1, (2005)
- ⁷⁷ D. Weidmann, F.K. Tittel, T. Aellen, M. Beck, D. Hofstetter, J. Faist, and S. Blaser, Mid-infrared trace-gas sensing with a quasi-continuous-wave Peltier-cooled distributed feedback quantum cascade laser, *Appl. Phys. B* **79**, 907 (2004)
- ⁷⁸ D. Weidmann, G. Wysocki, C. Oppenheimer, F.K. Tittel, Development of a compact quantum cascade laser spectrometer for field measurements of CO₂ isotopes, *Appl. Phys. B* **80**, 255 (2005)
- ⁷⁹ D. Weidmann, C. Roller, C. Oppenheimer, A. Fried, and F. Tittel, Carbon isotopomers measurement using mid-IR tunable laser sources, *Isotopes in Environmental and Health Studies* **41**, 293, (2005)
- ⁸⁰ M. Taslakov, V. Simeonov, M. Froidevaux, and H. van den Bergh, Open-path ozone detection by quantum - cascade laser, *Applied Physics B: Lasers and Optics* **82**, 501, (2006)
- ⁸¹ S. Sato, M. Saito and M. Miyagi *Appl. Spectrosc.* **47**, 1665, (1993)
- ⁸² Hvozdar, S. Gianordoli, G. Strasser, W. Schrenk, K. Unterrainer, E. Gornik, C.S.S.S. Murthy, M. Kraft, V. Pustogow, B. Mizaikoff, A. Inberg, N. Croitoru, Spectroscopy in the gas phase with GaAs/AlGaAs quantum - cascade lasers, *Applied Optics* **39**, 6926, (2000)
- ⁸³ C. Charlton, F. de Melas, A. Inberg, N. Croitoru, and B. Mizaikoff, Hollow - waveguide gas sensing with room-temperature quantum cascade lasers, *IEEE Proceedings: Optoelectronics* **150**, 306 (2003)
- ⁸⁴ C. Charlton, B. Temelkuran, G. Dellemann, and B. Mizaikoff, Midinfrared sensors meet nanotechnology: Trace gas sensing with quantum cascade lasers inside photonic band-gap hollow waveguides, *Applied Physics Letters* **86**, 194102/1 (2005)
- ⁸⁵ W.H. Webber, J.T. Remillard, R.E. Chase, J.F. Richert, F. Capasso, C. Gmachl, A.L. Hutchinson, D.L. Sivco, J.N. Baillargeon, and A.Y. Cho, Using a Wavelength-modulated Quantum Cascade Laser to Measure NO Concentrations in the Part-per-Billion Range for Vehicle Emission Certification, *Appl. Spectrosc.* **56**, 706 (2002)
- ⁸⁶ A. Elia, P.M. Luga, and C. Giancaspro, Photoacoustic detection of nitric oxide by use of a quantum-cascade laser, *Optics Letters* **30**, 988, (2005)
- ⁸⁷ B.W.M. Moeskops, S.M. Cristescu, and F.J.M. Harren, Sub-part-per-billion monitoring of nitric oxide by use of wavelength modulation spectroscopy in combination with a thermoelectrically cooled, continuous-wave quantum cascade laser, *Optics Letters* **31**, 823 (2006)
- ⁸⁸ W.T. Rawlins, J.M. Hensley, D.M. Sonnenfroh, D.B. Oakes, and M.G. Allen, Quantum cascade laser sensor for SO₂ and SO₃ for application to combustor exhaust streams, *Applied Optics* **44**, 6635, (2005)
- ⁸⁹ M. T. McCulloch, N. Langford, and G. Duxbury, Real time trace level detection of carbon dioxide and ethylene in car exhaust gases *Applied Optics* **44**, 2887, (2005)

- ⁹⁰ R.E. Baren, M.E. Parrish, K.H. Shafer, C. N. Harward, Q. Shi, D.D. Nelson, J.B. McManus, and M.S. Zahniser, Quad quantum cascade laser spectrometer with dual gas cells for the simultaneous analysis of mainstream and sidestream cigarette smoke, *Spectrochimica Acta Part A* **60**, 3437 (2004)
- ⁹¹ K. Alving, E. Weitzberg, and J.M. Lundberg, *Eur. Respir. J.* **6**, 1368 (1993)
- ⁹² N. Wilson, and S. Pedersen, *Am. J. Respir. Crit. Care Med.* **162**, 48 (2000)
- ⁹³ S.S. Sehnert, L. Jiang, J.F. burdick, and T.H. Risby, *Biomarkers* **7**, 174 (2002)
- ⁹⁴ G.J. Fetzer, A.S. Pittner, and P.E. Silkoff, Mid-infrared laser absorption spectroscopy in coiled hollow optical waveguides, *Proceedings of SPIE-The International Society for Optical Engineering* **4957**(Optical Fibers and Sensors for Medical Applications III), 124, (2003)
- ⁹⁵ C.Roller, A.A. Kosterev, F. Tittel, K. Uehara, C. Gmachl, and D.L. Sivco, Carbonyl sulfide detection with a thermoelectrically cooled midinfrared quantum cascade laser, *Optics Letter* **28**, 2052 (2003)
- ⁹⁶ G. Wysocki, Matt McCurdy, S. So, D. Weidmann, C. Roller, R.F. Curl, and F.K. Tittel, Pulsed quantum-cascade laser-based sensor for trace-gas detection of carbonyl sulfide, *Applied Optics* **43**, 6040 (2004)
- ⁹⁷ G. Gagliardi, F. Tamassia, P. De Natale, C. Gmachl, F. Capasso, D.L. Sivco, J.N. Baillargeon, A.L. Hutchinson, and A.Y. Cho, Sensitive detection of methane and nitrous oxide isotopomers using a continuous wave quantum cascade laser, *The European Physical Journal D* **19**, 327 (2002)
- ⁹⁸ G. Gagliardi, S. Borri, F. Tamassia, F. Capasso, C. Gmachl, D.L. Sivco, J.N. Baillargeon, A.L. Hutchinson, A.Y. Cho, A frequency-modulated quantum - cascade laser for spectroscopy of CH₄ and N₂O isotopomers, *Isotopes in Environmental and Health Studies* **41**,313, (2005)
- ⁹⁹ S. Schilt, L. Thévenaz, E. Courtois, and P.A. Robert, Ethylene spectroscopy using a quasi-room-temperature quantum cascade laser, *Spectrochimica Acta Part A* **58**, 2533 (2002)
- ¹⁰⁰ A. Elia, F. Rizzi, C. Di Franco, P.M. Lugara, and G. Scamarcio, Quantum cascade laser -based photoacoustic spectroscopy of volatile chemicals: Application to hexamethyldisilazane, *Spectrochimica Acta, Part A: Molecular and Biomolecular Spectroscopy*, **64**, 426, (2006)
- ¹⁰¹ A. Cheesman, J.A. Smith, M.N.R. Ashfold, N. Langford, S. Wright, and G. Duxbury, Application of a Quantum Cascade Laser for Time-Resolved, in Situ Probing of CH₄/H₂ and C₂H₂/H₂ Gas Mixtures during Microwave Plasma Enhanced Chemical Vapor Deposition of Diamond, *Journal of Physical Chemistry A*, **110**, 2821, (2006)
- ¹⁰² M. Kölhed, M. Haberkorn, V. Pustogov, B. Mizaikoff, J. Frank, B. Karlberg, and B. Lendl, Assessment of quantum cascade lasers as mid infrared light sources for measurement of aqueous samples, *vibrational Spectroscopy* **29**, 283 (2002)
- ¹⁰³ J.Z. Chen, Z. Liu, C.F. Gmachl, and D.L. Sivco, Silver halide fiber-based evanescent-wave liquid droplet sensing with room temperature mid-infrared quantum cascade lasers, *Optics Express*, **13**, 5953, (2005)
- ¹⁰⁴ A. Edelmann, C. Ruzicka, J. Frank, B. Lendl, W. Schrenk, E. Gornik, and G. Strasser, Towards functional group-specific detection in high-performance liquid chromatography using mid-infrared quantum cascade lasers, *Journal of Chromatography A* **934**, 123 (2001)
- ¹⁰⁵ M. Koelhed, S. Schaden, B. Karlberg, and B. Lendl, On-line hyphenation of quantum cascade laser and capillary electrophoresis, *Journal of Chromatography, A* **1083** 199 (2005)
- ¹⁰⁶ B. Lendl, J. Frank, R. Schindler, A. Müller, M. Beck, and J. Faist, Mid-Infrared Quantum Cascade Laser for Flow Injection Analysis, *Anal. Chem.* **72**, 1645 (2000)

Table I: Milestones in the development of Quantum cascade lasers.

Year	Milestones	Puplication	
1994	First QCL	Science 264, 533-556	J. Faist et al.
1995	CW operation	Appl. Phys. Lett. 68, 3057-3062	J. Faist et al.
1996	Room temperature operation with high power	Appl. Phys. Lett. 67, 3680-3682	J. Faist et al.
1997	Room temperature operation in single mode (DFB)	Appl. Phys. Lett. 70, 2670-2672	J. Faist et al.
1998	new material used: GaAs/AlGaAs	Appl. Phys. Lett. 73, 3486-3488	C. Sirtori et al.
2002	CW operation above room temperature	Science 295, 301-305	M. Beck et al.
2004	QCL grown using Metal-Organic Chemical Vapor Deposition	J. of Crystal Growth 272, 526	D.Bour et al.

Table II: Comparison of the AlGaAs/GaAs and AlInAs/AlInAs//InP quantum cascade lasers.

<i>Parameter</i>	<i>AlInAs/AlGaAs//InP</i>	<i>AlGaAs/GaAs</i>
Possible type	F-P multimode / DFB - mono mode	F-P - multimode / DFB - mono mode
Continuous wave	Demonstrated up to 310 K	Demonstrated up to 140 K
Pulsed mode	Above room temperature	Above Room temperature
Possible range	(4.2 to 17.5 microns)	(7 to 22.5) microns
Tuneability range	0.40%	unknown
Average powers	2 mW typical, 250 mW max.	1 mW range
Line width DFB	3 .. 5 nm (pulsed), 1 .. 2 nm (CW)	unknown
Lifetime	>10 years	>10 years

Figure Captions

Figure 1. (a) Scheme of a quantum well: a narrow-gap semiconductor embedded into two broader-gap semiconductors. Continuum of the conduction band breaks into discrete states. Three states are shown in the enlarged view on the right. A typical form of the electron wave functions, is indicated. Note that the wave functions penetrate into the barriers as a result of the finite depth of the quantum well. (b) Excitation and relaxation as two complementary processes of electron transitions between two energetic states. Various ways of energy exchange are involved, including photon absorption and photon emission. (c) Tunneling. Provided that the barrier between two quantum wells is made so narrow that the penetrating wave functions of the electrons overlap in it, the electrons are free to move in the whole quantum system, although they do not possess energy higher than the barriers. We speak from coupled quantum wells. (The wave functions of the electrons are squared in order to become a measure of the probability function).

Figure 2. Transmission electron micrograph of a laser heterostructure. The darker layers correspond to the barriers, and the brighter ones to the quantum wells. (Courtesy of the Institute of Physics, University of Neuchâtel, Switzerland.)

Figure 3. (a) Scheme of the laser structure under bias. The structure consists of two functional sub-structures: injectors and active cells. The injectors (left and right) serve for injection (on one side) and for the extraction (on the other side) of the electrons into and from the active cell (in the middle). The optical transition as a generation mechanism - takes place inside the active cell. Pairs of the active cells and injectors are reproduced typically in 20 to 40 periods in a laser structure. A single electron, when successfully passing the whole structure, can emit 20 or 40 photon respectively. (b) Active cell close-up. An electron is injected into the upper state (E3). It undergoes an optical transition E3-E2. The energetic difference between the states determines the wavelength of the emitted photon. The energetic difference E2-E1 is tuned to be in resonance with the longitudinal optical phonon. As a very efficient transition mechanism it serves for evacuation of the electrons from the state E2. A condition for population inversion in the system E3 and E2 is created.

Figure 4. A scheme of the QCL fabrication process flow.

Figure 5. A Fabry-Pérot laser spectrum (a). The spacing of the modes is determined by the physical length of the resonator, and it is typically in the range of 0.5 - 2 cm⁻¹. The total width of the emission spectrum may range from 0.4 % to 10 % of the emission wavelength, depending on the quantum design. The position of the emission maximum is only determined by the MBE growth of the material. Laser may be applied in spectroscopy of broadened absorption lines typically in liquids. (b) Distributed feedback laser spectrum.

The position of the emission peak is determined by the grating period incorporated in the laser resonator. The line-width is in the range of 1-2 nm (for the CW laser operation).

Figure 6. Different cell designs for absorption measurements: (a) single path cell, (b) cell equipped with Brewster windows to suppress optical interference fringes, (c) cell with single reflection, (d) Multi Path Cell, (e) Hollow wave guide acting as light pipe and gas cell

Figure 7. Different cell designs for Photoacoustic measurements: (a) simple resonant cell, (b) cell equipped with acoustic baffle for reducing the noise of the gas stream, (c) cell with additional Brewster windows, (d) Multipass PA cell, (e) Helmholtz resonator, (f) tuning fork for quartz enhanced PAS.

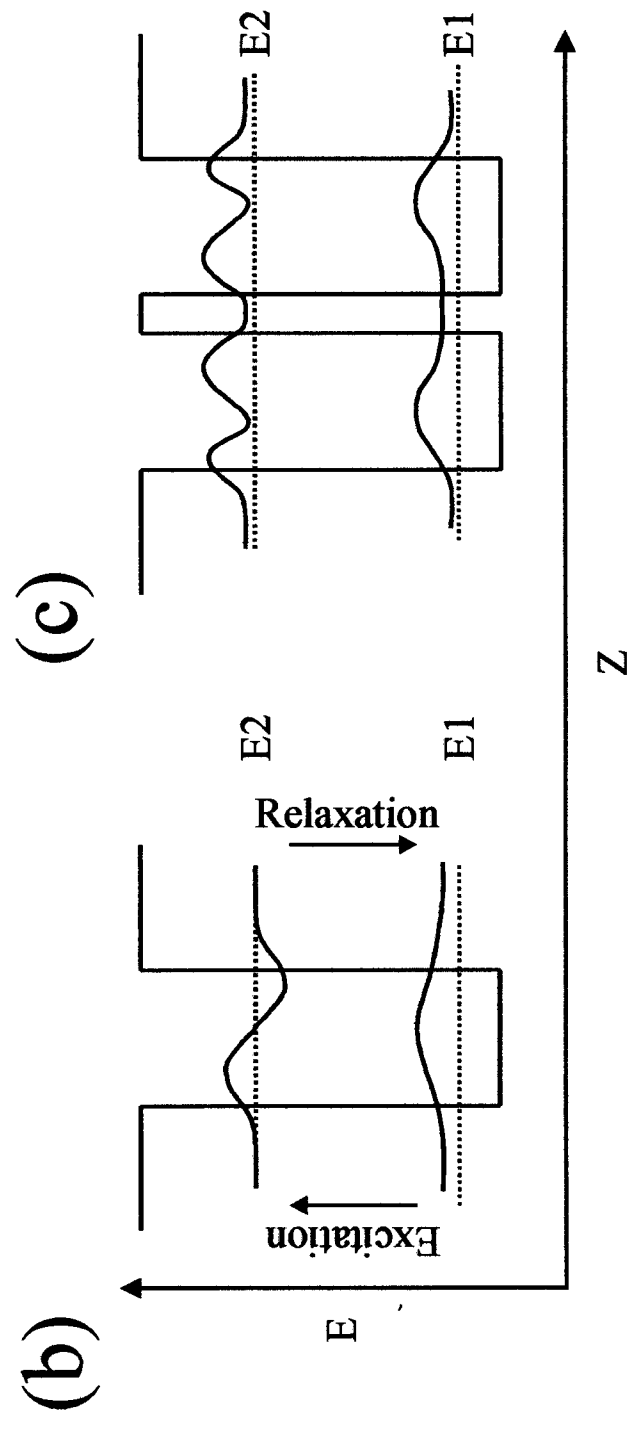
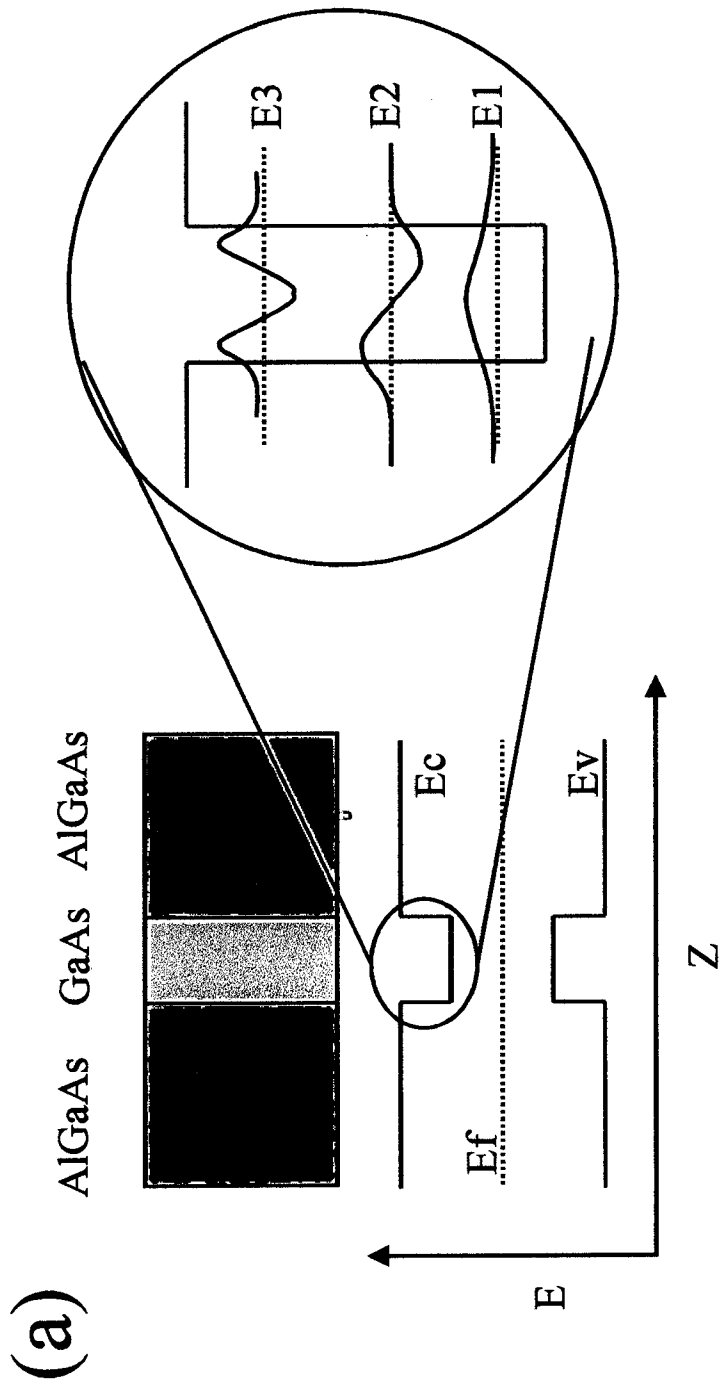


Figure 1

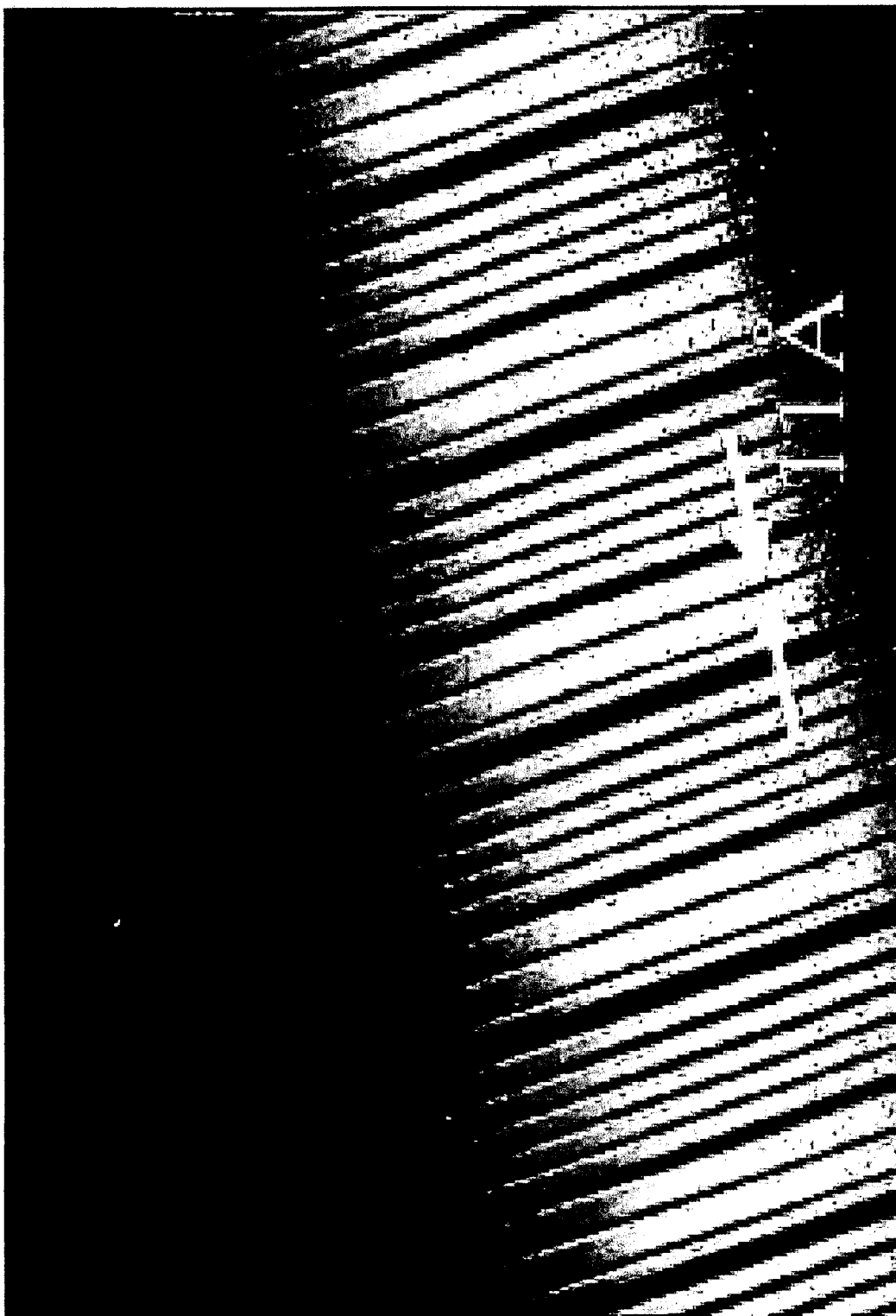
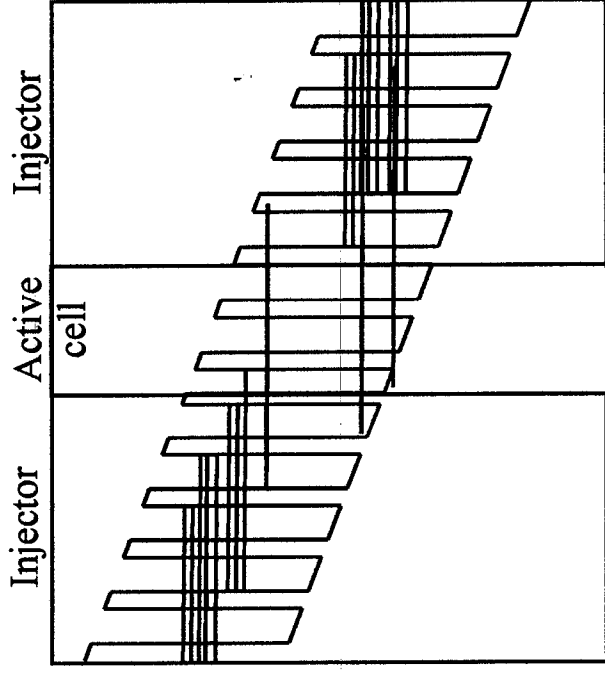


Figure 2

(a)



(b)

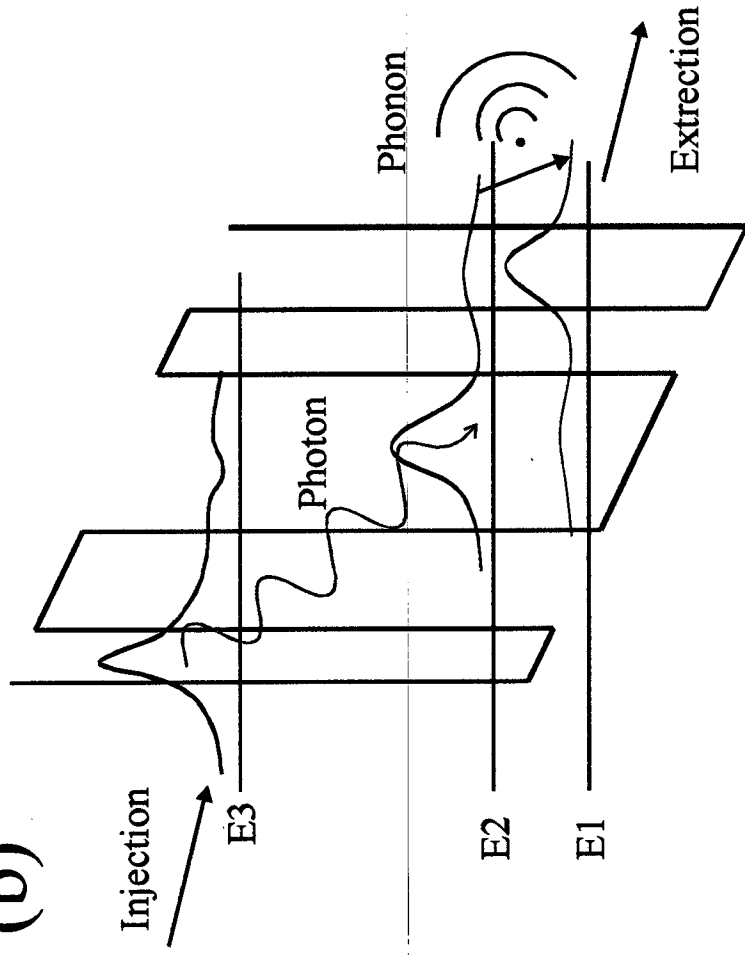


Figure 3

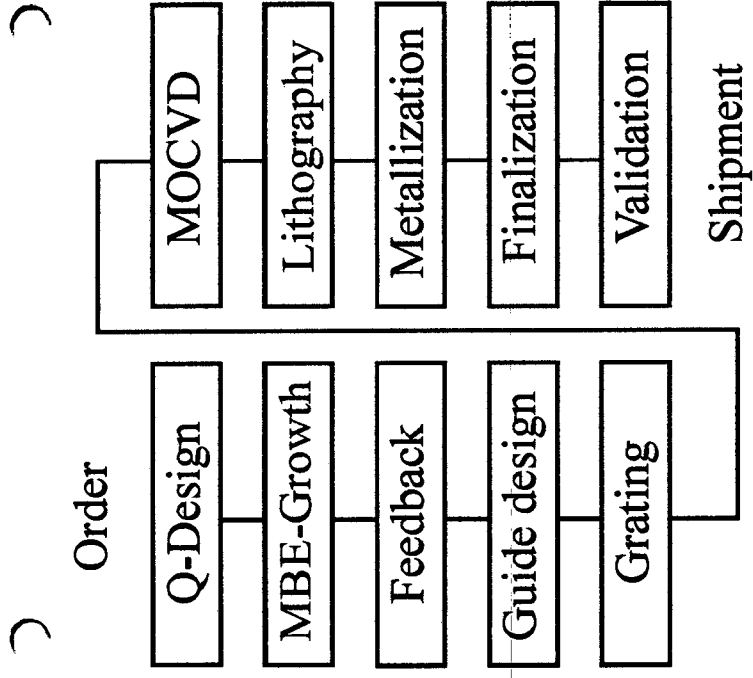


Figure 4

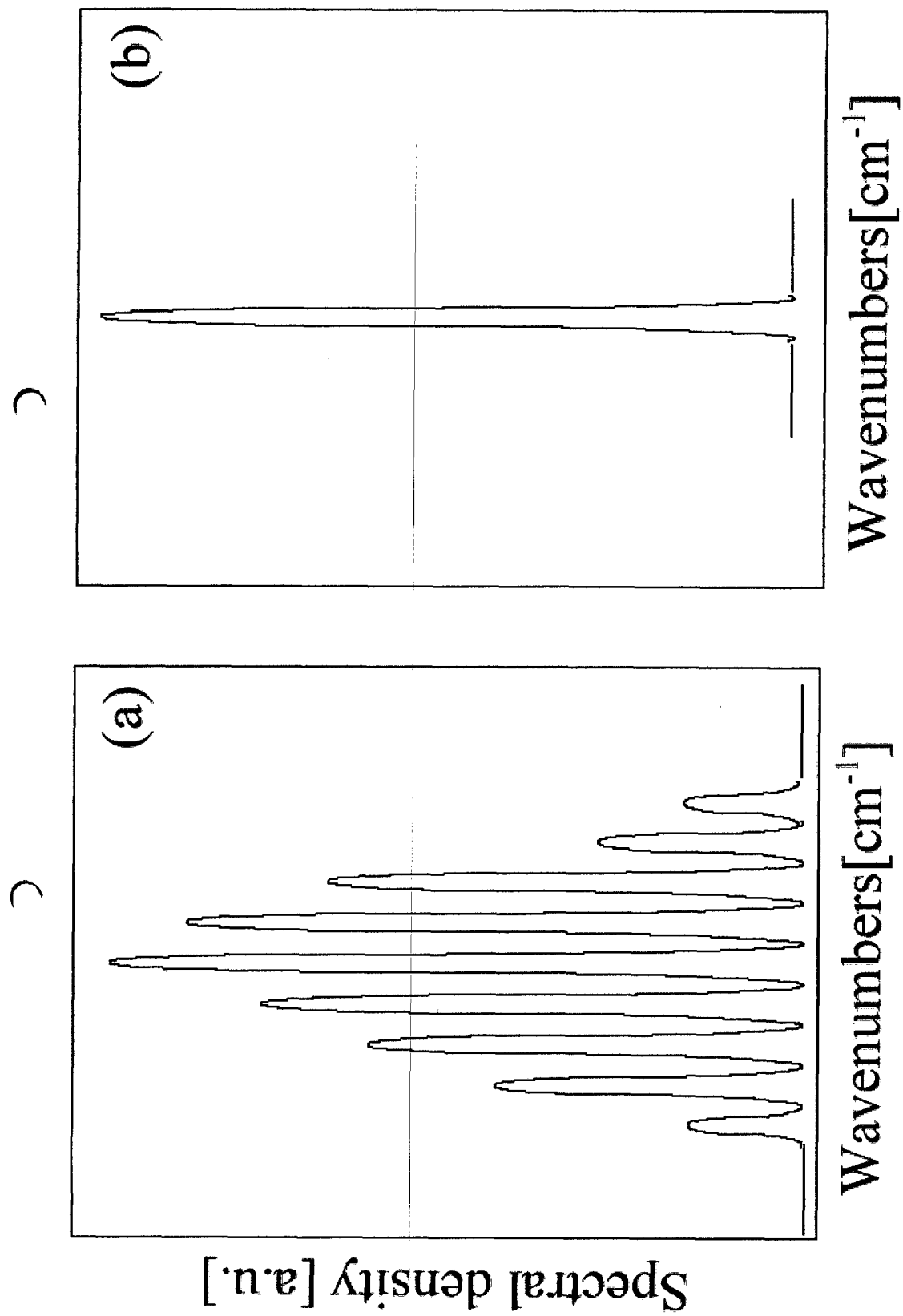


Figure 5

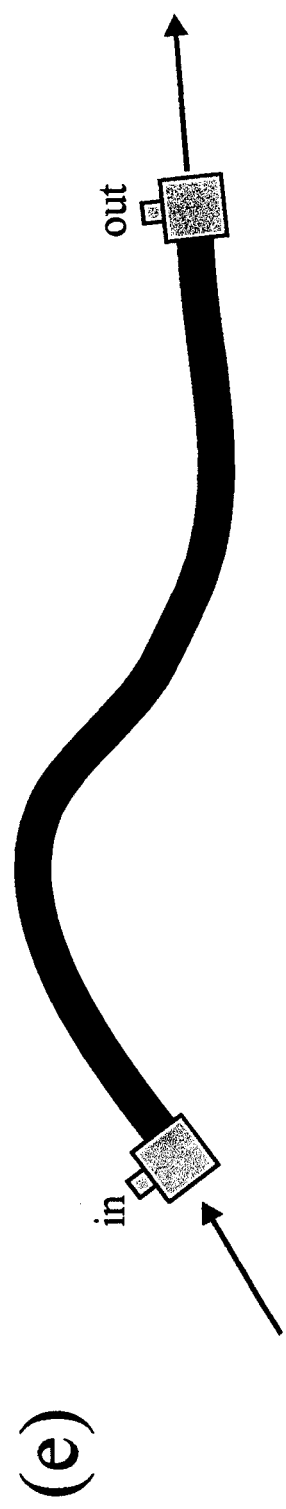
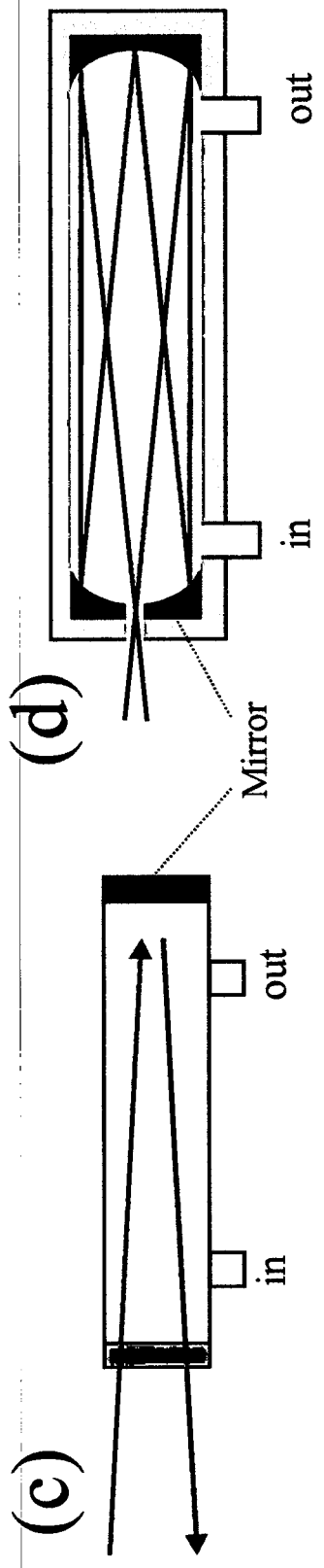
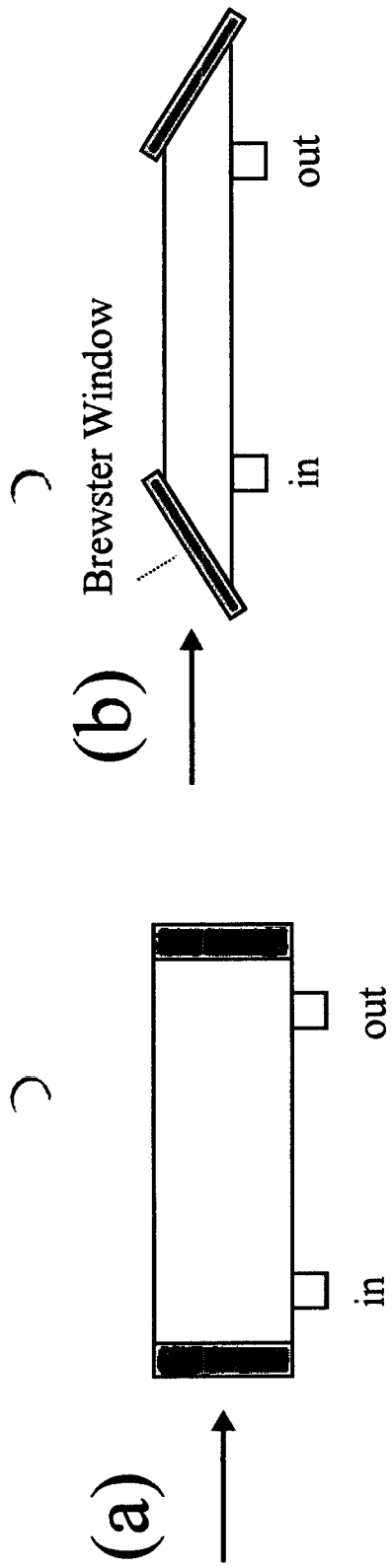


Figure 6

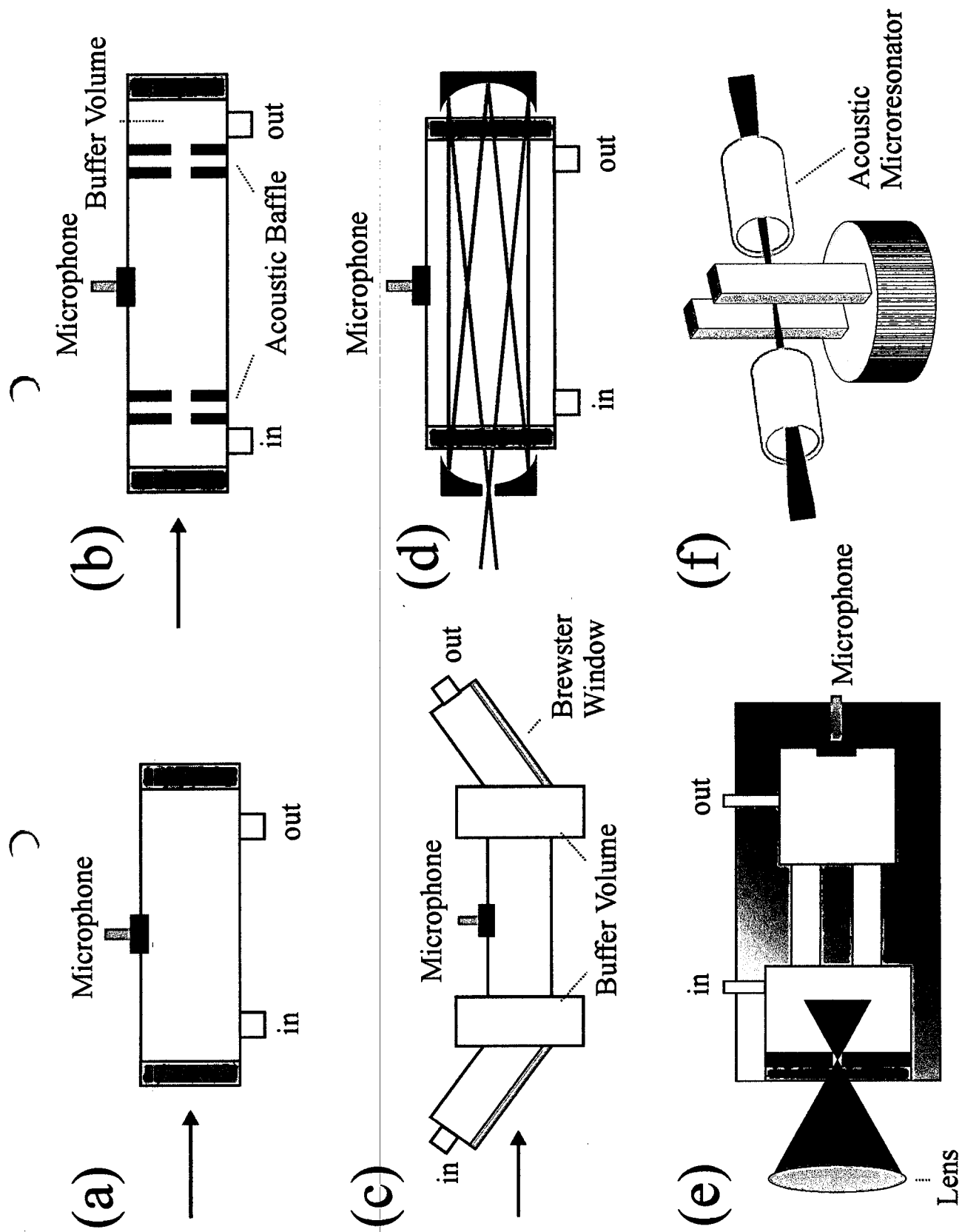


Figure 7

Curriculum Vitae

DI Stefan Schaden

Address:

Simmeringer Hauptstrasse 192a/1/20
1110 Vienna, Austria
Tel.: +43 (0)650 4255558
E-Mail: e9625044@stud3.tuwien.ac.at

Personal data:

Date of birth:	18.04.1978
Place of birth:	Vienna, Austria
Nationality	Austria
Marital status	single

Education

09/03 – until now	PhD thesis at the Institute of Chemical Technologies and Analytics, Vienna University of Technology <i>"Application of Mid-Infrared Quantum Cascade Lasers for Quantitative Analysis in Aqueous Phase"</i>
08/03	Master of Science (honors)
10/96 – 08/03	Studies in Technical Chemistry, Vienna University of Technology Specialisation on Analytical and Physical Chemistry Diploma thesis at the Institute of Chemical Technologies and Analytics <i>"Quantitative Determination of CO₂ and Glucose in Water Using MID-IR Quantum Cascade Lasers"</i>
05/99 – 12/99	Military service NBC defence
08/88-10/96	Wirtschaftskundliches Bundesrealgymnasium Wien XI, Gottschalkgasse

Professional Experience

10/01 – 06/02	Tutor at the Institute of Physical Chemistry, Vienna University of Technology
09/00, 08/97, 08/96, 07/95, as well as 07/94	Summer intern in the chemical laboratories of the <i>Power Plant Station Simmering</i> , Vienna <ul style="list-style-type: none">• established new analytical methods• performed routine analyses (chemical parameters)
08/98	Summer intern in the chemical laboratories of <i>Wienstrom GmbH, staatlich autorisierte Prüf- und Versuchsanstalt für Mineralölprodukte</i> , Vienna <ul style="list-style-type: none">• performed routine analyses (chemical and physical parameters)

Language Skills

- German (native)
- English (very good)
- French (basic)

Computer Skills

- Microsoft Office (Word, Excel, PowerPoint)
- Divers instrument and data processing software

Publications

Schaden, S.; Hvozda, L.; Müller, A.; Lendl, B. "*Quantum cascade lasers: a promising light source for vibrational spectroscopy*" 2006, submitted for publication

Schaden, S.; Domínguez-Vidal, A.; Lendl, B. "*Quantum cascade laser modulation for correction of matrix induced background changes in aqueous samples*" 2006, submitted for publication

Schaden, S.; Domínguez-Vidal, A.; Lendl, B. "*Online reaction monitoring in liquid phase using two mid-IR quantum cascade lasers simultaneously*" 2005, accepted for publication.

Schaden, S.; Domínguez-Vidal, A.; Lendl, B. "*Simultaneous measurement of two compounds in aqueous solution with dual quantum cascade laser absorption spectroscopy*" 2005, accepted for publication.

Koelhed, M.; Schaden, S.; Karlberg, B.; Lendl, B. "*On-line hyphenation of quantum cascade laser and capillary electrophoresis.*" *Journal of Chromatography, A* 2005, 1083(1-2), 199-204.

Schaden, S.; Haberkorn, M.; Frank, J.; Baena, J. R.; Lendl, B. "*Direct determination of carbon dioxide in aqueous solution using mid-infrared quantum cascade lasers.*" *Applied Spectroscopy* 2004, 58(6), 667-670.

Oral Presentations

Schaden S. "*Quanten Kaskaden Laser als Lichtquelle für Messungen in wässriger Phase*" 1. ASAC Dissertanten-Forum, June 10-11, 2005, Tulln, Austria

Poster Presentations

Schaden, S.; Haberkorn, M.; Frank, J.; Ritter, W.; Koelhed, M.; Karlberg, B.; Lendl, B. "*Quantum Cascade Laser for Determination of Solutes in Liquid Phase*" 5th QCL-Workshop, September 23-24, 2004, Freiburg, Germany

Schaden, S.; Haberkorn, M.; Frank, J.; Lendl, B. "*Quantitative Analysis of CO₂ in Water using a MID-IR Quantum Cascade Laser*" 2nd International Conference on Advanced Vibrational Spectroscopy, August 24-29 2003, Nottingham, England